Critical Power Characteristics of Axially Heterogeneous Tight Bundle Designs

by

Xingang Zhao

Diplôme d'ingénieur, Energy and Environmental Engineering (2014)
Institut National des Sciences Appliquées de Lyon

Diplôme d'ingénieur, Nuclear Engineering (2014)
Institut National des Sciences et Techniques Nucléaires de Saclay

SUBMITTED TO THE DEPARTMENT OF NUCLEAR SCIENCE AND ENGINEERING
IN PARTIAL FULFILLMENT OF THE REQUIREMENTS FOR THE DEGREE OF

MASTER OF SCIENCE IN NUCLEAR SCIENCE AND ENGINEERING

AT THE

MASSACHUSETTS INSTITUTE OF TECHNOLOGY

February, 2016

Signature of Author ……...
Xingang Zhao
Department of Nuclear Science and Engineering
January 6, 2016

Certified by …...……..……..
Jacopo Buongiorno, Ph.D.
Professor and Associate Department Head of Nuclear Science and Engineering
Director, Center for Advanced Nuclear Energy Systems (CANES)
Thesis Supervisor

Certified by ...….…….……..
Koroush Shirvan, Ph.D.
Research Scientist of Nuclear Science and Engineering
Thesis Co-supervisor and Reader

Accepted by ...…….…….....……..
Ju Li, Ph.D.
Battelle Energy Alliance Professor of Nuclear Science and Engineering
Professor of Materials Science and Engineering
Chair, Department Committee on Graduate Students

Critical Power Characteristics of Axially Heterogeneous Tight Bundle Designs

by

Xingang Zhao

Submitted to the Department of Nuclear Science and Engineering on January 6, 2016 in Partial Fulfillment of the Requirements for the Degree of

Master of Science in Nuclear Science and Engineering

Abstract

Accurate prediction of the dryout critical power in fuel rod bundles is challenging and has important implications for the economy and safety of Boiling Water Reactors (BWRs). This is especially true for the tight bundle design of the Resource-Renewable BWR (RBWR) proposed by Hitachi, Ltd. Unlike a traditional square lattice BWR fuel bundle, the RBWR bundle is a relatively short tight hexagonal lattice with axially heterogeneous fuel composition for purpose of providing actinide breeding and burning capabilities. The RBWR's different core geometry, combined with higher power-to-flow ratio and larger coolant void fraction, demands a reevaluation of the standard BWR thermal hydraulic models. One of the key constraints in BWR design is the thermal margin to dryout occurrence, referred to as the Minimum Critical Power Ratio (MCPR).

In this thesis, different approaches for predicting critical power of tight bundles are investigated through empirical and mechanistic formulations. Previous work at MIT focused on collecting dryout database representative of RBWR fuel bundle geometry and operating conditions, and derived a best-estimate model for the prediction of critical quality/power, named M1-CISE4 (modified CISE4 version 1) correlation, which was based on the CISE4 formulation. This model showed significant scatter when compared to experimental data in its range of validity. This work supplements tight bundle data with relevant critical heat flux (CHF) data for tubes and annuli to better understand the effect of different parameters. An updated correlation, M2-CISE4 (modified CISE4 version 2), is proposed and analyses reveal that the dependence of critical power on such parameters as non-uniform axial and radial power distribution profiles as well as heated length requires further investigations via sub-channel analysis, using the code VIPRE-01. Results of radial quality distribution at the axial location of dryout are then incorporated and yield the M3-CISE4 (modified CISE4 version 3) correlation development. Another approach utilized in the prediction of dryout databases is the three-field model, which relies on a mechanistic system of mass balance equations to resolve relevant fields (liquid film, entrained droplets, and vapor) within the annular flow regime. The introduction of sub-channel analysis is able to reduce the predicted standard deviation with both M3-CISE4 and three-field model against tight bundle database that includes eight different data sets with a total of 565 measurements with various axial and radial power distributions.

Lastly, the MCPR evaluation of the two current RBWR designs, RBWR-AC and TB2, is performed using the models above and values are compared against the conventional BWR steady-state design limit.

Thesis Supervisor: Jacopo Buongiorno, Ph.D.
Title: Professor and Associate Head, Department of Nuclear Science and Engineering

Thesis Co-supervisor and Reader: Koroush Shirvan, Ph.D.
Title: Research Scientist, Department of Nuclear Science and Engineering

Acknowledgments

I would like to express my most profound gratitude to my former and late thesis supervisor, Professor Mujid S. Kazimi, for providing me with the opportunity to work on this exciting project. His guidance and insights have guided me to become a better researcher, his patience and generosity have helped me to become a better man. His knowledge as well as his smile will be missed by many, and I am so honored to have him as my first mentor at MIT. May your soul rest in peace, and I will miss you, Professor Kazimi.

I am very thankful to have Professor Jacopo Buongiorno as my thesis supervisor. He took me as his student immediately after the passing of Professor Kazimi, and his renowned expertise in reactor thermal-hydraulics has helped tremendously to the completion of my work. The discussions we had during group meetings have always been of great value, along with his comments and suggestions on the thesis.

I owe a great debt to my thesis co-supervisor and reader, Dr. Koroush Shirvan, for his continuous support and help throughout my thesis. I was deeply impressed and influenced by his diligence, rigorous attitude, incisive thinking, and unending desire for learning. He assisted me with every single step of my research: literature review, code learning, data analysis, and troubleshooting. He always prioritized my questions no matter how busy he was. More than an advisor, he is a real friend who helped and encouraged me at different moments.

My thanks are extended to Professor Yingwei Wu, visiting professor from Xi'an Jiaotong University, who provided me with files from previous work on critical power prediction and sub-channel analysis at the start of my project.

I also wish to thank all my NSE classmates for their hospitality and support. My special thanks go to my fellow friends, in particular Lulu Li, Yinan Cai and Zhaoyuan Liu, who have always been of priceless help both academically and socially.

This research work is partly funded by Hitachi, Ltd., which we acknowledge for their financial support.

Finally I would like to thank my father Nan Zhao and my mother Fengqin Zhang, for their unconditional love. They have made unimaginable sacrifices sending their only child abroad for over seven years now. I would never be able to pursue my study here without having such supportive parents.

Table of Contents

List of Figures

List of Tables

Nomenclature

AC: Actinide Consumer

APD: Axial Power Distribution

BAPL: Bettis Atomic Power Laboratory

BFBT: BWR Full-size Fine-mesh Bundle Test

BOC: Beginning of Cycle

BWR: Boiling Water Reactor

CFD: Computational Fluid Dynamics

CHF: Critical Heat Flux

CPR: Critical Power Ratio

CR: Conversion Ratio

DNB: Departure from Nucleate Boiling

EOC: End of Cycle

EPRI: Electric Power Research Institute

FR: Fast Reactor

JAEA: Japan Atomic Energy Agency

JAERI: Japan Atomic Energy Research Institute

LWR: Light Water Reactor

M1-CISE4: Modified CISE4 version 1

M2-CISE4: Modified CISE4 version 2

M3-CISE4: Modified CISE4 version 3

MCPR: Minimum Critical Power Ratio

MDNBR: Minimum Departure from Nuclear Boiling Ratio

MEFISTO: Mechanistic Film Sub-channel Tool

MIT: Massachusetts Institute of Technology

NASCA: Nuclear reactor Advanced Sub-Channel Analysis

NRC: Nuclear Regulatory Commission (U.S.)

NSE: Nuclear Science and Engineering (department of)

NUPEC: Nuclear Power Engineering Corporation

OAF: Onset of Annular Flow

ONB: Onset of Nucleate Boiling

OTC: One-Through Cycle

PECP: Predicted over Experimental Critical Power

PWR: Pressurized Water Reactor

RBWR: Resource-renewable BWR

RMWR: Reduced-Moderation Water Reactor

SD: Standard Deviation

TB2: Transuranic Burner

TRU: Transuranic

UCB: University of California, Berkeley

U-M: University of Michigan

VIPRE: Versatile Internals and Component Program for Reactors; EPRI

1. Introduction

1.1. Background

By the end of the 20th century, a Boiling Water Reactor (BWR) design aiming to provide long-term energy supply, referred to as the Resource-Renewable BWR (RBWR), was proposed by Hitachi, Ltd. (Takeda et al., 1995). Over 90% of the world's commercial power producing nuclear reactors are water cooled and moderated. Except for its reactor core, the RBWR is fully based on the most advanced and proven BWR technology.

Similar to a Gen-IV fast reactor (FR), the RBWR is capable of consuming actinides of the current light water reactor (LWR) spent fuel as well as breeding new nuclear fuel. Sustainability can be attained with the RBWR, i.e. fissile material inventory stays the same throughout the lifetime of the fuel in the reactor. This will extend current uranium ore reserves to last by over 1,000 years, a solution to the global increase in energy demand. Moreover, by burning transuranics (TRUs) in the spent fuel, the RBWR can reduce the long-term radioactivity by orders of magnitude. Figure 1 shows natural uranium requirement and TRU inventory for the next 100 years in the U.S., assuming a 2.5% nuclear energy demand growth rate. The RBWR design is able to achieve similar performance as a FR with a conversion ratio (CR) of 1.0 in terms of uranium utilization and reduce the TRU inventory in the system to half way between FRs and current once-through cycle (OTC) LWRs. Additionally, the RBWR is an attractive option in terms of potential economic performance and ease in licensing compared to FRs for which zero commercial experience is available.

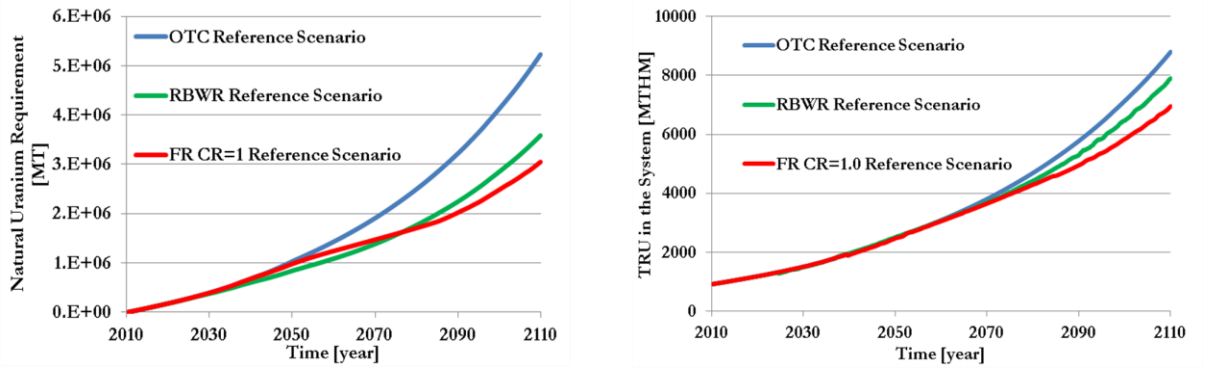

Figure 1. Natural uranium requirement (left) and TRU inventory (right) for OTC LWR, RBWR, and FR scenarios (reproduced from Passerini and Kazimi, 2012).

With the objective of providing actinide breeding and burning capabilities, the RBWR core design has different features from a conventional BWR in order to achieve a harder neutron spectrum: the fuel bundles are shorter (~1/3, to facilitate neutron leakage) with a tight hexagonal lattice (to reduce volume occupied by water) and axially heterogeneous, blanket-fissile-blanket-fissile-blanket axial zoning (to achieve negative void coefficient of reactivity). Figure 2 compares the RBWR geometry to that of a regular BWR, and Figure 3 depicts its axial fuel composition.

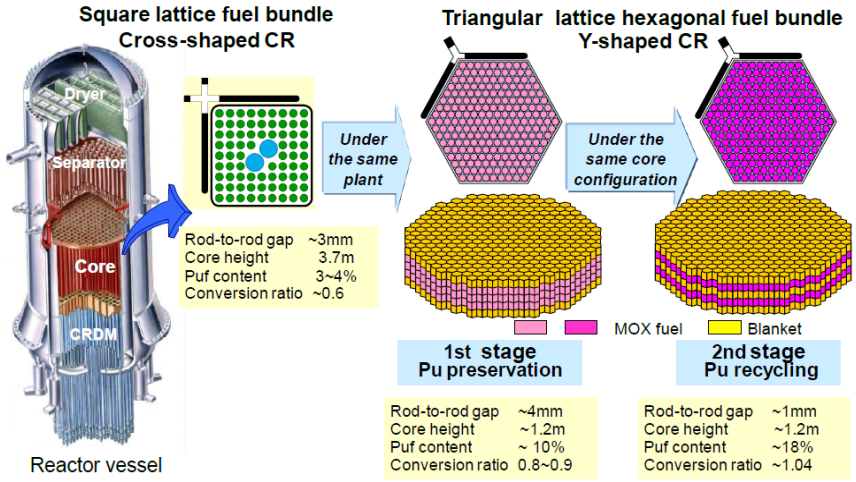

Figure 2. Geometry of a BWR square (left) and an RBWR hexagonal (right) fuel bundle (from Uchikawa et al., 2009).

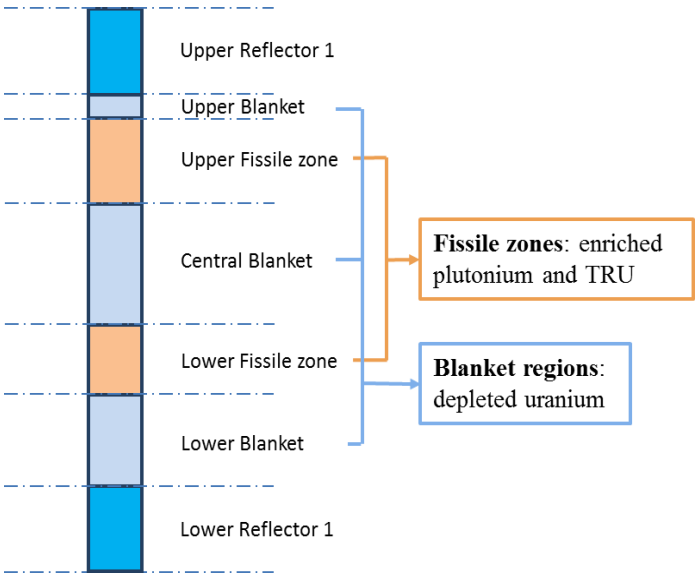

Figure 3. RBWR heterogeneous axial fuel composition (reproduced from Shirvan, 2013).

Compared to a regular BWR, the RBWR coolant flowrate is much lower (~1/3) to increase the coolant void fraction (from 30-40% to ~60%) for reduced neutron moderation. The lower coolant flowrate also gives rise to higher coolant exit quality (from ~15% to ~40%). The two RBWR designs selected for this study are: AC (Actinide Consumer) as a breeder reactor, and TB2 (Transuranic Burner) as a burner reactor[1]. Table I compares main design parameters between RBWR-AC and TB2, and Figure 4 illustrates the double-humped axial power distribution profile for both designs.

Table I. Overall design parameters of RBWR-AC and RBWR-TB2 (reproduced from Shirvan and Kazimi, 2015).

Item	RBWR-AC	RBWR-TB2
Thermal power [MWt]	3926	3926
Fuel rod diameter [cm]	1.005	0.72
Core height [m]	1.347	1.015
Number of fuel bundles	720	720
Number of rods per assembly	271	397
Coolant average flow rate [kt/h]	22	22
Core average pressure [MPa]	7.2	7.2
Inlet enthalpy [kJ/kg]	1250	1250
Assembly average mass flux [kg/m^2-s]	896	573
Hydraulic/Heated Diameter [mm]	4.1/4.4	6.1/6.6
Core radial power peaking factor	1.3	1.2

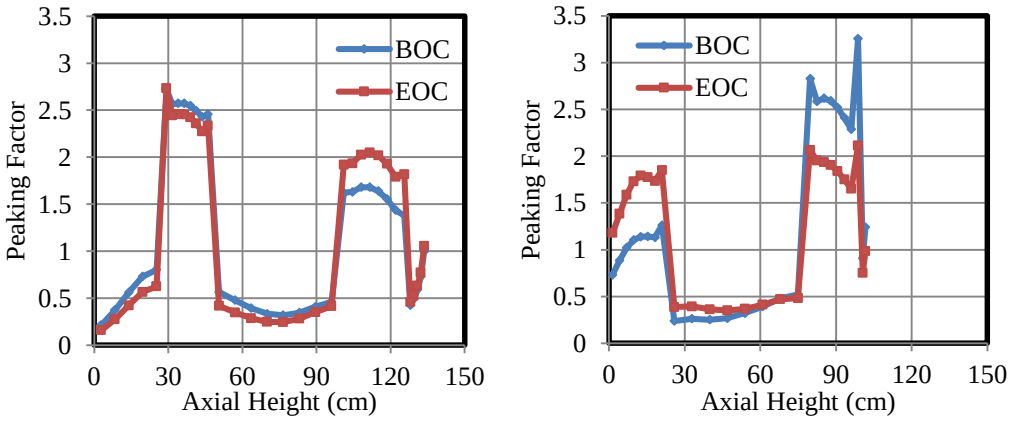

Figure 4. RBWR-AC (left) and TB2 (right) relative axial power distribution (from Downar and Kazimi, 2015).

[1] A breeder reactor is capable of generating at least the same amount of fissile material as it consumes, while the goal of a burner reactor is to destroy transuranics rather than to increase fissile fuel.

1.2. Motivation

Different core geometry, combined with higher power-to-flow ratio and larger void fraction conditions, demands re-examination of the standard BWR thermal hydraulic models for the RBWR application. One of the most important constraints on the operation of a BWR is the thermal margin to dryout occurrence, also known as the Minimum Critical Power Ratio (MCPR). Dryout, referred to as the evaporation and disappearance of liquid film in annular flow, constitutes the practical limit for the BWR type reactor power, and its accurate prediction is of crucial importance for safe operation.

As presented in Figure 5, limited dryout experimental data and few critical power correlations for tight bundles are available. The first tight bundle experiment was carried out at Bettis Atomic Power Laboratory (BAPL) in 1975. Twenty years later, when the RBWR design was conceived, Hitachi developed a modified CISE correlation (referred here as H-CISE), which was based on the CISE4 formulation (Gaspari et al., 1974), to predict the MCPR. The JAEA (Japan Atomic Energy Agency) and Toshiba Corporation tight bundle tests were then conducted to better represent RBWR geometry and operating conditions compared to BAPL experiments. Following those tests, the U.S. RBWR projects started in 2006, led by MIT, University of Michigan (U-M), and UC Berkeley (UCB). MIT was in charge of the thermal hydraulic assessment in cooperation with Hitachi and conducted by Prof. Kazimi, Dr. Hu, and later on Dr. Shirvan and Prof. Wu. Different correlations, standard or modified versions, have been used for predicting the MCPR of the RBWR that resulted in a wide range of predictions. In the near future, Hitachi plans to carry out a new dryout test dedicated to its RBWR design.

Recent work at MIT by Shirvan et al. (2013) focused on collecting dryout database representative of RBWR fuel bundle geometry and operating conditions, i.e. BAPL, JAEA and Toshiba test sets which will be detailed in section 2.3, and derived a best-estimate model for the prediction of critical quality/power, named as M1-CISE4 (modified CISE4 version 1) correlation. Like the initial Hitachi correlation (H-CISE), M1-CISE4 is grounded in the CISE4 critical quality - boiling length type formulation which depends on bundle-averaged thermal hydraulic conditions. This model

showed significant scatter when compared to experimental data in its validity range. In order to better quantify the effect of different parameters, and help validate the updated models, round tube (detailed in section 2.1) and annulus (section 2.2) dryout data that are representative of the RBWR hydraulic diameter and operating conditions are integrated in the database.

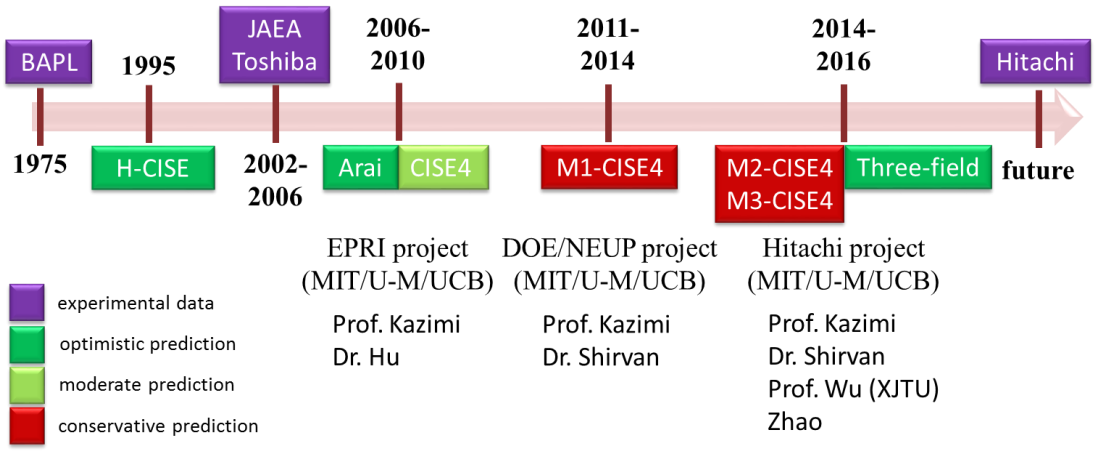

Figure 5. Dryout research timeline for tight bundles and more specifically RBWR.

The original CISE4 formulation only depends on bundle-averaged pressure, mass flux, boiling length, and the ratio of heated to wetted perimeters. This one-dimensional analysis approach neglects the intra-assembly channel mixing for a rod bundle, which would result in an under-prediction of the critical power. But on the other hand, the fact that it also neglects the local rod peaking within the bundle could compensate for the critical power underestimation. Sub-channel analysis is capable of providing radial flow and quality distribution within a bundle, and thus capturing the effect of inter-channel mixing as well as non-uniform radial heating. Moreover, the configuration of spacer grids also has an impact on the dryout, and can be embodied in sub-channel analysis codes. Therefore, in order to reduce the spread in prediction of critical power data, sub-channel analysis will be employed in this work.

Additionally, the non-uniform axial power distribution (APD) may, if not dominantly, influence the critical power, and its effect is difficult to be captured in simple 1-D correlations like CISE4 due to the strong interference between various parameters. Besides the sub-channel analysis in which APD will be specified and accounted for in each case, it has been shown that the influence

of APD on dryout can be captured via the three-field model (Anglart, 2010). The latter relies on a mechanistic approach to resolve relevant field (liquid film, entrained droplets, and vapor) mass balance equations within the annular flow regime, and is considered as one of the most promising mathematical tools to achieve the purpose of accurate critical power prediction (Okawa et al., 2003).

1.3. Thesis Objective and Outline

The objective of the thesis is to derive best-estimate critical power prediction models that can correctly capture the unique features of axially heterogeneous tight bundle designs, more specifically those of an RBWR.

The thesis will start with the assessment of the previously derived M1-CISE4 correlation against experimental data for tubes, annuli, and tight bundles (Chapter 2). An updated correlation, M2-CISE4 (modified CISE4 version 2), will be developed and evaluated in Chapter 3. Effects of different parameters on the critical power (predicted and experimental) will be surveyed and discussed. Chapter 4 will focus on sub-channel analysis of tight bundles with the code VIPRE-01 which provides radial quality distribution information to be incorporated in Chapter 5: M3-CISE4 (modified CISE4 version 3) correlation development and assessment. Chapter 6 will present the three-field model with its governing equations and constitutive relations, as well as its prediction of dryout against experiments. The MCPR evaluation of RBWR-AC and TB2 will be investigated in Chapter 7 with all the models mentioned earlier. Chapter 8 summarizes the observations and conclusions drawn from the work performed for the thesis, and discusses recommended future research.

2. M1-CISE4 Correlation Assessment

The first step of the thesis consists of evaluating the ability of previously derived M1-CISE4 correlation by Shirvan et al. (2013) to accurately predict the dryout critical power for all the three types of heated geometries: tubes, annuli, and tight bundles. As shown in Equation (1), a one-dimensional critical quality - boiling length type correlation was opted as it was deemed easier and simpler than other models which would require sub-channel analysis for tight bundle cases. The critical quality only depends on bundle-averaged hydraulic & heated diameter, exit pressure, mass flux, and boiling length. For this work, all data processing and critical power modeling were performed in Matlab. The M1-CISE4 is given by:

$$x_{cr} = \frac{D_e}{D_h} \times \frac{a \times L_b}{b + L_b} \tag{1}$$

where

$$a = [1 + 1.481 \times 10^{-4} \left(1 - \frac{P}{P_c}\right)^{-3} 0.7G]^{-1} \quad \text{if } G \leq G^*,$$

and

$$a = \left(1 - \frac{P}{P_c}\right) / (\frac{0.7G}{1000})^{1/3} \quad \text{if } G > G^*,$$

with

$$G^* = 3375 \left(1 - \frac{P}{P_c}\right)^3;$$

$$b = 0.199(\frac{P_c}{P} - 1)^{0.4} G {D_e}^{1.2}.$$

x_{cr} = critical quality; D_e = hydraulic diameter (m); D_h = heated diameter (m); L_b = boiling length (m); P = exit pressure (MPa); P_c = critical pressure (MPa); G = mass flux (kg/m^2-s). Terms a and b were adjusted in M1-CISE4 so as to fit tight bundle data.

2.1. Tube Data

The Thompson and Macbeth (1964) vertical, uniformly heated round tube dryout database is used to compare with the predicted critical power using M1-CISE4.Tests were performed at a variety of tube diameters and operating conditions. In order to be compatible with the RBWR design

specifications, a total of 390 burnout data points are selected, and ranges of parameters are summarized in Table II.

Table II. Dryout experiment test parameters for tubes.

Test	APD	Number of data	Pressure [MPa]	Mass flux [kg/m^2-s]	Diameter [mm]	Heated length [m]
Thompson & Macbeth (1964)	Uniform	390	1 - 7.1	241 - 1,980	3.9 - 7.8	0.86 - 3.12

The results of tube critical power prediction by M1-CISE4 are presented in Figure 6. The average predicted over experimental critical power (PECP) is equal to 0.87 with a standard deviation (SD) of 0.10. In other words, M1-CISE4 under-estimates the tube data by 13%.

One can see from Figure 6 that M1-CISE4 markedly under-predicts the critical power at pressures higher than 4 MPa, at mass fluxes over 1,500 kg/m^2-s, and for tube diameter of 5.6 mm. The trend of increasing PECP with increasing heated length is observed.

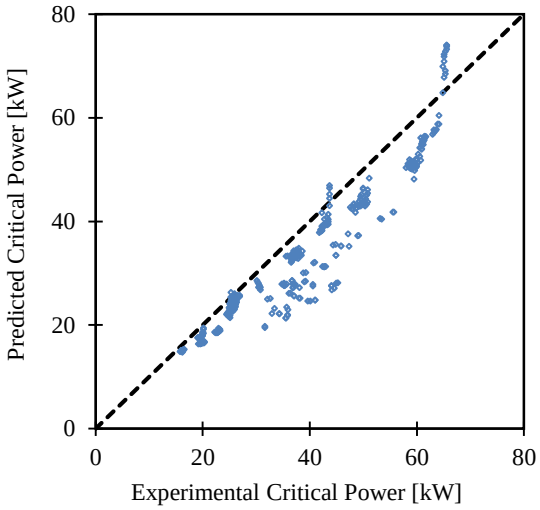

(a)

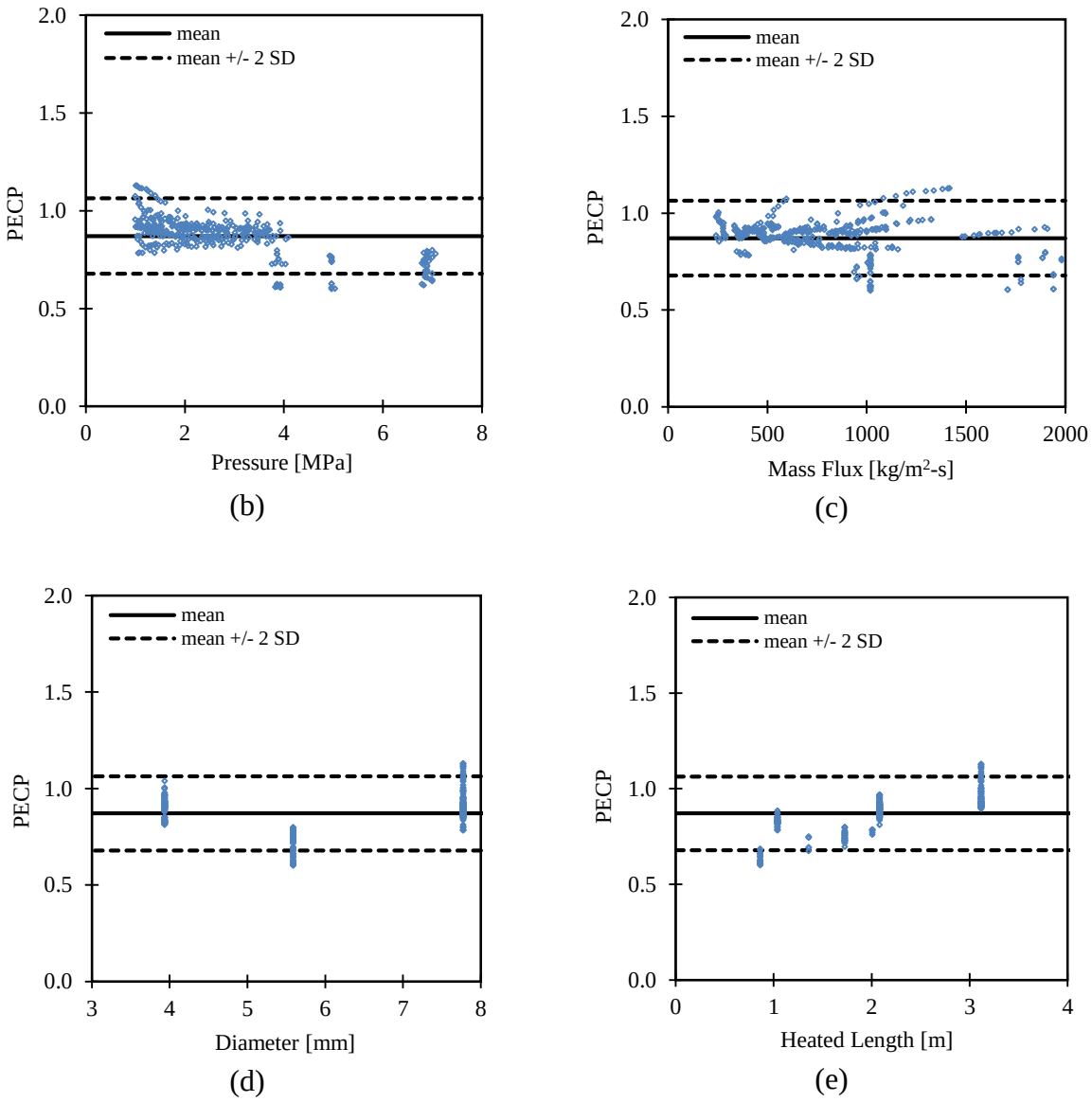

Figure 6. M1-CISE4: tube critical power results.
(a) predicted vs. experimental critical power; (b) PECP vs. pressure; (c) PECP vs. mass flux; (d) PECP vs. tube diameter; (e) PECP vs. heated length.

2.2. Annulus Data

Four references have been used for the evaluation of internally heated annuli critical power prediction, as presented in Table III with selected parameter ranges.

In the first reference (Beus and Seebold, 1981), the annulus is 2.13 m long and tests are performed by employing three different APDs: the first test section with a uniform power distribution; the second with 1.52 m uniform and 0.61 m alternate high and low heat flux segments (with local-to-average heat flux ratios of 1.27 and 0.16 respectively); and the third with a 5.46 cm hot patch (with a peak-to-average heat flux ratio of 2.19) near the outlet, as shown in Figure 7. Experimental data indicate that the thermal performance of the annulus was unaffected by the alternate high and low heat flux profile or the presence of hot patch compared to the uniform power distribution.

Table III. Dryout experiment test parameters for annuli.

Test	APD	Number of data	Pressure [MPa]	Mass flux [kg/m^2-s]	Hydraulic diameter [mm]	Heated diameter [mm]	Heated length [m]	Axial peaking factor
Beus and Seebold (1981)	Uniform	22	5.5 - 11	336 - 1,363	5.6	15.2	2.13	1.0
	Alternate	11						1.27
	Alternate with hot patch	9						2.19
Beus and Humphreys (1979)	Alternate	18	5.5 - 11	290 - 1,248	5.5	14.8	2.13	1.76
	Alternate with hot patch	14						2.7
Mortimore and Beus (1979)	Uniform	15	8.3 - 11	332 - 1,396	5	13.3	2.13	1.0
	Hot patch of 1.5 heat flux ratio	12						1.5
	Hot patch of 2.25 heat flux ratio	14						2.25
Janssen and Kervinen (1963)	Uniform	282	4.1 - 10.2	354 - 1,980	8.5	22.3; 24.6	1.8 - 2.7	1.0

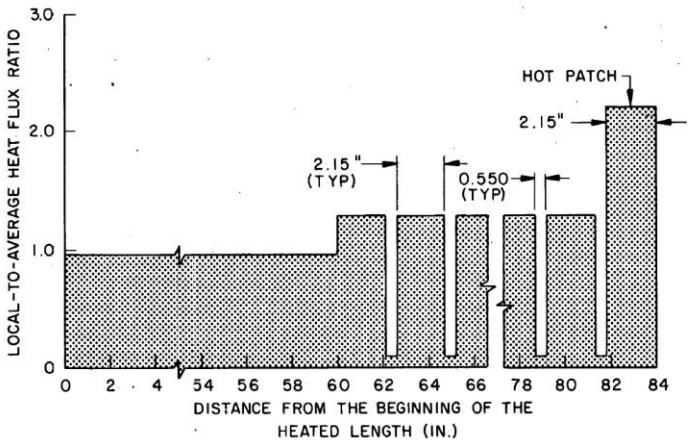

Figure 7. First annulus data reference: axial heat flux profile for the third test section (from Beus and Seebold, 1981).

The experimental configurations in the second reference (Beus and Humphreys, 1979) are very similar to those in the first reference. Tests are performed by employing two different APDs: the first test section with 1.83 m uniform and 0.3 m square wave alternating heat flux segments (with a maximum-to-average heat flux ratio of 1.76); and the second with a 1.12 cm hot patch (with a peak-to-average heat flux ratio of 2.7) near the outlet, as shown in Figure 8. Like the first reference, no significant critical heat flux (CHF) penalty due to the non-uniform heat flux profile was observed in the experiments.

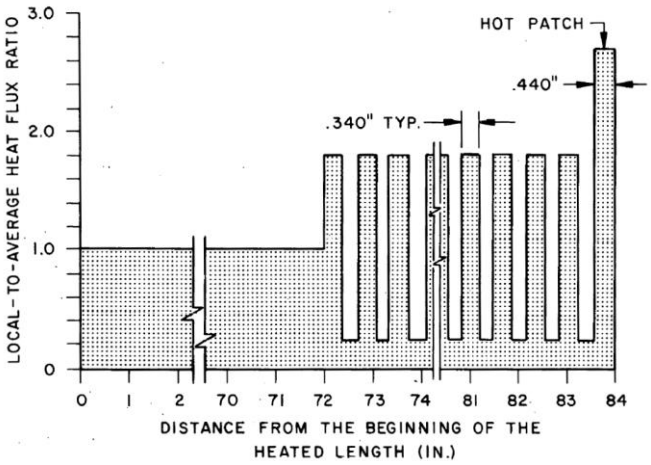

Figure 8. Second annulus data reference: axial heat flux profile for the second test section (from Beus and Humphreys, 1979).

Experiments performed in the third reference (Mortimore and Beus, 1979) are under similar conditions as in the two previous sources. Three different test sections are employed with: (1) axially uniform heat flux over the entire length of 2.13 m; (2) axially uniform heat flux over 2.08 m with hot patch over the last 5.08 cm with a 1.5 heat flux ratio; and (3) axially uniform heat flux over 2.08 m with a hot patch over the last 5.08 cm with a 2.25 heat flux ratio. Experimental results suggest that the hot-patches did not affect CHF over the range of variables tested.

In the last reference (Janssen and Kervinen, 1963), the rod is uniformly heated in annular geometry with ranges of parameters quite different from those in the other references. The major disparity occurs by a significantly larger hydraulic diameter (8.5 mm) which is well beyond that of the RBWR designs (4-6 mm). The pressure and mass flux ranges are also wider, and the heated length can reach up to 2.7 m compared to 1-1.3 m in an RBWR.

The comparison between experimental and predicted critical power (with M1-CISE4) is illustrated in Figure 9. The average PECP is 0.83 with a SD of 0.09. The last reference has the most data but yields significant under-estimation of critical power (mean PECP of 0.81 for the last data source only). It can be noticed that the effect of pressure is well captured by M1-CISE4, though no low pressure (less than 4 MPa) data is available. The effect of hydraulic-over-heated-diameter (D_e/D_h) is also well captured. The PECP slightly increases with increasing mass flux, whilst it decreases when the hydraulic diameter is larger. The PECP trend as a function of heated length for annulus data differs from that for tubes, as shown in Figure 6(e) and Figure 9(f).

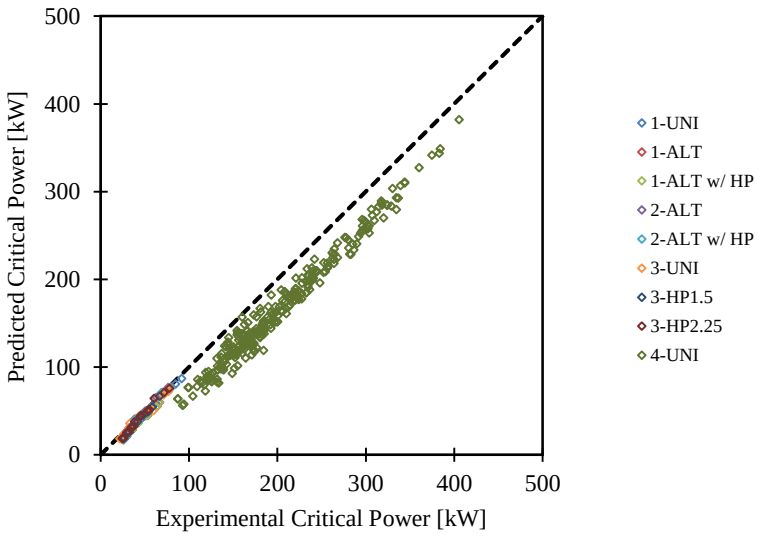

(a)[1]

[1] *Legend*: "1-UNI" = first reference - uniform; "1-ALT" = first reference - alternate; "1-ALT w/ HP" = first reference - alternate with hot patch; "2-ALT" = second reference - alternate; "2-ALT w/ HP" = second reference - alternate with hot patch; "3-UNI" = third reference - uniform; "3-HP1.5" = third reference - hot patch of 1.5 heat flux ratio; "3-HP2.25" = third reference - hot patch of 2.25 heat flux ratio; "4-UNI" = fourth reference - uniform.

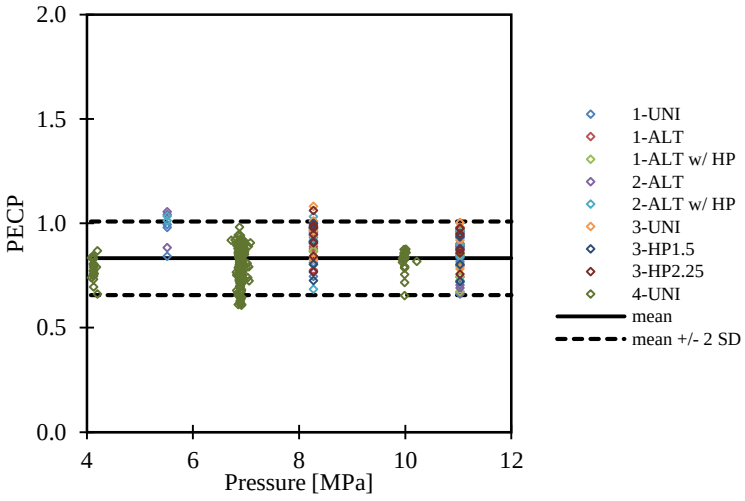
2.0
1.5
1.0
0.5
0.0
PECP
4
6
8
10
12
Pressure [MPa]
1-UNI
1-ALT
1-ALT w/ HP
2-ALT
2-ALT w/ HP
3-UNI
3-HP1.5
3-HP2.25
4-UNI
mean
mean +/- 2 SD

(b)

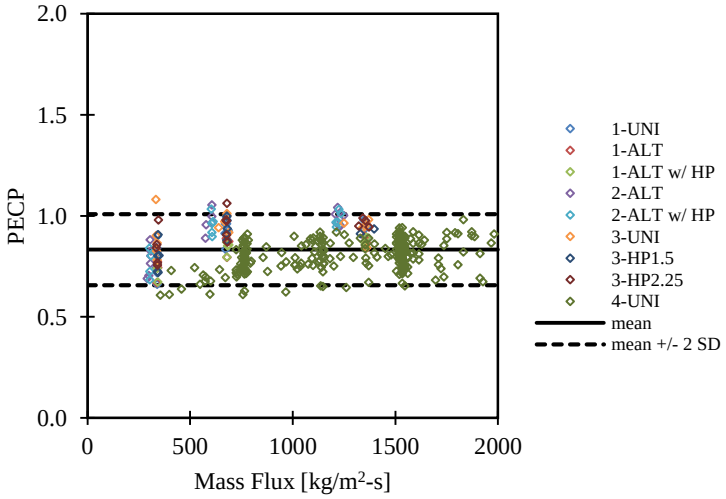
2.0
1.5
1.0
0.5
0.0
PECP
0
500
1000
1500
2000
Mass Flux [kg/m²-s]
1-UNI
1-ALT
1-ALT w/ HP
2-ALT
2-ALT w/ HP
3-UNI
3-HP1.5
3-HP2.25
4-UNI
mean
mean +/- 2 SD

(c)

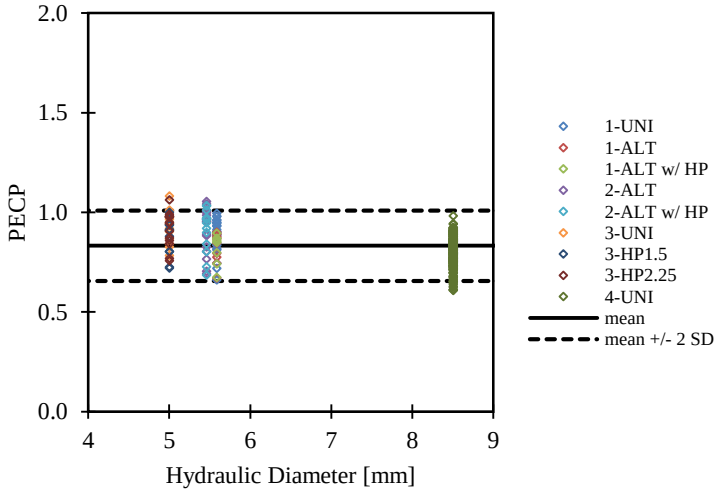
2.0
1.5
1.0
0.5
0.0
PECP
4
5
6
7
8
9
Hydraulic Diameter [mm]
1-UNI
1-ALT
1-ALT w/ HP
2-ALT
2-ALT w/ HP
3-UNI
3-HP1.5
3-HP2.25
4-UNI
mean
mean +/- 2 SD

(d)

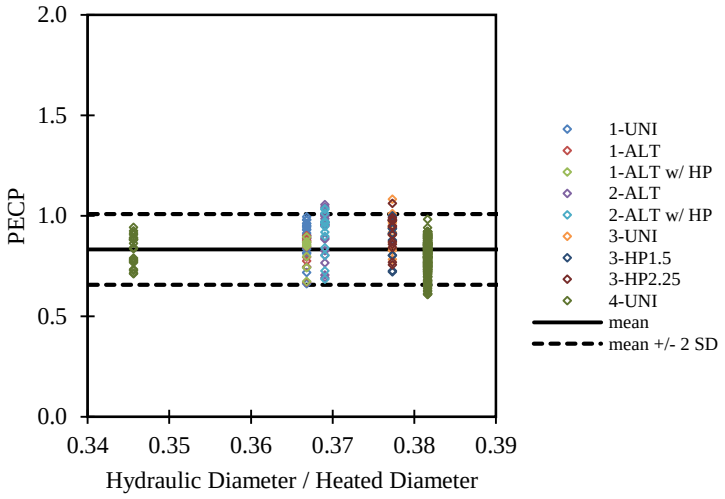

(e)

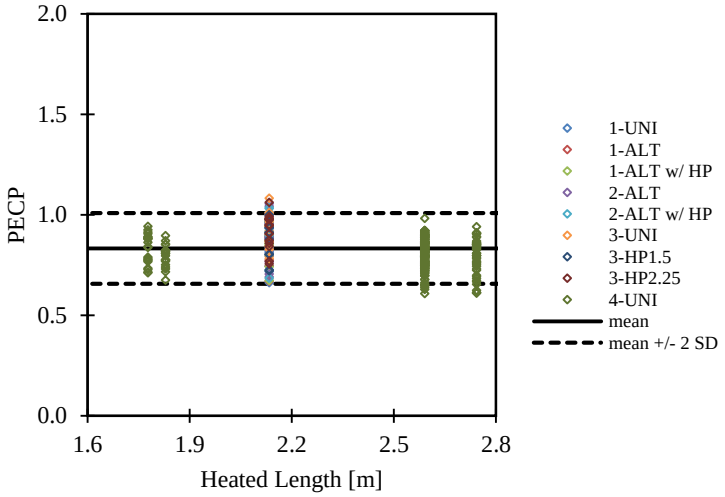

(f)

Figure 9. M1-CISE4: annulus critical power results.
(a) predicted vs. experimental critical power; (b) PECP vs. pressure; (c) PECP vs. mass flux; (d) PECP vs. hydraulic diameter; (e) PECP vs. hydraulic/heated diameter; (f) PECP vs. heated length.

2.3. Tight Bundle Data

The tight lattice rod bundle critical power experimental tests used as calibration database for the M1-CISE4 correlation and corresponding parameter ranges are listed in Table IV. Unlike in Shirvan et al. (2013), the limited data publically available from BAPL are not included due to its

unconventional geometric configuration (parallelogram shape channel box). As listed in Table IV, the selected experiments were carried out in JAEA and Toshiba Corporation. They differ in bundle geometry, including the number and arrangement of heater rods, shape, tightness, and heated length of the bundle, as well as working conditions such as axial and local power distribution, pressure, and mass velocity.

Table IV. Dryout experiment test parameters for tight lattice bundles.

Test	Number of rods	APD	Number of data	Pressure [MPa]	Mass flux [kg/m^2-s]	Hydraulic diameter [mm]	Heated diameter [mm]	Heated length [m]
JAEA-A (Kureta and Akimoto, 2003)	7	Uniform	129	1 - 8.5	298 - 2,489	2.35	3.56	1.8
JAEA-B (Liu et al., 2004)	7	Double-humped	116	2 - 8.4	300 - 1,381	2.86	4.34	1.26
JAEA-C (Liu et al., 2007)	37	Double-humped	117	2 - 9	206 - 1,005	4.42	5.32	1.26
JAEA-D (Liu et al., 2007)	37	Double-humped	147	2 - 9	300 - 1,500	3.71	4.45	1.26
Toshiba-1 (Yamamoto et al., 2006)	7	Stepped cosine	6	7	472 - 1,744	4.85	7.29	1.6
Toshiba-2 (Yamamoto et al., 2006)	7	Stepped cosine	13	7	489 - 1,961	5.91	9.03	0.8; 1.6
Toshiba-3 (Yamamoto et al., 2006)	7	Stepped cosine	6	7	600 - 1,711	7.03	10.95	1.6
Toshiba-4 (Yamamoto et al., 2006)	14	Stepped cosine	31	1 - 8	385 - 1,764	5.74	9.55	1.6

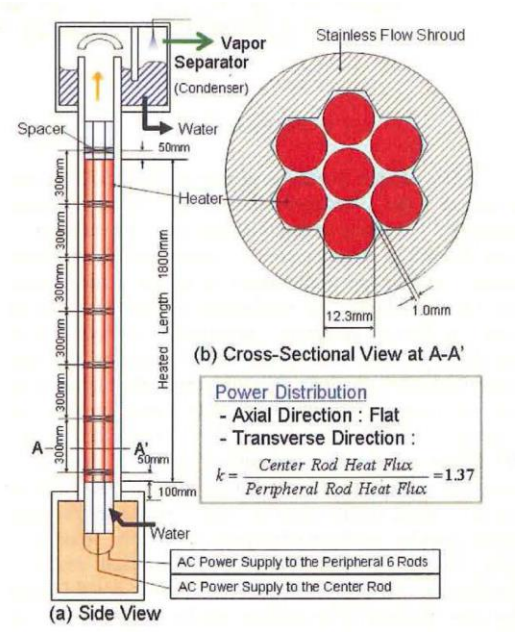

Figure 10. JAEA-A: schematic view (from Kureta et al., 2002).

The JAEA-A test section (Kureta and Akimoto, 2003) simulates the fuel assembly of a reduced-moderation water reactor (RMWR) designed by the Japan Atomic Energy Research Institute (JAERI[1]), a water-cooled breeder reactor with a core of tight triangular fuel rod arrangement. As shown in Figure 10, the bundle contains 7 heater rods (one center rod and six peripheral rods) of 12.3 mm in diameter with rod-rod gap of 1 mm and rod-shroud gap of 0.5 mm. The test section is uniformly heated along the 1.8 m bundle length. The center rod operates with a nominal radial local peaking factor (R_f) of 1.3.

The JAEA-B test section (Liu et al., 2004) also simulates the RMWR tight lattice bundle behavior but employs an axial 12-step double-humped power distribution, as outlined in Figure 11 and Figure 12. Its geometry is very similar to that of JAEA-A, but with a larger rod diameter (13 mm) and gaps (1.3 mm of rod-rod gap and 0.65 mm of rod-shroud gap). The heated length is significantly reduced to 1.26 m. A nominal R_f value of 1.4 was chosen in this experiment.

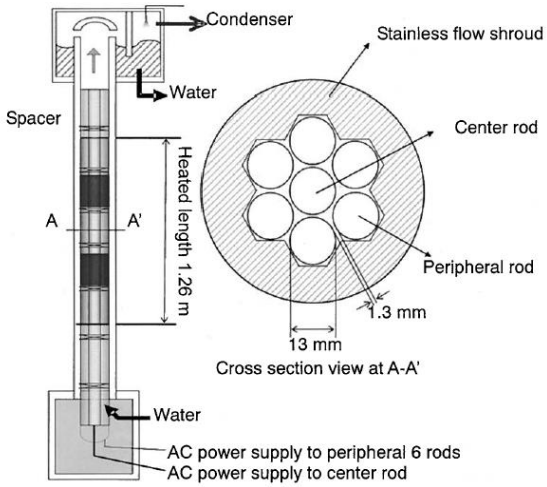

Figure 11. JAEA-B: schematic view (from Liu et al., 2004).

[1] It merged with Japan Nuclear Cycle Development Institute and became JAEA in 2005.

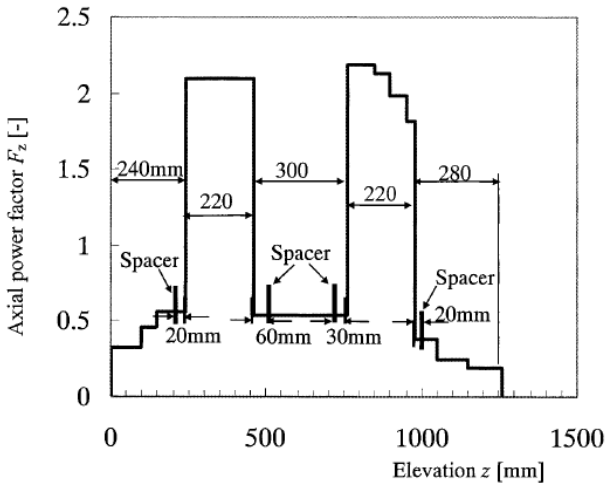

Figure 12. JAEA-B: axial power distribution profile (from Liu et al., 2004).

The JAEA-C and JAEA-D experiments (Liu et al., 2007) use a 37-rod bundle with 13 mm rod diameter and were performed with a double-humped APD. The cross-sectional configuration is shown in Figure 13, and the axial power shape is illustrated in Figure 14. JAEA-C bundle has a 1.3 mm rod-rod gap and 1.05 mm rod-shroud gap, whilst JAEA-D bundle is tighter with a 1 mm rod-rod gap and 0.75 mm rod-shroud gap. The heated length is equal to 1.26 m in both cases. The 37-rod experiments mainly focused on uniformly heated transverse conditions (R_f = 1.0).

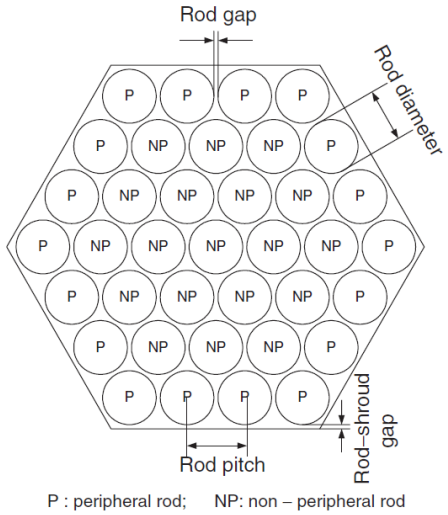

Figure 13. JAEA-C & D: 37-rod bundle configuration (from Liu et al., 2007).

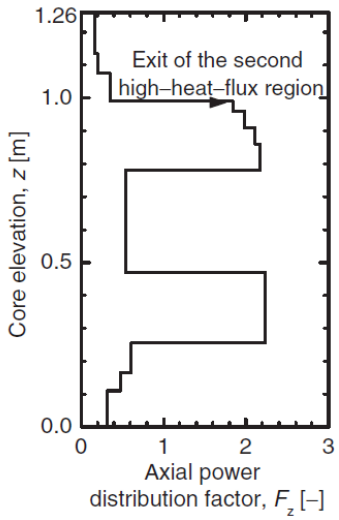

Figure 14. JAEA-C & D: axial power distribution profile (from Liu et al., 2007).

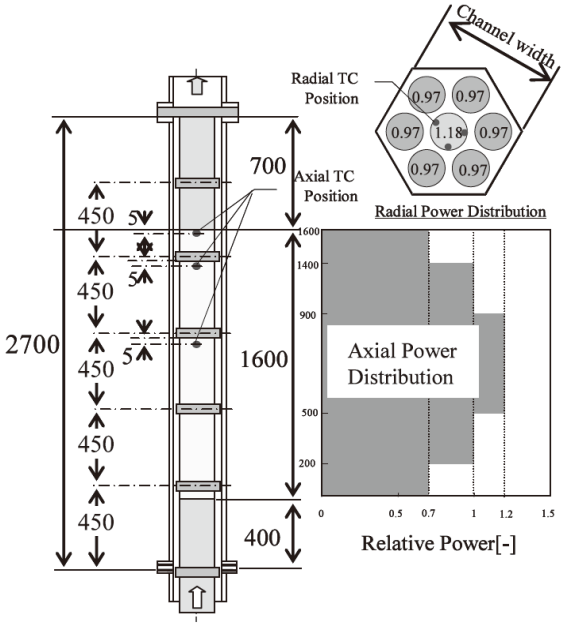

Figure 15. Toshiba 7-rod bundle: schematic view and axial power distribution profile (from Yamamoto et al., 2006).

The Toshiba test sets (Yamamoto et al., 2006) were performed with two types of tight bundles: one is a 7-rod bundle with a hexagonal channel box (Figure 15), and the other is a 14-rod bundle with a rectangular channel box. The first three test sections use the same 7-rod bundle but differ in bundle tightness: 0.8 mm rod-rod gap and 2.2 mm rod-shroud gap for Toshiba-1, 1.3 mm rod-rod gap and 2.57 mm rod-shroud gap for Toshiba-2, 1.8 mm rod-rod gap and 2.99 mm rod-shroud gap for Toshiba-3. Toshiba-4 uses the 14-rod bundle with a 1.3 mm rod gap and 2.7/3.78 mm rod-

shroud gap[1]. All the four experiments have the same rod diameter of 10.8 mm and heated length of 1.6 m (except for Toshiba-2 in which some data were obtained with a reduced length of 0.8 m), and employed a stepped-cosine shape APD[2], as shown in Figure 15. The nominal radial peaking factor equals to 1.18 for the three 7-rod bundle tests, and 1.15 for the 14-rod bundle test (Figure 16).

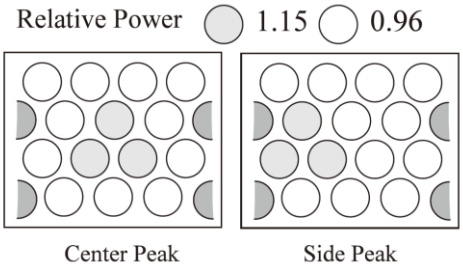

Figure 16. Toshiba 14-rod bundle: radial power distribution (from Yamamoto et al., 2006).

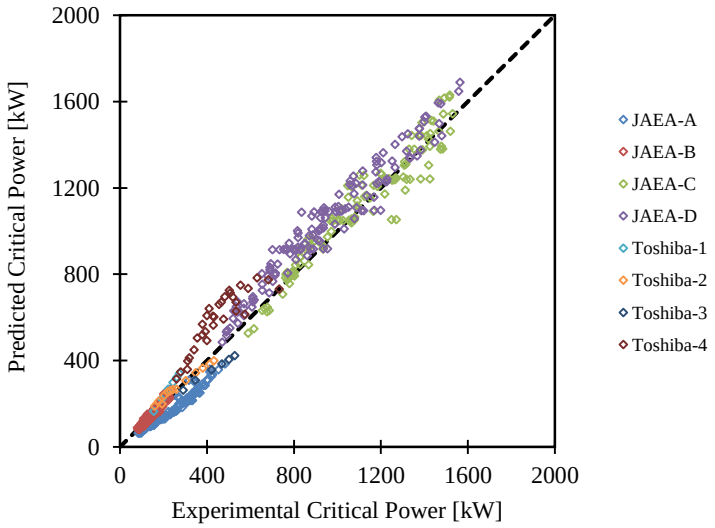

(a)

[1] Erratum in Yamamoto et al. (2006): Toshiba-4 (14-rod) channel width should be 52.2 mm × 49.8 mm.

[2] In the case of the short heated length of 0.8 m in Toshiba-2, the upper half of the heated region does not exist in Figure 15, i.e. the APD shape becomes outlet-peak instead of stepped-cosine.

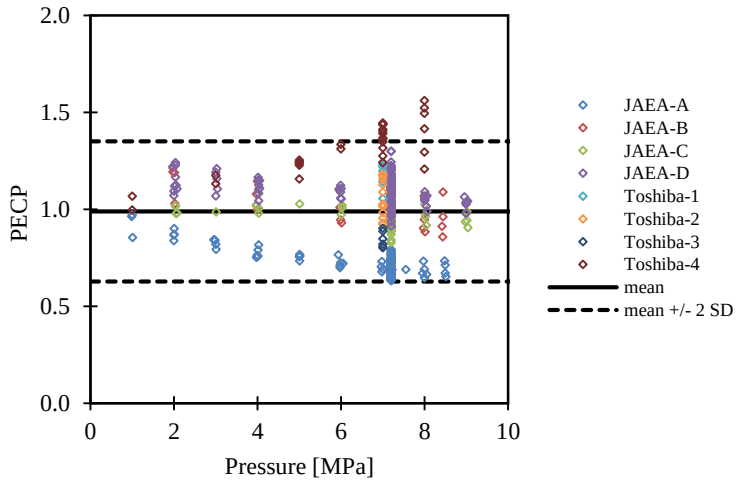
2.0
1.5
1.0
0.5
0.0
PECP
0
2
4
6
8
10
Pressure [MPa]
JAEA-A
JAEA-B
JAEA-C
JAEA-D
Toshiba-1
Toshiba-2
Toshiba-3
Toshiba-4
mean
mean +/- 2 SD

(b)

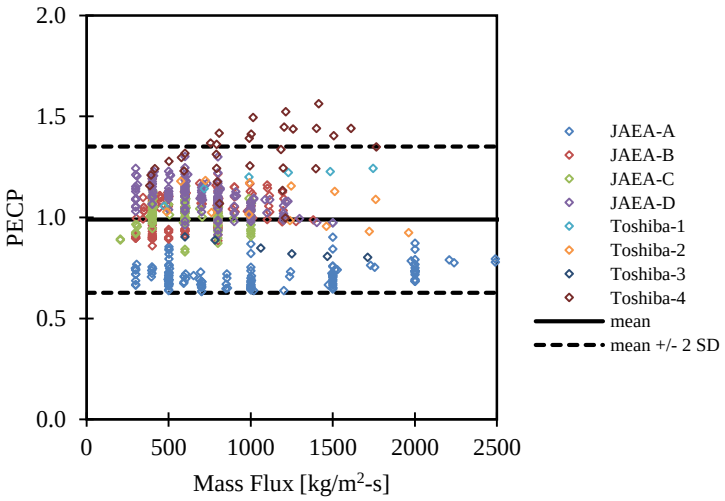
2.0
1.5
1.0
0.5
0.0
PECP
0
500
1000
1500
2000
2500
Mass Flux [kg/m2-s]
JAEA-A
JAEA-B
JAEA-C
JAEA-D
Toshiba-1
Toshiba-2
Toshiba-3
Toshiba-4
mean
mean +/- 2 SD

(c)

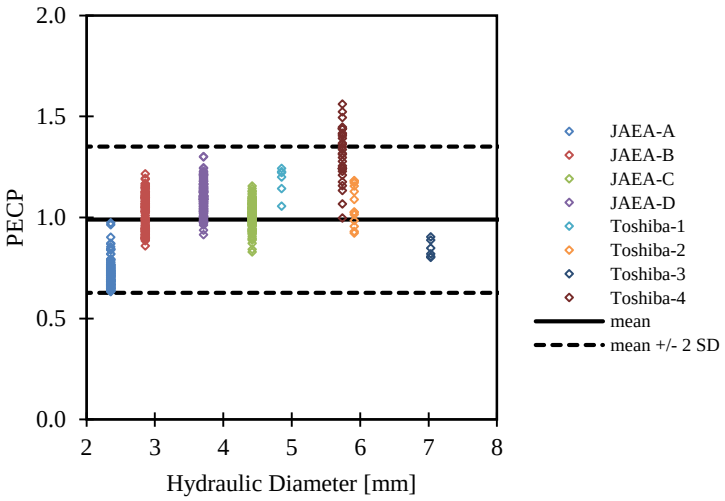
2.0
1.5
1.0
0.5
0.0
PECP
2
3
4
5
6
7
8
Hydraulic Diameter [mm]
JAEA-A
JAEA-B
JAEA-C
JAEA-D
Toshiba-1
Toshiba-2
Toshiba-3
Toshiba-4
mean
mean +/- 2 SD

(d)

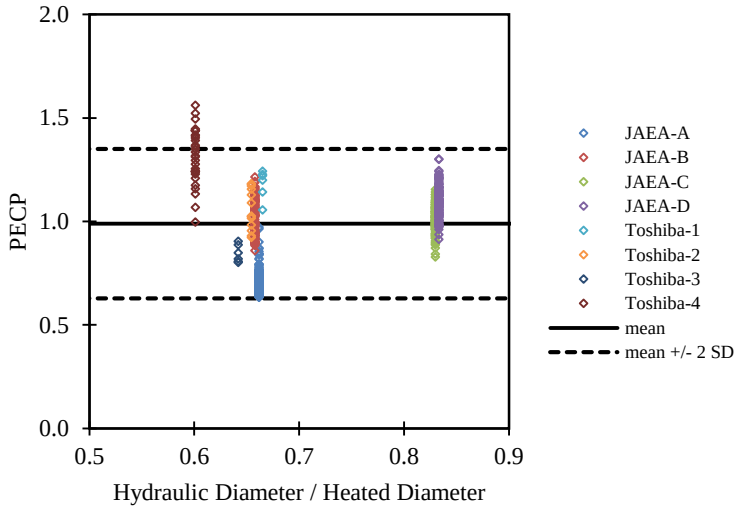

(e)

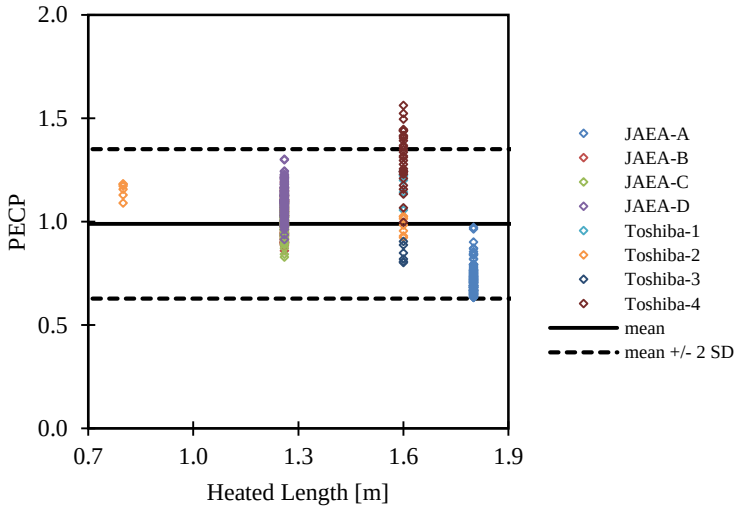

(f)

Figure 17. M1-CISE4: tight bundle critical power results.
(a) predicted vs. experimental critical power; (b) PECP vs. pressure; (c) PECP vs. mass flux; (d) PECP vs. hydraulic diameter; (e) PECP vs. hydraulic/heated diameter; (f) PECP vs. heated length.

As for position where dryout occurred, for uniform and stepped-cosine APD cases (JAEA-A, Toshiba 1 through 4), it first occurred at bundle exit; for double-humped shape APD (JAEA-B through D), it occurred earlier at the outlet[1] if the mass velocity was low (in general below 600

[1] also called complete dryout

kg/m^2-s but varies with different tests), or near the end of the second hump[1] if the mass velocity was high.

The results of tight lattice bundle critical power prediction by M1-CISE4 are reported in Shirvan et al. (2013) and independently replicated for further investigation and improvement. The average PECP equals to 0.99 with a SD of 0.18. Figure 17 depicts the parameter effects on the overall performance of M1-CISE4 (reflected by values of PECP), and more detailed discussion about the dependence of critical power on different parameters (pressure, mass flux, bundle tightness, heated length, APD, R_f, etc.) is included in the next chapter.

2.4. Conclusion

About 800 round tube and annulus data that are representative of the RBWR flow characteristics have been integrated in the database of over 550 tight bundle data to validate the formerly derived M1-CISE4 correlation. As presented in the previous sections, M1-CISE4 under-predicts tube and annulus dryout data by respectively 13% and 17% in average within the selected parameter ranges. An updated critical power correlation is necessary to improve the prediction with regard to tube and annulus geometry.

In terms of parameter effects, it is tough to draw conclusions based on the overall PECP results (Figure 6, Figure 9, and Figure 17). Sensitivity analysis will be performed and detailed in the next chapter along with the updated correlation, namely M2-CISE4.

[1] also called spot dryout

3. M2-CISE4 Correlation Development and Assessment

3.1. Methodology

As discussed in chapter 2, the M1-CISE4 correlation significantly under-estimates tube and annulus critical power (by 13% and 17% respectively), and does not account for the rod radial heating factor (even though this was somewhat covered in the original CISE4 formulation by the presence of hydraulic-to-heated diameter ratio term and counter-balanced by the non-consideration of intra-assembly flow mixing in the one-dimensional modeling). The scatter in PECP results between different test sets and even within certain experiments also needs to be addressed.

The updated critical power correlation, referred to as M2-CISE4, will focus on predicting tube and annulus data as accurately as possible and aim to achieve an average PECP of 1.0 for tight bundles. The impact of different parameters should be correctly captured.

The methodology for the development of M2-CISE4 is as follows:

- ✓ Calibrate the correlation by modifying coefficients and exponents in *a* and *b* terms to fit tube data as closely as possible;
- ✓ Calibrate the correlation by modifying coefficients and exponents in *a*, *b* and (D_e/D_h) terms to fit annulus data as closely as possible;
- ✓ Introduce the R_f factor, and calibrate the correlation by modifying coefficients and exponents in *a*, *b* and (D_e/D_h) terms to fit tight bundle data (average PECP = 1.0).

Like the original CISE4 and M1-CISE4, the updated M2-CISE4 correlation does not account for the non-uniform axial power distribution, since annuli experiments with non-uniform heating up to 2.7 times the average heat flux did not show any significant impact on critical power. Also as dryout is a global phenomenon, its dependence on local heat flux is not supposed to be over-arching. However, literature review suggests that the shape of non-uniform APD upstream the location of dryout could affect the critical power, as presented later in section 3.3.4.

The effect of radial peaking factor (R_f) on experimental critical power has been surveyed, and different test sections yield quite different results: in JAEA-A, critical power drops by 7% when

R_f increases from 1.0 to 1.3; in JAEA-C & D, critical power decreases by about 20% when R_f changes from 1.04 to 1.19; whereas in JAEA-B and Toshiba-4, R_f has no impact on critical power. Exact heater rod configuration cannot be modeled in 1-D analysis, and local flow distribution remains unknown. Hence, a constant R_f is preferred to a geometry dependent radial peaking factor in M2-CISE4. The value of R_f is set to be 1.1 as suggested by the hot assembly local peaking in an RBWR (Downar and Kazimi, 2015).

3.2. M2-CISE4 Correlation

The updated M2-CISE4 correlation is presented in Equation (2).

$$x_{cr} = \left(\frac{D_e}{D_h}\right)^{0.8} \times \frac{a \times L_b}{b + L_b} \times R_f^{-1} \tag{2}$$

where

$$a = \left[1 + 1.481 \times 10^{-4} \left(1 - \frac{P}{P_c}\right)^{-3} G\right]^{-1} \quad \text{if } G \leq G^*,$$

and

$$a = \left(1 - \frac{P}{P_c}\right) / \left(\frac{G}{1000}\right)^{1/3} \quad \text{if } G > G^*,$$

with

$$G^* = 3375 \left(1 - \frac{P}{P_c}\right)^3;$$

$$b = 0.279 \left(\frac{P_c}{P} - 1\right)^{0.4} G {D_e}^{1.4}.$$

x_{cr} = critical quality; D_e = hydraulic diameter (m); D_h = heated diameter (m); L_b = boiling length (m); P = exit pressure (MPa); P_c = critical pressure (MPa); G = mass flux (kg/m^2-s); R_f = 1.1 (constant radial peaking factor for tight bundles).

Its range of validity is listed in Table V.

Table V. Parameter ranges for the M2-CISE4 correlation.

Parameter	Tube		Annulus		Tight Bundle	
	Low	High	Low	High	Low	High
Pressure [MPa]	1.0	7.1	4.1	11.0	1.0	9.0
Mass Flux [kg/m^2-s]	241	1,980	290	1,980	206	2,489
Hydraulic Diameter [mm]	3.9	7.8	5.0	8.5	2.4	7.0
Heated Diameter [mm]	3.9	7.8	13.3	24.6	3.6	11.0
Hydraulic-to-heated Diameter Ratio	1.00	1.00	0.35	0.38	0.60	0.83
Heated Length [m]	0.86	3.12	1.80	2.70	0.80	1.80
Number of Heater Rods					7; 14; 37	
APD	uniform		uniform; alternate; outlet peak		uniform; double-humped; stepped-cosine	

3.3. Results and Discussion

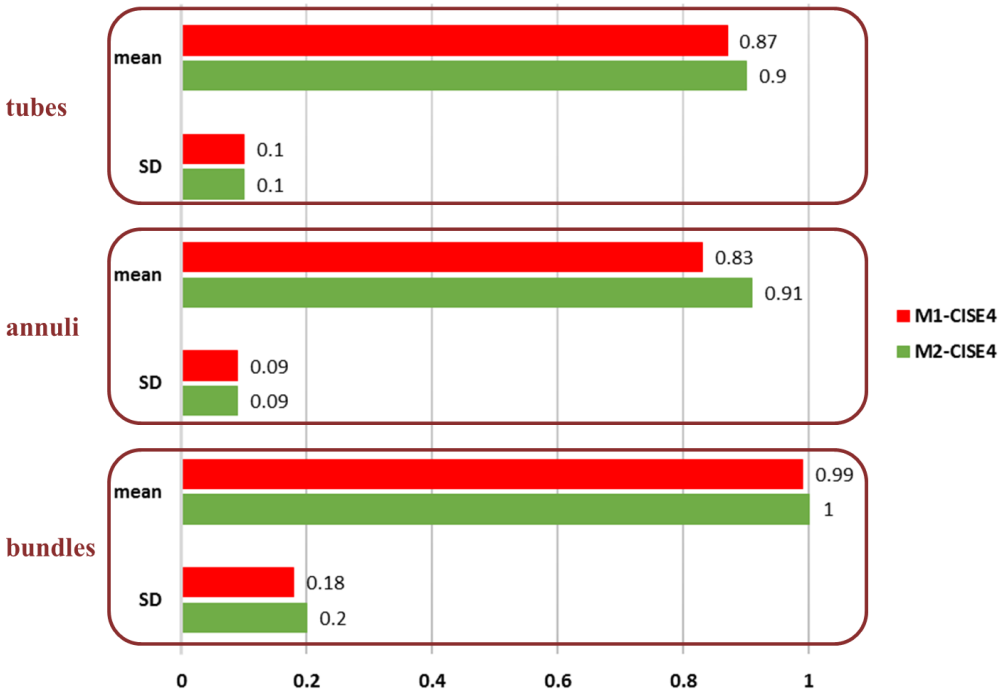

Figure 18. Predicted/experimental critical power (PECP) mean and SD values for tubes, annuli, and tight bundles with M1-CISE4 and M2-CISE4 correlations.

As can be seen in Figure 18, in average M2-CISE4 outperforms its previous version (M1-CISE4) for the tube and annulus database by 3% and 8% respectively, but remains conservative for both

geometries. On the other hand, M2-CISE4 is still unable to reduce the scatter in tight bundle results due to significant discrepancies between different tests and even within some tests, as recapitulated in Table VI, leading us to go for a parameter effect survey.

Table VI. PECP mean and SD values for all test sections with M1-CISE4 and M2-CISE4 correlations.

Correlation		M1-CISE4				M2-CISE4			
Parameter range		all		nominal[1]		all		nominal	
Test section		mean	SD	mean	SD	mean	SD	mean	SD
Tubes		0.87	0.10	0.72	0.05	0.90	0.10	0.74	0.04
Annuli		0.83	0.09	0.79	0.10	0.91	0.09	0.87	0.10
Bundles	JAEA-A	0.72	0.06	0.68	0.03	0.72	0.09	0.68	0.03
	JAEA-B	1.03	0.09	1.04	0.08	1.03	0.11	1.05	0.10
	JAEA-C	1.01	0.06	1.02	0.07	1.02	0.08	1.03	0.07
	JAEA-D	1.10	0.07	1.10	0.08	1.09	0.08	1.09	0.08
	Toshiba-1	1.18	0.07	1.20	0.04	1.22	0.10	1.23	0.06
	Toshiba-2	1.06	0.10	1.08	0.10	1.16	0.16	1.18	0.15
	Toshiba-3	0.84	0.04	0.85	0.04	0.91	0.02	0.91	0.03
	Toshiba-4	1.32	0.13	1.38	0.06	1.42	0.12	1.46	0.09
	all bundles	0.99	0.18	0.99	0.18	1.00	0.20	0.99	0.20

Table VI reveals that the performance of M2-CISE (and M1-CISE) is not markedly altered when we only focus on RBWR representative operating conditions, except for tube cases in which the under-estimation of critical power can reach up to more than 25% at nominal conditions. This under-prediction could result from various reasons including data uncertainties and applicability of bundle formulation for tubes. Interestingly, as shown in Figure 19, the comparison of the tube data at 7 ± 0.5 MPa to the 2006 CHF look-up table (Groeneveld et al., 2007) also resulted in similar under-estimation. The 2006 CHF look-up table consists of a normalized data bank for a vertical 8 mm water-cooled tube, and is widely used for the prediction of tube CHF due to its relatively high accuracy and reliability. It gives rise to an average PECP of 0.96 (SD of 0.08) with our tube database if the entire range of validity is covered (which outperforms M2-CISE), but also under-

[1] Nominal conditions refer to: pressure from 6.5 to 7.5 MPa, and mass flux from 500 to 1,500 kg/m^2-s.

predicts experiments by 20% at 7 ± 0.5 MPa. The prediction of annulus critical power has been improved with M2-CISE4 mainly due to the modification of the scaling factor (i.e. hydraulic-to-heated diameter ratio term) exponent.

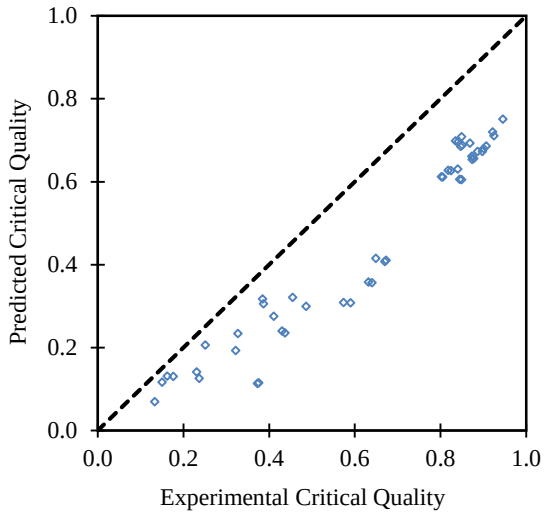

Figure 19. Look-up table: tube critical quality results (at 7±0.5 MPa).

Sensitivity analysis will be performed in the following sub-sections to investigate the impact of different parameters on the dryout critical power of tight bundles.

3.3.1. Effect of Pressure

It is generally well established for a traditional BWR fuel bundle that the critical power would increase at low pressure before reaching its peak value between 4 and 6 MPa and then decrease at high pressure. However, this trend is not observed with our tight bundle database in which critical power decreases as pressure becomes higher, as shown in Figure 20. This feature is also confirmed in tubes and annuli. The pressure effect is correctly captured by M2-CISE4, even though the correlation over-estimates Toshiba-4 data.

An RBWR operates under the same pressure as a conventional BWR; that is, around 7.2 MPa.

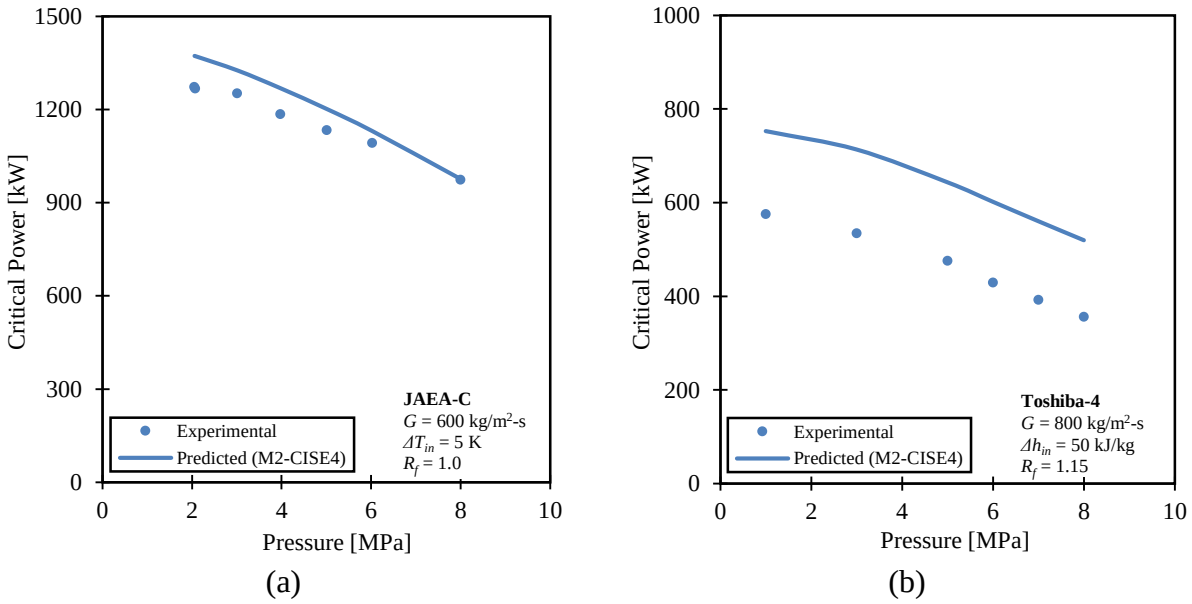

Figure 20. Pressure effect on tight bundle critical power (M2-CISE4). (a) JAEA-C; (b) Toshiba-4.

3.3.2. Effect of Mass Flux and Bundle Tightness

The two plots in Figure 21 compare experimental versus predicted (by M2-CISE4) critical power as a function of mass flux. One can conclude that the trend of increasing critical power with increasing mass flux is properly captured by M2-CISE4. Idem for the tightness: a tighter bundle would have a lower critical power. However, for Toshiba-1, 2 & 3 data sets (Figure 21(b)), the magnitude of tightness effect is not as well represented by M2-CISE4 as for JAEA-C & D (Figure 21(a)): the 0.8 mm gap case (Toshiba-1) is over-predicted, and the 1.8 mm gap case (Toshiba-3) is under-predicted. The bundle tightness is directly related to the inter-channel mixing: tighter bundle means smaller rod-rod gap, allowing less coolant mixing among sub-channels. Unfortunately, flow mixing cannot be modeled in 1-D bundle analysis.

In RBWR designs, the AC has a rod-rod gap of 1.3 mm versus 2.2 mm for the TB2. Hydraulic diameter is 4.1 mm (AC) versus 6.1 mm (TB2), and nominal mass flux (average assembly) is 896 kg/m^2-s (AC) versus 573 kg/m^2-s (TB2).

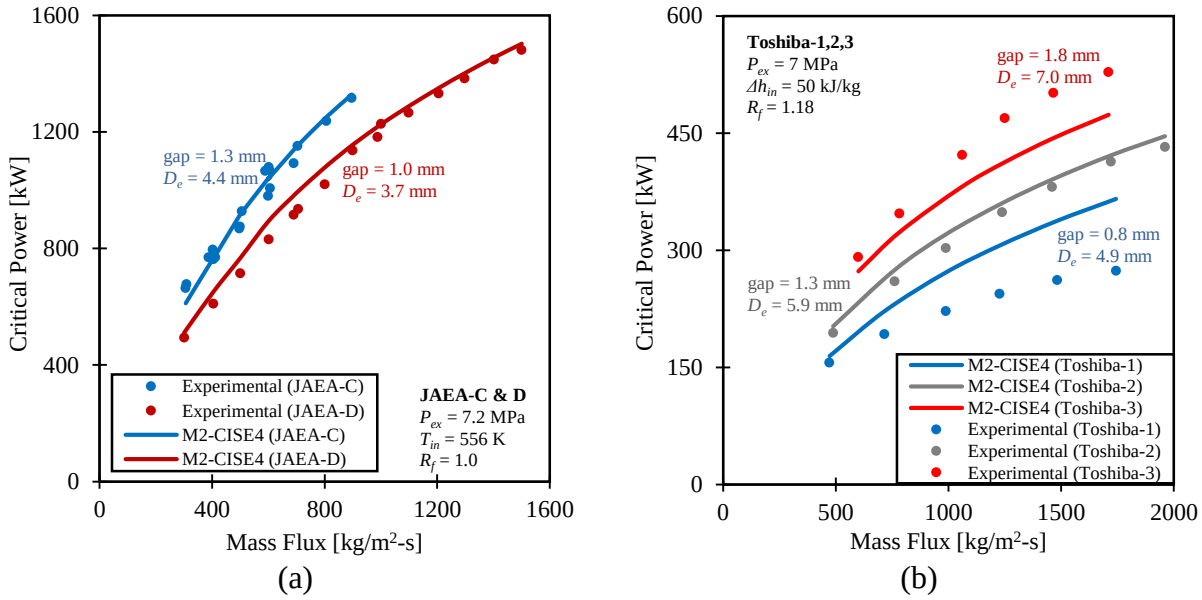

Figure 21. Mass flux and tightness effect on tight bundle critical power (M2-CISE4). (a) JAEA-C & D; (b) Toshiba-1,2,3.

3.3.3. Effect of Inlet Condition

As plotted in Figure 22, a higher inlet temperature (or enthalpy) results in a lower critical power. This trend is correctly captured by M2-CISE4.

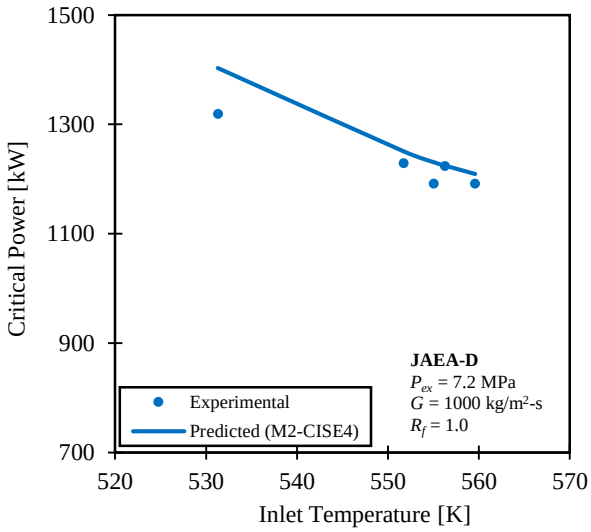

Figure 22. Inlet temperature effect on tight bundle critical power (M2-CISE4).

An RBWR operates with an inlet enthalpy of 1250 kJ/kg, which corresponds to an inlet temperature of 557.5 K (284.4 °C).

3.3.4. Effect of Heated Length and Axial Peaking Condition

Figure 23 shows the dependence of critical power on heated length and axial power distribution. This plot compares results of Toshiba-2 test section between two different lengths and APD profiles: the stepped-cosine shape and longer bundle (1.6 m) dryout is nicely predicted by M2-CISE4, while the downstream-peaked profile and shorter bundle (0.8 m) dryout is over-estimated by 30%. Theoretically, a longer heated/boiling length yields a higher critical quality/power. The critical quality - boiling length curve reaches a plateau when the channel is long enough (Figure 13.21 in Todreas and Kazimi, 2012) for the annular flow regime to become fully-developed (the droplet deposition rate catches up and is in equilibrium with the entrainment rate). The heated length sensitivity is quite different from what has been observed in tubes (Figure 6(e)) and annuli (Figure 9(f)). This higher sensitivity of critical power in tight bundles may be due to intra-assembly flow mixing, configuration (number and location) of spacer grids, as well as the difference in APD profile. Unfortunately, tight bundle experiments changed more than one parameter[1], so their effect on dryout cannot be investigated separately.

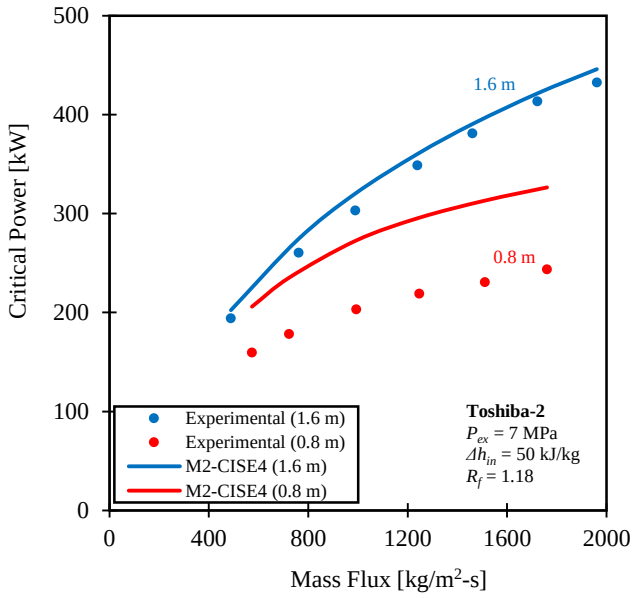

Figure 23. Heated length and APD effect on tight bundle critical power (M2-CISE4).

[1] In Toshiba-2, both heated length and APD were modified between the 1.6 m case and the 0.8 m case; between JAEA-A and B tests, not only length and APD but also bundle geometry (rod diameter, bundle tightness) and radial power peaking factor changed.

While inter-channel mixing and spacer grid effect cannot be analyzed without sub-channel analysis, it is worthwhile, at the current stage, to investigate more in details the effect of non-uniform APD profiles on critical power.

It is well known that a different APD may change the position of dryout occurrence and could affect the heat removal performance. However, quantifying the effect of non-uniform APD on critical power and including it into simple correlations are much more complicated. As mentioned earlier in section 3.1, the reason why M2-CISE4 does not have a specific term for the APD is because our annuli data displayed no significant impact of non-uniform axial heating on critical power. Moreover, unlike the departure from nucleate boiling (DNB) which is a local phenomenon, the dryout critical power should not be very dependent on local heat flux. The shape of an APD does affect the onset of nucleate boiling (ONB) point and thus the boiling length, which has been accounted for in the CISE4 formulation.

Experiments performed to investigate the non-uniform APD effect initially reported quite inconsistent results: some revealed non dependence of critical power on APD, others showed significant penalty from uniform to cosine shape APD. It turned out later that the confusing conclusions regarding the influence of APD were not due to lab-to-lab uncertainties, but rather other factors. One major factor is that the effect of axial heating condition depends not only on the peaking profile itself, but also on the channel geometry, presence and configuration of spacer grids, and flow conditions. The consensuses from various studies including Adamsson and Anglart (2010), Anglart (2010), Todreas and Rohsenow (1965), and Yang et al. (2006) are: (a) the absence of a strong dependence of dryout on APD: a different APD may change critical power by up to 15% at BWR type conditions; (b) in general, inlet-peak profiles yield the highest level of critical power; outlet-peak profiles yield the lowest; middle-peaked (cosine) profiles behave in between; uniform shape results in higher critical power than cosine and outlet-peak profiles but remains unclear when compared to inlet-peak cases. This partially explains the over-estimation of downstream-peaked (which would lead to the lowest critical power) 0.8 m bundle data by M2-CISE4. The RBWR employs a double-humped shape APD (Figure 4) which is not beneficial to

the critical power. The AC fuel bundle has a heated length of 1.35 m, versus 1.02 m for the shorter TB2.

The JAEA-B test (Liu et al., 2004) reported that under the same operating conditions, the double-humped axial power shape results in much lower critical quality compared to the uniform APD (JAEA-A test) as displayed in Figure 24. Figure 24 also compares predicted critical quality with M2-CISE4 between the two test sections. The difference in predicted results is significant: under-estimation of over 30% for JAEA-A, and slight over-estimation for JAEA-B. However, one cannot conclude from the presented results that such difference is due to APD only. In fact, multiple parameters come into play in this comparison: heated length, bundle geometry (hydraulic diameter, tightness), radial peaking, and APD. As discussed in the previous paragraph, the APD effect is supposed to alter critical power/quality by less than 15%. The radial power peaking should have very little impact on JAEA-A and B tests based on analysis in section 3.1. The heated length and bundle tightness effects are directly related to inter-channel mixing phenomenon, which requires sub-channel analysis. Furthermore, Nakatsuka et al. (2003) also reported much higher PECP values for the double-humped JAEA-B test than for the axially uniform JAEA-A test by using the Arai's correlation developed with axially uniformly heated BAPL data, which are consistent with results using M2-CISE4 (Table VI).

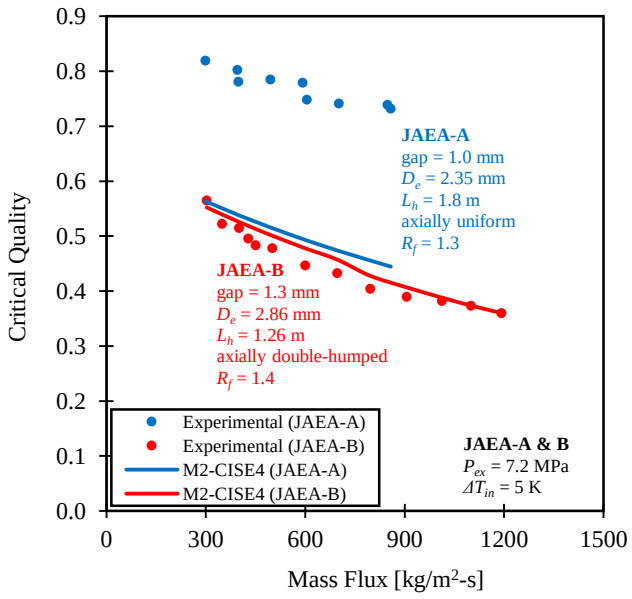

Figure 24. JAEA-A & B experimental vs. predicted (M2-CISE4) critical quality.

3.3.5. Effect of Radial Peaking Condition

The impact of radial peaking factor (R_f) on experimental critical power was discussed in section 3.1. Due to inconsistencies observed among test sections, a constant value of R_f = 1.1 that corresponds to the RBWR hot bundle local peaking factor was used in M2-CISE4.

However, it is not appropriate to put a power ratio term in a quality formulation, properly speaking. Sub-channel analysis is required to get the local quality distribution inside a bundle and further improve the critical power prediction.

3.3.6. Recommendations

As the parametric studies above reveal, the effect of bundle tightness, heated length, non-uniform APD and radial heating cannot be perfectly captured by M2-CISE4 mainly because of the 1-D approach in which intra-assembly flow mixing is neglected and spacer grid modeling is missing. The sub-channel analysis will be able to take into account these two factors, and also the exact APD profile. Additionally, as introduced in section 1.2, the impact of APD on dryout critical power which may reach up to 15% could be properly represented in the mechanistic approach three-field model, along with other parameter effects.

3.4. Conclusion

The updated dryout critical power correlation, namely M2-CISE4, predicts better but still conservative results for tube and annulus data compared to its previous version (M1-CISE4). The 1-D critical quality - boiling length formulation only depends on bundle-averaged thermal hydraulic parameters and is not able to model inter-channel mixing and spacer grids which both have important consequences on tight bundle critical power. Hence, such parameter effects as bundle tightness, heated length, radial peaking, and APD cannot be entirely captured, and tight bundle dryout prediction with M2-CISE4 still shows significant scatter in PECP results with regard to the whole database.

It is important to mention that all the eight tight bundle dryout tests data have been retrieved from corresponding published papers (original data unavailable, unlike tubes and annuli). This creates an extra source of uncertainty (data extraction) in addition to existing and unavoidable uncertainties with experiments themselves.

In order to further improve the M2-CISE4 correlation, sub-channel analysis is necessary. The next chapter will present the sub-channel code VIPRE-01 and focus on its application for tight bundles. Results of radial quality distribution in VIPRE-01 for each bundle case will be incorporated in M3-CISE (Chapter 5), improved and ultimate version of CISE4 based tight bundle critical power correlation.

Another dryout prediction methodology, the mechanistic approach three-field model, will be investigated and evaluated against experimental data (tubes, annuli, tight bundles) in Chapter 6.

4. Sub-channel Analysis of Tight Bundles

4.1. Objective

The assessment of the M2-CISE4 correlation reveals that a sub-channel level modeling of tight bundles is necessary if further improvement on dryout prediction is desired. A sub-channel code (such as VIPRE-01) is able to introduce higher mechanistic models and provide much more detailed local information (flow, quality, void fraction, temperature, etc.).

The purpose of this chapter is to characterize tight bundle radial quality distribution at the axial location of dryout to be included in our correlation (Chapter 5) via sub-channel analysis with the code VIPRE-01 (MOD-02). Section 4.2 will give a brief presentation of the code and its input layout; in sections 4.3 and 4.4, VIPRE-01 will be benchmarked against the computational fluid dynamics (CFD) code STAR-CCM+ for tight bundles under single-phase flow conditions and against sub-channel level experimental data and simulations in other work for tight bundles under two-phase flow conditions, respectively. The JAEA and Toshiba bundle modeling results will be presented and discussed in section 4.5.

4.2. Code Overview: VIPRE-01

4.2.1. Description

VIPRE-01 (Versatile Internals and Component Program for Reactors; EPRI) is a thermal-hydraulic and safety analysis code. It was developed on the strengths of the COBRA series of codes by Battelle Pacific Northwest Laboratories for the Electric Power Research Institute (EPRI) to help evaluate nuclear reactor core thermal-hydraulic parameters and safety limits including minimum departure from nuclear boiling ratio (MDNBR), critical power ratio (CPR), fuel and clad temperatures, and reactor coolant state in normal and assumed accident conditions.

VIPRE-01 MOD-01 was accepted by the U.S. NRC (Nuclear Regulatory Commission) for PWR licensing applications. VIPRE-01 MOD-02 is an improved and updated version of VIPRE-01 MOD-01, and was developed to address, in particular, issues related to generic BWRs. This up-to-date version has been benchmarked and qualified for both PWR and BWR applications.

Like most other core thermal-hydraulic codes, the VIPRE-01 modeling structure is based on sub-channel level analysis. The core (or section of symmetry) is defined as an array of quasi 1-D parallel flow channels that communicate laterally by diversion crossflow and turbulent mixing (a brief review of coolant mixing in rod bundles will be given later in section 4.2.2). Given the geometry of the core (rod bundle) and coolant channels, along with the boundary conditions, VIPRE-01 calculates single- and two-phase flow velocity, pressure, and thermal energy fields and fuel rod temperatures by solving the finite-difference equations for mass, energy, and momentum conservation for an interconnected array of channels assuming incompressible thermally expandable homogeneous flow. The equations are solved with no time step or channel size restrictions for stability. Empirical models are included for subcooled boiling and vapor/liquid slip in two-phase flow.

Two correlations in VIPRE-01, Hench-Levy and Hench-Gillis critical quality correlations, can be used to compute CPR of BWRs. The GEXL correlation is the only model that has NRC approval for BWRs and is used for licensing calculations. However, GEXL is not available in the academic distribution of VIPRE code and its applicability for other than GE fuel bundles is not determined. Additionally, none of these correlations has been validated against tight lattice fuel bundles, hence the CPR analysis will not be performed in VIPRE-01 for the thesis.

A detailed mathematical modeling description of VIPRE-01 can be found in Volume 1 of the code manual (Stewart et al., 2011a).

4.2.2. Input Layout

This section provides a brief presentation of VIPRE-01 (MOD-02) input layout. Detailed input instructions can be found in Volume 2 of the code manual (Stewart et al., 2011b).

VIPRE code input is organized into groups which reflect a generalized logical approach to setting up a problem. The code requires input of five sections prior to running a problem: the geometry of the problem (described in the groups GEOM, AXLV and RODS), the physical properties of the working fluid (group PROP), the boundary conditions (group OPER), the constitutive models for

the flow and heat transfer solutions (groups CORR, DRAG, GRID and MIXX), and the numerical solution method to be used (group CONT).

The geometry group GEOM is used to input bundle and channel dimensions, channel interconnections, and axial node spacing. The input for the PROP group defines the physical properties of the working fluid. The geometric and material properties of the heat conducting or heat source elements are specified in the RODS group input, including APD profiles and radial peaking factors. The input for the group OPER is used to define the operating conditions for a problem (system pressure, inlet conditions, power/heat flux, etc.). Empirical correlations used in VIPRE-01 to model single/two-phase flow effects (single/two-phase friction factors/multipliers, subcooled void correlations, and bulk void relations) and the heat exchange between the rods and the coolant along the boiling curve are collected in the CORR group. The exchange of energy and momentum between adjacent channels due to turbulent mixing is described in the group MIXX. The friction input group DRAG includes pressure losses due to frictional drag for both axial and transverse flow. The group GRID is used to model any irreversible axial pressure loss that occurs over a relatively short distance in a channel (e.g. pressure loss associated with spacer grids and orifices). Modeling of axial variation in geometry variables can be realized in the input group AXLV. The last group, CONT, consists of parameters that control the execution of the code and sets options for the output features.

Important constitutive models:

- **Two-phase friction multiplier**

The two-phase friction multiplier is the traditional means of modeling the effect of two-phase flow on the pressure drop due to friction. It is applied as a multiplier on the single-phase friction pressure drop calculated assuming the total flow is single-phase liquid only. The analytical homogeneous model (HOMO) is applied in this work in which the two-phase flow is considered to be a single fluid with the properties of the mixture. This is a fairly reasonable approximation of the flow field at relatively high pressures and high mass velocities (with small bubbles), but is less satisfactory for low pressure and low mass flux conditions.

The EPRI correlation is the default model for the two-phase friction multiplier in VIPRE-01, and is also applied in section 4.5. Based on the homogeneous model, the EPRI correlation incorporates the mass flux dependence observed in some two-phase pressure drop data. Its formulation is given as:

$$\Phi_{lo}^2 = 1.0 + x \cdot (\frac{\rho_f}{\rho_g} - 1) \cdot C_F \tag{3}$$

where

$$C_F = 1.02x^{-0.175}G^{-0.45} \quad \text{if } P \geq 600\ psia,$$

and

$$C_F = 0.357x^{-0.175}G^{-0.45}(1 + \frac{10P}{P_c}) \quad \text{if } P < 600\ psia.$$

Φ_{lo}^2 = two-phase friction multiplier; x = flow quality; ρ_f = density of the saturated liquid (lbm/ft^3); ρ_g = density of the saturated steam (lbm/ft^3); G = mass flux (Mlbm/hr-ft^2); P = exit pressure (psia); P_c = critical pressure (psia).

However, its applicability has not been proved under such conditions as low pressures (< 4 MPa), low mass velocities (< 500 kg/m^2-s), and small hydraulic diameters (< 6 mm).

- **Void/quality relation**

The void/quality correlation is used to model the relationship between flow quality and void fraction in two-phase flow. In VIPRE-01, the recommended and default EPRI (Lellouche-Zolotar) drift flux correlation (Stewart et al., 2011a) may not be appropriate because operating conditions in this work are sometimes beyond its range of validity. Only the well-established Chexal-Lellouche (also called new EPRI) drift flux model which is used in most safety analysis codes such as RELAP5 (INL, 2001) for the void fraction prediction is able to cover these conditions (except for small hydraulic diameters[1]) and will be applied in this work.

[1] Shirvan et al. (2013) discovered that for tight bundle geometry the Chexal-Lellouche correlation tended to over-estimate the void fraction in the 10-25% quality region.

- **Mixing mechanisms**

The mechanisms of mixing phenomenon in rod bundles are complicated, and a detailed review was carried out by Conboy (2010). In the category of natural mixing (which is not caused by mechanical protrusions into the actual flow channels, vs. forced mixing) in single-phase, the mechanisms of sub-channel cross-flow include: (1) diversion cross-flow, (2) turbulent interchange, and (3) molecular diffusion.

Diversion cross-flow refers to the redistribution of fluid which occurs due to naturally arising radial pressure gradients in a flow field. These gradients come from heterogeneity in sub-channel geometry or of fluid properties as a result of heating. This directional flow effect is fully captured in VIPRE-01 by defining the channel-to-channel gap width. Besides the directional flow effect, the redistribution of energy and momentum is largely caused by the movement of turbulent flow structures across adjacent sub-channels, also known as turbulent interchange/mixing. In this non-directional mechanism, no net exchange in mass is typically assumed. Heat transfer due to molecular diffusion is of very little importance in nuclear reactor cores, since mass velocities are relatively high and temperature gradients are relatively small.

As was just noted, turbulent mixing is usually assumed to cause a lateral enthalpy flux without any associated net mass-flow. However, fluid interchange is required so as to provide heat exchange, which can be represented by a turbulent crossflow term w' (mass flow rate per unit length). The corresponding exchange of energy between adjacent channels is modeled as a source term Q_m in the VIPRE-01 energy equation such as:

$$Q_m = \Delta x \sum w' \Delta h \tag{4}$$

where Δh is the difference in mixture enthalpy between the two neighboring sub-channels, and four types of correlation are available in VIPRE-01 to predict the turbulent crossflow w'. For the single-phase benchmark (section 4.3), the simplest and most commonly used correlation is applied:

$$w' = \beta \bar{G} S \tag{5}$$

where β refers to the mixing coefficient, $\bar{G}$ is the average mass flux in the adjacent channels, and S is the gap width. According to Conboy (2010), the value for β generally ranges from 0.006 to 0.012 based on various studies. A sensitivity analysis will be performed.

In multi-phase, similar mixing mechanisms are present as in single-phase flow (diversion cross-flow, turbulent interchange, molecular diffusion), though in general they can occur differently among the two phases and are highly sensitive to two-phase flow regime. In addition, a new mechanism, namely two-phase void drift, is introduced to describe the tendency of a vapor phase within liquid phase along interconnected channels to redistribute itself according to a certain equilibrium void distribution, and is believed to behave independently of local pressure gradients. In a bundle comprised of sub-channels of different shapes and sizes, this equilibrium would favor higher void fractions in larger channels than in smaller ones. Most sub-channel codes including VIPRE-01 considers an incompressible but thermally expandable mixture fluid (a single phase in effect) for multi-phase analysis, thus two-phase turbulent mixing in VIPRE-01 is assumed to be the same as in single-phase flow. Void drift mechanism can be modeled using a construct developed by Rowe et al (1990) to calculate the equilibrium void fraction in a given sub-channel. However, this model has not yet been added in modern sub-channel codes.

Starting from the two-phase benchmark (section 4.4 and beyond), a new model given by Brynjell-Rahkola et al. (2009) will be opted for turbulent mixing crossflow (w') in VIPRE-01:

$$w' = 0.035 Re^{-0.1} \frac{S}{l} \overline{D_e} \bar{G} \tag{6}$$

where Re is the Reynolds number based on average flow in the adjacent channels, S is the gap width, l refers to the centroid distance of two neighboring channels, $\overline{D_e}$ is the averaged hydraulic diameter of the two connected channels, and $\bar{G}$ is the average mass flux in the adjacent channels. This model was incorporated in VIPRE-W (Westinghouse version of VIPRE-01) sub-channel analysis code (Sung et al., 1999), which was validated against sub-channel void measurement data from an 8×8 fuel assembly design under typical BWR conditions provided by NUPEC (Nuclear Power Engineering Corporation) for the BFBT (BWR Full-size Fine-mesh Bundle Test) benchmark (Neykov et al., 2006).

- **Spacer grid loss coefficient**

Spacer grids have become indispensable for promotion of mixing among sub-channels and enhancement of droplet deposition rates despite their inherent disadvantages including increases in pressure drop. In a sub-channel code like VIPRE-01, spacers are modeled as local pressure losses. The form loss due to the presence of spacers can be calculated from the formula as follows:

$$\Delta P_{grid} = K_{grid} \frac{\rho v^2}{2} \tag{7}$$

where K_{grid} is the grid loss coefficient, ρ and v refer to the density and velocity of the fluid in the channel (a two-phase multiplier independent of the two-phase friction multiplier[1] will be applied to local form losses if it is two-phase flow). Rehme and Trippe (1980) showed that the grid loss coefficient can be represented by relating a modified drag coefficient K_v to the relative blockage of the flow cross section[2] ε:

$$K_{grid} = K_v \cdot \varepsilon^2 \tag{8}$$

K_v is a function of the Reynolds number (decreases with increasing *Re*), but is very weakly dependent of *Re* for $Re > 10^4$. The grid loss coefficient K_{grid} is not only affected by the blockage ratio ε but also by the length of the spacer and its leading edge. According to a literature review including Rehme and Trippe (1980), Holloway et al. (2003), Tamai et al. (2004), and Caraghiaur et al. (2009), the value for K_{grid} mostly ranges from 0.4 to 1.5.

4.3. VIPRE-01 Benchmark: Single-phase Flow

While VIPRE-01 performance has been established for regular BWR applications, its applicability for tight hexagonal lattice bundles (RBWR) needs to be confirmed. Four test cases with single-phase turbulent flow conditions are modeled in VIPRE-01, and results are compared to STAR-CCM+ (version 9.06.011), a widely recognized CFD solver known for highly accurate and reliable simulation solutions in single-phase for rod-bundle geometries. In STAR-CCM+, selected physics

[1] VIPRE-01 uses the Romie multiplier on all local loss coefficients.

[2] The relative blockage is defined as the cross-section blocked in the axial direction divided by the undistributed flow cross-section.

models are: segregated flow, constant density (except for heat generation in test case #2 where polynomial density and segregated fluid temperature are applied), realizable K-Epsilon two-layer all y+ wall treatment. The convergence is achieved when the residual parameters reach steady-state, typically after 1000 iterations.

Test case #1: (Kureta et al., 2008)

The first test case deals with a 14-rod tight bundle. One quarter of the bundle (section of symmetry) is modeled in VIPRE-01 in which 10 channels are interconnected. The sub-channel scheme and the CFD mesh scene (mesh base size = 0.325 mm, i.e. one quarter of the rod-rod gap) are shown in Figure 25; bundle parameters and working conditions are presented in Table VII. No heat is generated in this case. Turbulent mixing group is omitted in VIPRE-01, and spacers are not modeled.

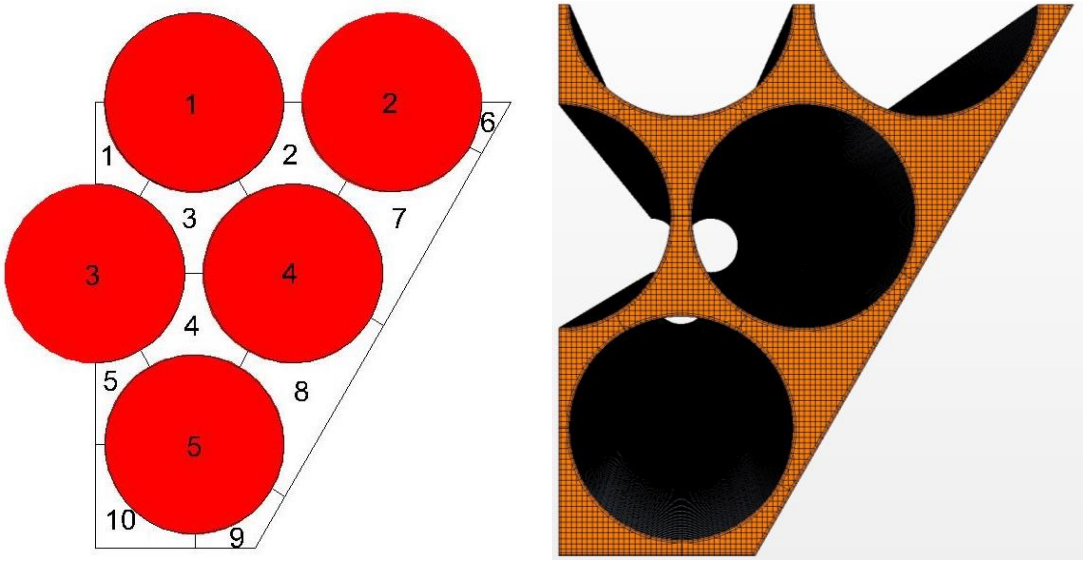

(a) (b)

Figure 25. VIPRE-01 single-phase verification test case #1 geometric view. (a) Sub-channel scheme; (b) CFD (STAR-CCM+) mesh scene.

Figure 26 illustrates the CFD outflow velocity profile, and Figure 27 presents the outflow mass flux as a function of sub-channel number for which the two codes agree closely with each other. The VIPRE-01 input file is attached in Appendix A.

Table VII. VIPRE-01 single-phase verification test case #1 parameters.

Configuration	1/4 bundle, 10 channels
Rod diameter	13.69 mm
Gap rod-rod	1.3 mm
Gap rod-shroud	1.0 mm
Length	0.3 m
Heat generation sensitivity study	-
Turbulent mixing sensitivity study	-
Exit pressure	7.2 MPa
Inlet temperature	285 °C
Mass flux (bundle-averaged)	1000 kg/m^2-s

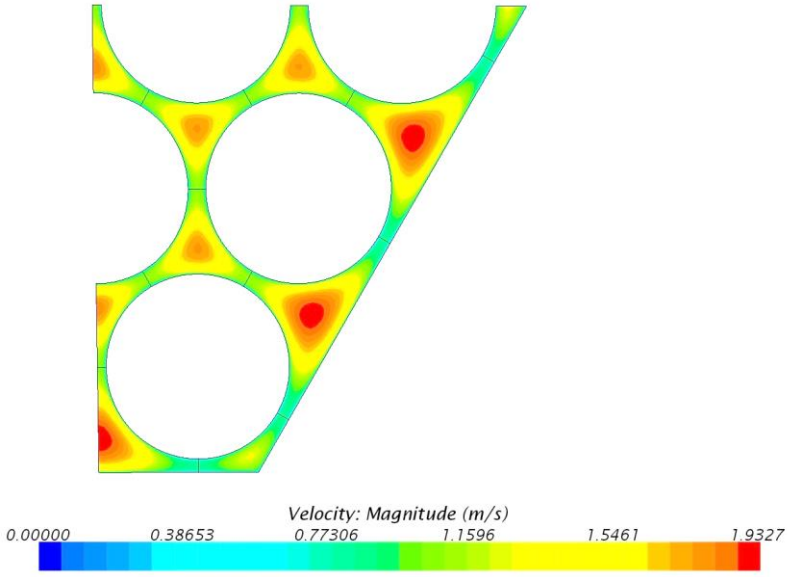

Figure 26. VIPRE-01 single-phase verification test case #1 outflow velocity (CFD).

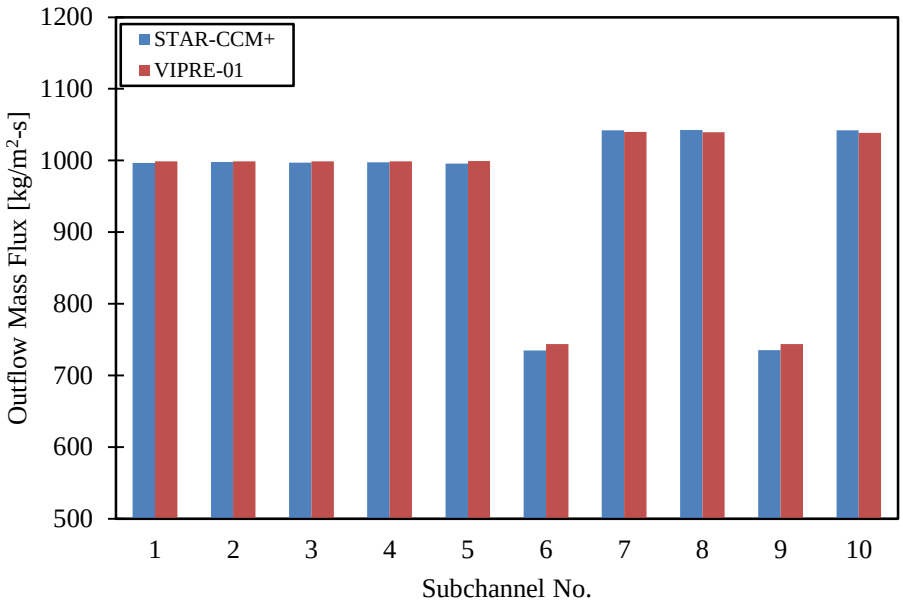

Figure 27. VIPRE-01 single-phase verification test case #1 outflow mass flux.

Test case #2-4: (Yamamoto et al., 2006)

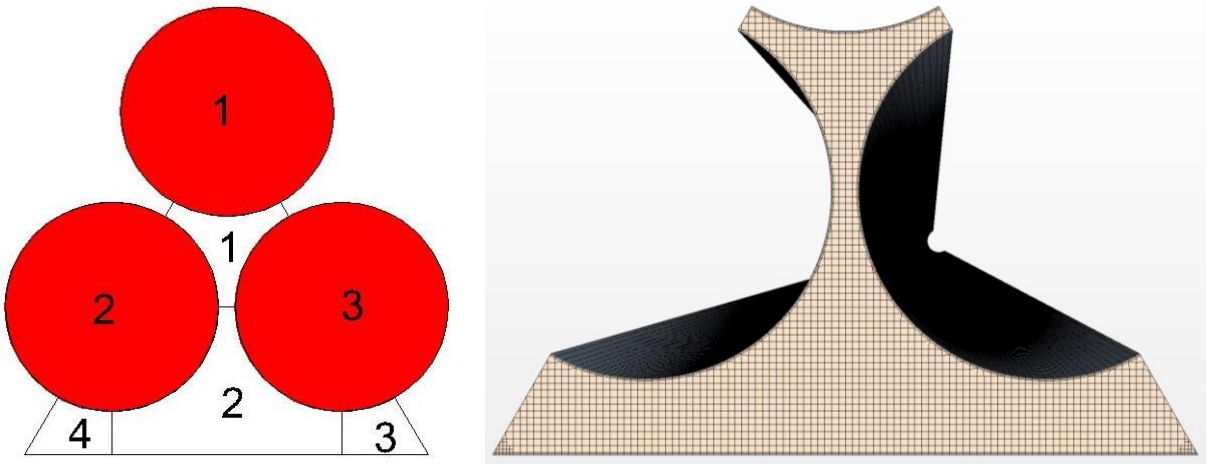

(a) (b)

Figure 28. VIPRE-01 single-phase verification test case #2-4 geometric view. (a) Sub-channel scheme; (b) CFD (STAR-CCM+) mesh scene.

The three following test cases correspond to the Toshiba 7-rod bundle geometries (Figure 15) but with a reduced length of 0.5 m due to high computational cost of CFD. The sub-channel scheme and the CFD mesh scene (mesh base size is one quarter of the rod-rod gap) are shown in Figure 28; bundle parameters and working conditions are presented in Table VIII. Sensitivity studies are performed on heat generation and turbulent mixing (in VIPRE-01). Spacers are not modeled.

Table VIII. VIPRE-01 single-phase verification test case #2-4 parameters.

Test case #	2	3	4
Test set ID	Toshiba-1	Toshiba-2	Toshiba-3
Configuration	1/6 bundle, 4 channels		
Rod diameter	10.8 mm		
Gap rod-rod	0.8 mm	1.3 mm	1.8 mm
Gap rod-shroud	2.2 mm	2.57 mm	2.99 mm
Length	0.5 m		
Heat generation sensitivity study	0; 100 kW/m^2		
Turbulent mixing sensitivity study	yes		
Exit pressure	7.2 MPa		
Inlet temperature	285 °C; 265 °C		
Mass flux (bundle-averaged)	1000 kg/m^2-s		

Figure 29 shows close agreement between VIPRE-01 and CFD outflow mass flux in each sub-channel for the three cases with no heat generation and no turbulent mixing modeling in VIPRE-01. The heat generation does not show any impact on the performance of VIPRE-01 as long as no boiling occurs (so it can be verified with CFD which was not extended to two-phase flow), as depicted in Figure 30 for Toshiba-1 test case in which an axially uniform heat flux of 100 kW/m^2 is assumed.

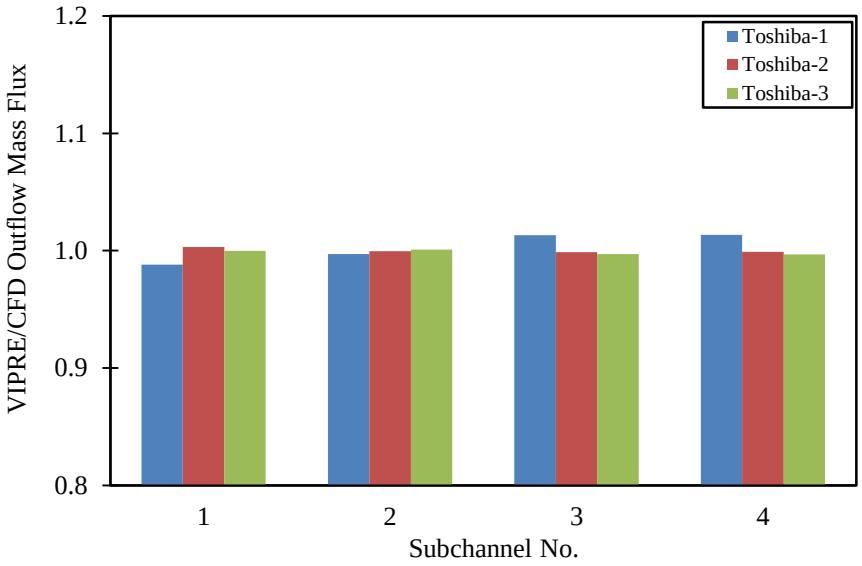

Figure 29. VIPRE-01 single-phase verification test case #2-4 outflow mass flux (adiabatic, no turbulent mixing).

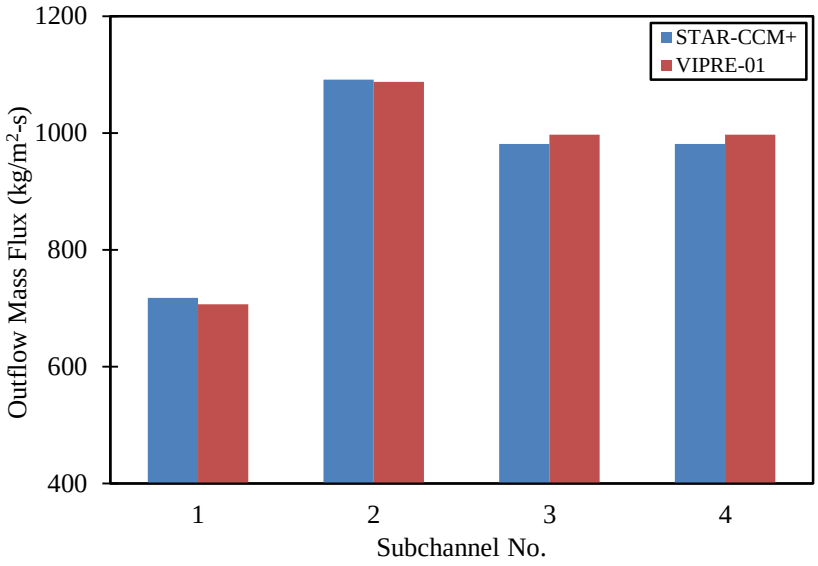

Figure 30. VIPRE-01 single-phase verification test case #2 outflow mass flux (axially uniform heat flux of 100 kW/m^2, no turbulent mixing).

One can notice from Figure 31 that the single-phase flow distribution computed by VIPRE-01 is not sensitive to turbulent mixing for Toshiba-1 bundle. The flow distribution is indeed more uniform with a higher mixing coefficient, but the degree of sensitivity is very weak. The VIPRE-01 input file for Toshiba-1 (test case #2) without heating and with a mixing coefficient of 0.01 is attached in Appendix A.

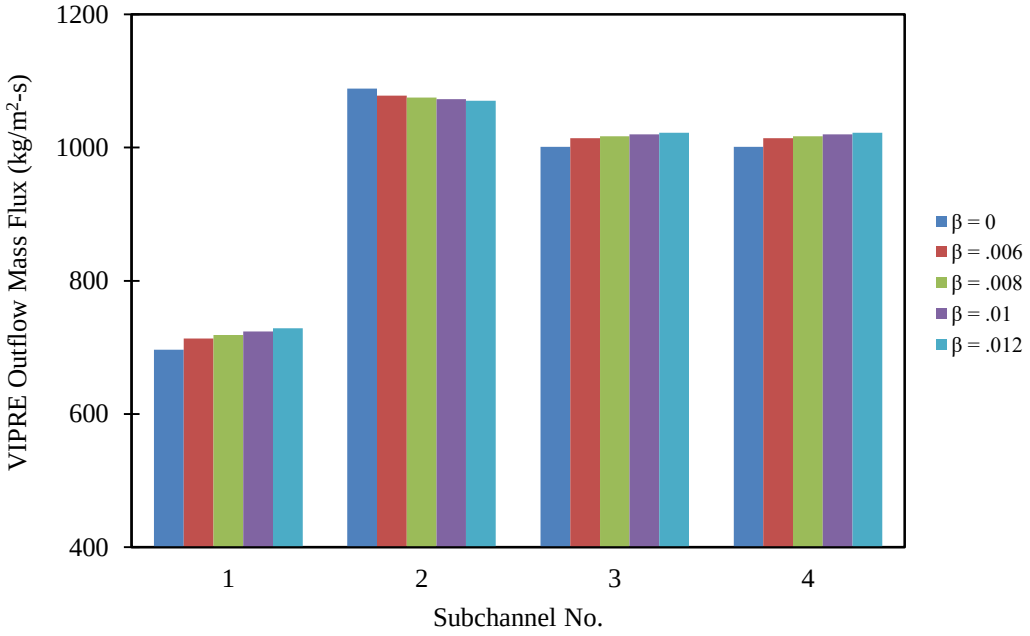

Figure 31. VIPRE-01 single-phase verification test case #2 outflow mass flux (adiabatic, sensitivity to turbulent mixing coefficient).

Under two-phase flow conditions though, the sensitivity to turbulent mixing is more significant. As plotted in Figure 32, for the case of a bundle average exit quality of 16.2%, the outflow quality in channel 1 decreases by 18% when the mixing coefficient increases from 0 to 0.01. Therefore, the accuracy and reliability of the turbulent mixing crossflow model is deemed of great importance in two-phase sub-channel analysis. The correlation (Equation 6) provided by Brynjell-Rahkola et al. (2009) will be used in this work.

To conclude, based on the four test cases above, in single-phase VIPRE-01 results agree well with CFD solutions. Radial flow distribution is not sensitive to turbulent mixing, and introducing rod power in the Toshiba assembly does not alter the performance of VIPRE-01 relative to CFD.

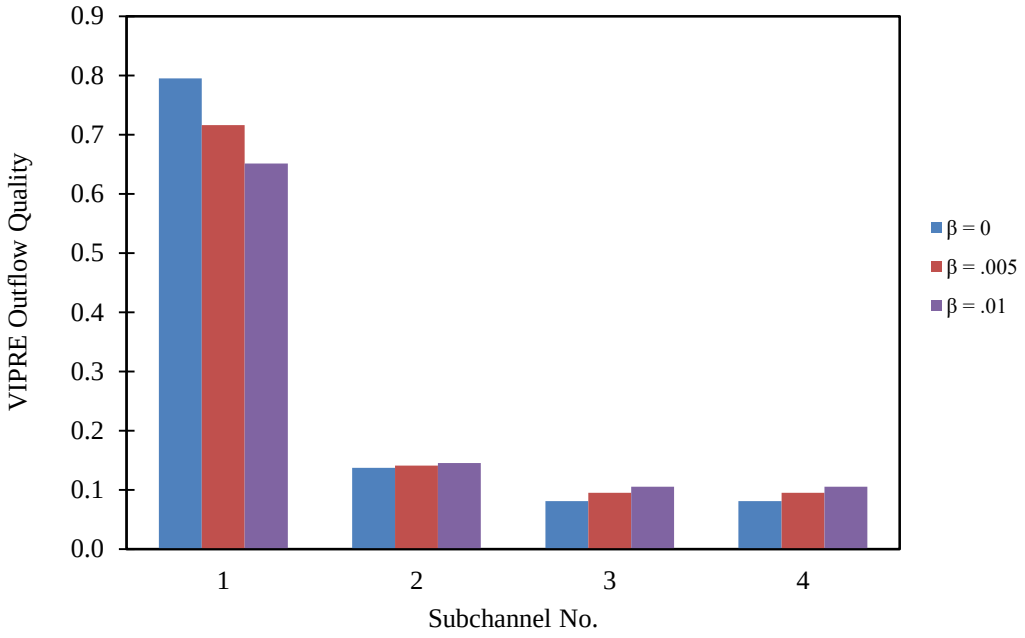

Figure 32. VIPRE-01 single-phase verification test case #2 outflow quality ($x_{avg,\,exit}$ = 0.16, sensitivity to turbulent mixing coefficient in two-phase).

4.4. VIPRE-01 Benchmark: Two-phase Flow

The verification of VIPRE-01 applicability for tight bundles in two-phase flow is much more complicated due to the lack of benchmark tools (like CFD in single-phase) and sub-channel level experimental data. The empirical nature of constitutive relations (two-phase friction multiplier, void/quality relation, etc.) used in VIPRE-01, the high sensitivity of multi-phase quality distribution to turbulent mixing (e.g. Figure 32), and the important role of spacer grids in the enhancement of mixing among sub-channels all contribute to the uncertainties associated with VIPRE-01 modeling. Very few relevant references are available, and two of them have been used as our test cases.

Test case #1: (Kureta et al., 2008)

The first case deals with the same 14-rod tight bundle as what was used for the single-phase benchmark (#1). The sub-channel configuration is presented in Figure 25(a), and parameters are listed in Table IX. Figure 33 visualizes the side view of the bundle with two honeycomb-type spacers of 0.5 mm thickness installed at the bottom and top in the unheated regions.

Table IX. VIPRE-01 two-phase verification test case #1 parameters.

Configuration	1/4 bundle, 10 channels
Rod diameter	13.69 mm
Gap rod-rod	1.3 mm
Gap rod-shroud	1.0 mm
Total length	0.3 m
Heated length	0.24 m
Total power[1]	25 kW
Exit pressure	0.1 MPa
Inlet temperature	90 °C
Mass flux (bundle-averaged)	382 kg/m^2-s

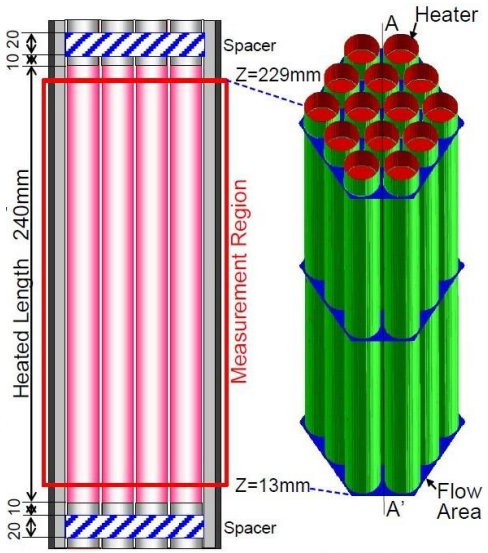

Figure 33. VIPRE-01 two-phase verification test case #1 side view (from Kureta, 2007).

Figure 34 shows a zoomed in photograph of the honeycomb-type spacer. Based on Tamai et al. (2004), K_{grid} = 0.5 is used in this study as a reasonable value.

[1] The rod power is not specified in Kureta et al. (2008) but the exit void fraction distribution is given in Figure 4 of the reference paper based on which the bundle-averaged exit void fraction can be computed and kept the same in VIPRE-01 while the power is being adjusted.

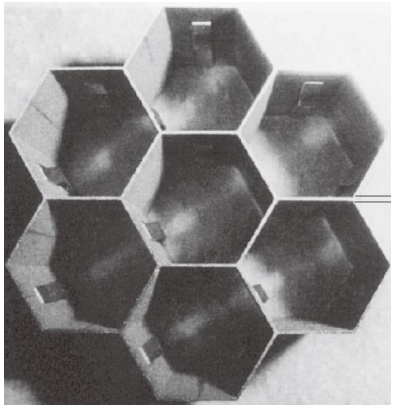

Figure 34. Photograph of honeycomb-type spacer (from Yamamoto et al., 2006).

Figure 35 compares the VIPRE-01 exit void fraction results to experimental data and also to the calculations by NASCA (Nuclear reactor Advanced Sub-Channel Analysis), a sub-channel code which has been widely used by the Japanese reactor vendors for the assessment of current BWR bundles. NASCA was developed based on the concept of two-fluid three-field description in which dryout is assumed to take place when the volumetric fraction of liquid film flow reaches a value smaller than 10^{-5}. The global tendency of the exit void distribution predicted by VIPRE-01 agrees with data and NASCA solution, i.e. inner channels (No. 1-5) yield higher voids than side (No. 7, 8, 10) and corner (No. 6 and 9) channels. However, VIPRE-01 predicts higher voids in corner channels than in side channels, which is opposite to what was measured or predicted in NASCA. Intuitively, side channels in this test case have the highest mass flux (Figure 36; also confirmed in single-phase benchmark, see Figure 27), and should yield the lowest quality and void fraction. This discrepancy may be due to, other than uncertainties with the experiment and constitutive models in codes (as discussed earlier in this section), the fact that VIPRE-01 does not account for void drift mixing mechanism which could drive void toward larger sub-channels with higher mass velocities. Sensitivity studies have been performed on turbulent mixing correlation and grid loss coefficient, but neither of them change the shape of the void fraction distribution in VIPRE-01 such that it could match the experimental or NASCA simulated results. Another issue with this test case is that the Reynolds number is only around 5,000 (due to low pressure and low mass velocity), a value at which the flow is not yet fully turbulent. In the transitional flow region, it is hard to obtain reliable experimental data and apply empirical fully developed turbulent models.

The VIPRE-01 input file is attached in Appendix B.

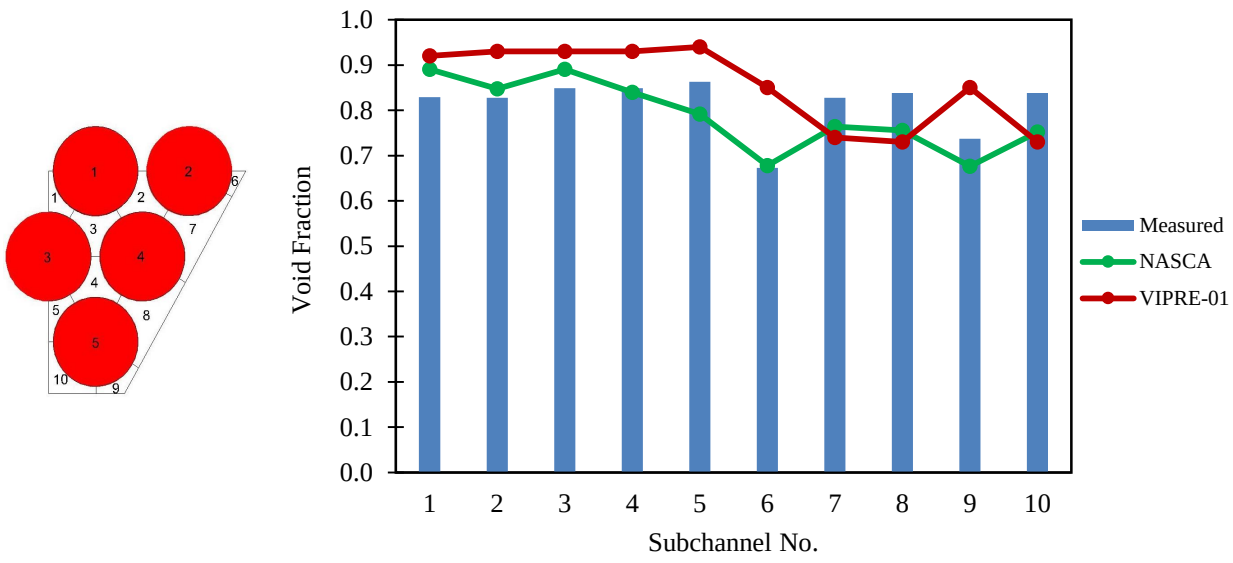

Figure 35. VIPRE-01 two-phase verification test case #1 exit void fraction (partially reproduced from Kureta et al., 2008).

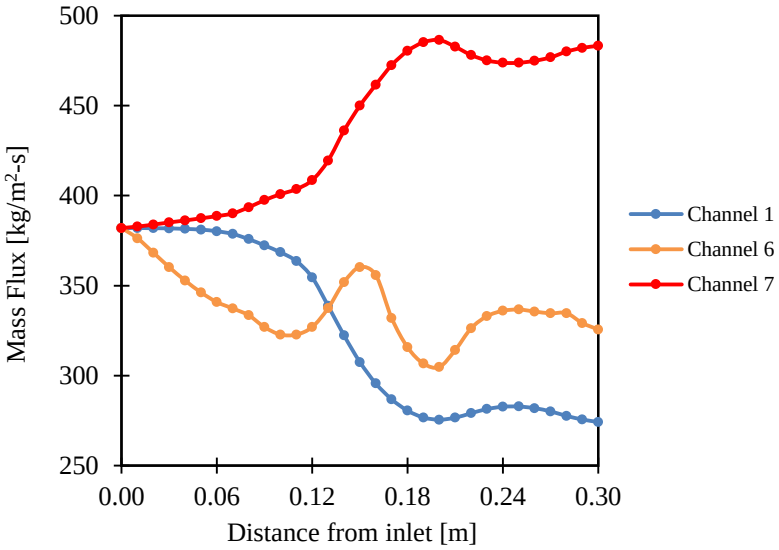

Figure 36. VIPRE-01 two-phase verification test case #1 mass flux axial distribution.

Test case #2: (Tamai et al., 2003)

This test case employs the geometry of the JAEA-C 37-rod tight bundle. The symmetry helps to reduce the analysis to 1/6 of the bundle as shown in Figure 37(a). Four spacers are located at the elevation of a low heat flux region at intervals of about 0.3 m apart (Figure 37(b)), avoiding the location where dryout could occur. The local pressure loss coefficient due to the spacer grids equals to 0.5, as assumed by the JAEA experimentalists (Tamai et al., 2003). The test parameters are listed in Table X.

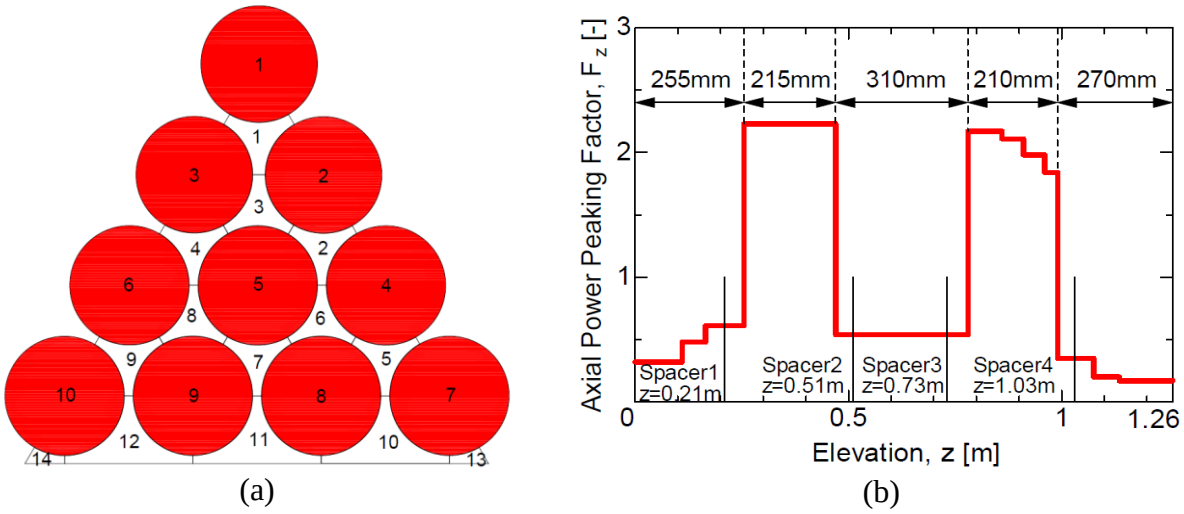

(a) (b)

Figure 37. VIPRE-01 two-phase verification test case #2 configuration. (a) Sub-channel scheme; (b) APD profile and spacer locations.

Results of VIPRE-01 are extracted and compared to those of the code NASCA. In the first simulation, the local power peaking profile is flat, and total power is 855 kW. The exit quality at each sub-channel is plotted in Figure 38. This figure clearly shows that the highest quality region is located around the center of the bundle (channel No.1). The trends displayed by VIPRE-01 and NASCA are the same, except for the two corner channels (No. 13 and 14) in which VIPRE-01 predicts higher exit quality than NASCA. Flow passing through these two channels and the three side channels (No. 10-12) is affected by the cold wall effect, leading to significantly lower quality than the inner channels (No. 1-9). The three side channels have the lowest exit quality in VIPRE-01. As discussed earlier in test case #1, the side channels have higher mass flux than the corner channels, and should *a priori* expect lower quality.

Table X. VIPRE-01 two-phase verification test case #2 parameters.

Configuration	1/6 bundle, 14 channels
Rod diameter	13 mm
Gap rod-rod	1.3 mm
Gap rod-shroud	1.05 mm
Total length	1.26 m
Heated length	1.26 m
Total power	855 kW; 951 kW
Exit pressure	7.2 MPa
Inlet temperature	556 K
Mass flux (bundle-averaged)	400 kg/m^2-s

The second simulation investigates the effect of a non-uniform local power profile, and Figure 39 presents the calculated exit quality distribution by NASCA and VIPRE-01 with a peripheral-to-inner rod power ratio of 1.3. The heater rods electric power is increased to 951 kW. It is important to note that the higher peripheral rod power leads to higher quality in channels secondly adjacent to shroud (No. 5-9). According to both NASCA and VIPRE-01, sub-channel No. 6 and No. 8 have the highest exit flow quality, and the quality distribution is more uniform than in the case of a flat local peaking (Figure 38). The VIPRE-01 input file for the side peak configuration is attached in Appendix B.

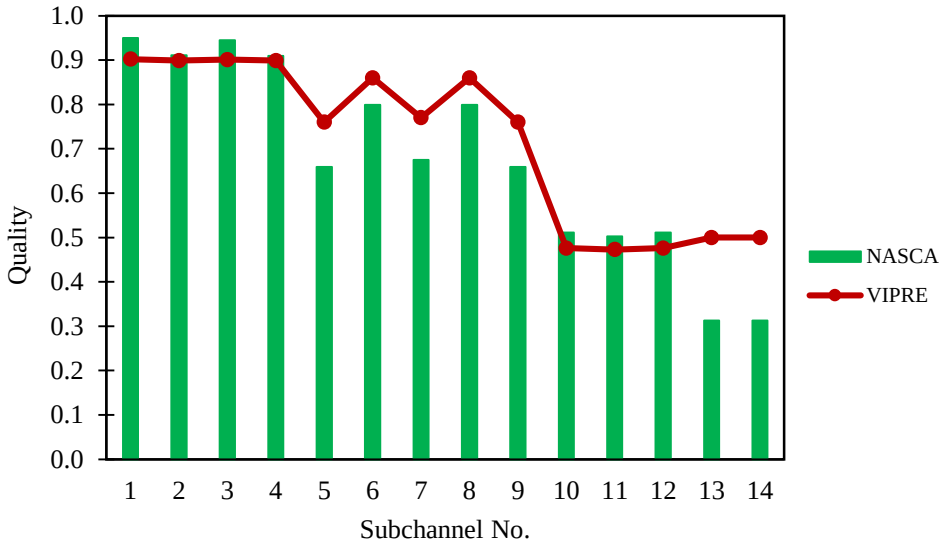

Figure 38. VIPRE-01 two-phase verification test case #2 exit quality - flat local power distribution (partially reproduced from Tamai et al., 2003).

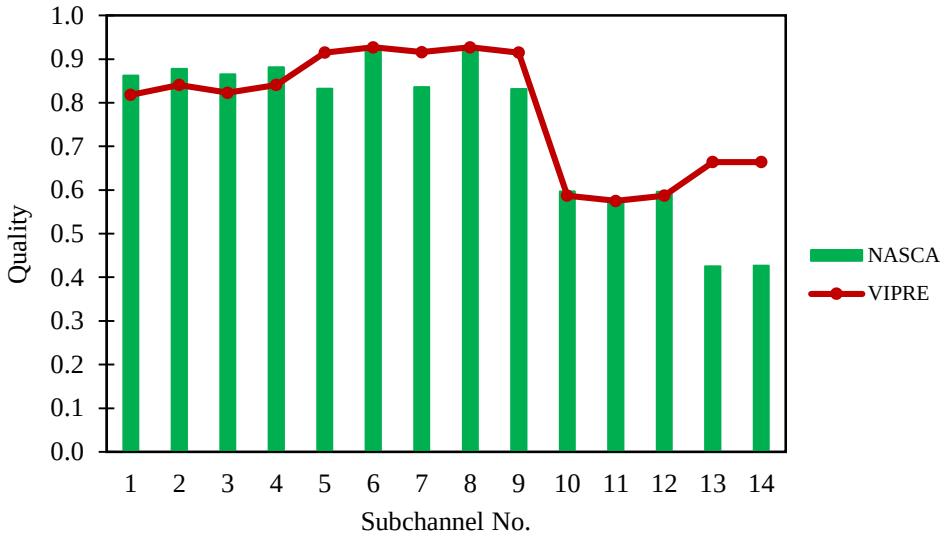

Figure 39. VIPRE-01 two-phase verification test case #2 exit quality - side peak local power distribution (partially reproduced from Tamai et al., 2003).

To summarize, the applicability of VIPRE-01 for tight bundles in two-phase flow has been verified with the 14-rod tight bundle data in Kureta et al. (2008) and NASCA code results. VIPRE-01 is capable of providing the same trend and magnitude of radial quality/void distribution as in the measurements and NASCA code. Regarding the inconsistencies, VIPRE-01 predicts higher quality/void values in corner channels than in side channels for the two selected test cases, which are opposite to published experimental and NASCA results. However, the impact of such discrepancy should be secondary, since the corner channels only make up a small fraction of the cross-sectional flow area and will not downgrade the overall performance of VIPRE-01. More experimental data are necessary for an advanced benchmark.

4.5. Results and Discussion

In this section, the eight test sets (JAEA and Toshiba) used for calibration of the tight bundle critical quality/power correlation will be modeled in VIPRE-01. For each data point, a quality distribution at the axial location of dryout will be given, and the local peak sub-channel quality to bundle-averaged quality ratio, i.e. $R_f\_x = \frac{x_{peak}}{x_{average}}$, will be extracted and used in the next two chapters.

The sub-channel schemes are presented in Figure 40. A selection of constitutive models for the flow and heat transfer solutions is summarized in Table XI (as discussed in section 4.2.2). Notice that Toshiba-4 bundle configuration is quite irregular (rectangular channel box in which four unheated half rods are present) and makes its modeling in VIPRE-01 more challenging. Regarding the two-phase friction multiplier, both the analytical homogeneous model (HOMO) and the EPRI correlation (default model in VIPRE-01) are applied for all the data points.

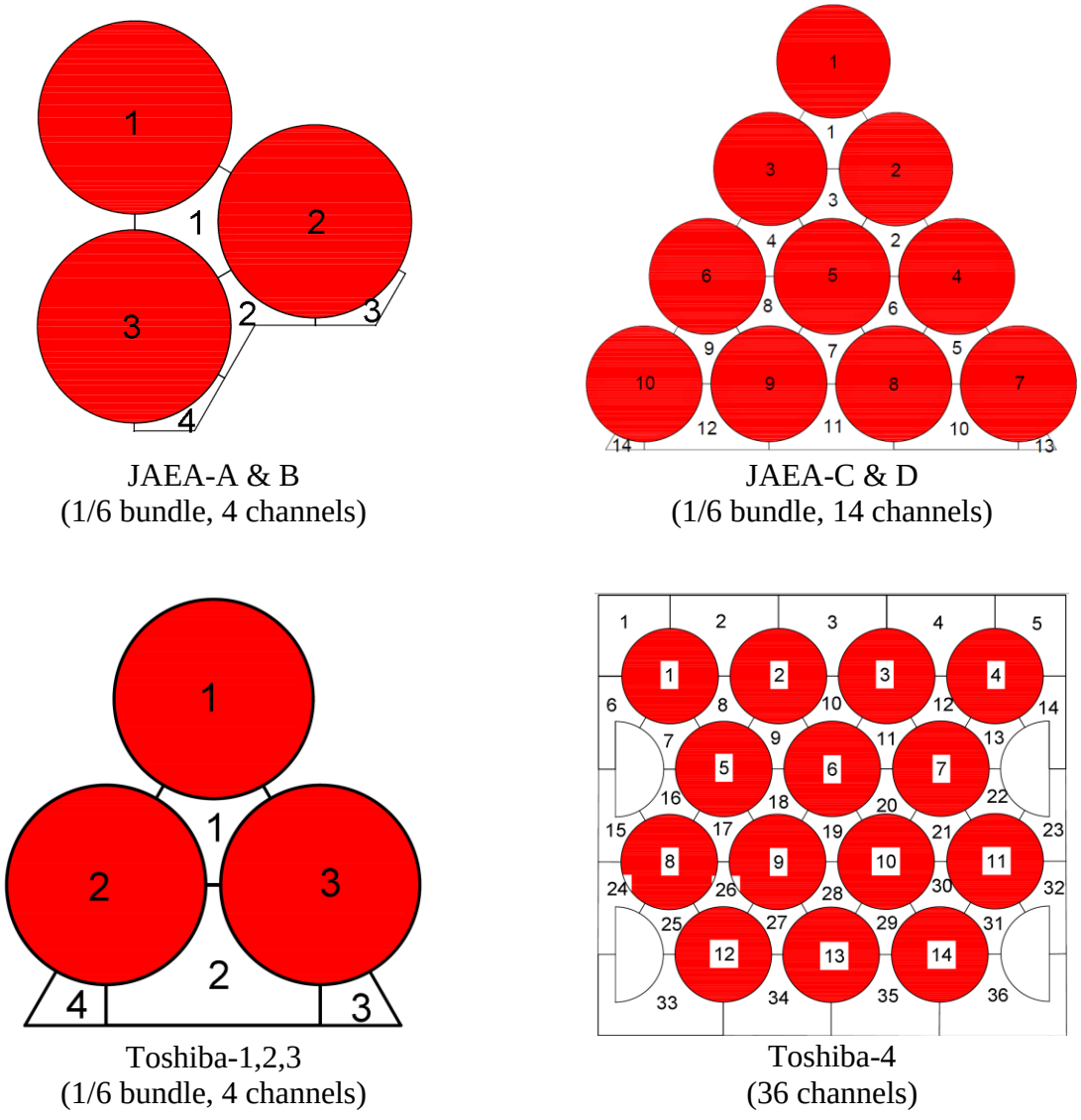

Figure 40. VIPRE-01 tight bundle test sections sub-channel schemes.

Table XI. VIPRE-01 principal constitutive models for tight bundle tests.

Group	Parameter/Correlation	Model/Value
CORR	Void Fraction	Chexal-Lellouche
	Two-phase Friction Multiplier	EPRI; HOMO
	Single-phase Forced Convection Heat Transfer Coefficient	Dittus-Boelter
	Flow Boiling Heat Transfer Coefficient	Chen
MIXX	Turbulent Momentum Factor	0.8 (recommended)
	Turbulent Crossflow	Equation (6)
DRAG	Axial Friction Factor[1]	$f = 94 \times Re^{-1}$ (laminar) $f = 0.15 \times Re^{-0.18}$ (turbulent)
GRID	Local Loss Coefficient	0.5 (JAEA)[2] 0.55 (Toshiba-1) 0.65 (Toshiba-2) 0.75 (Toshiba-3) 0.25 (Toshiba-4)

Based on the selected constitutive models, investigations have been made on the following two input parameters in VIPRE-01: axial noding and radial distribution of grid loss coefficient.

Typical BWR fuel assembly analysis often uses 25 uniform axial nodes, but a higher number (100 nodes for a heated length of 3.7 m) were selected by Brynjell-Rahkola et al. (2009) in order to effectively capture the highly non-uniform APD and other geometric features such as spacer grids. A finer-than-centimeter meshing size would no longer make any physical significance given the uncertainties of thermal-hydraulic models. A uniform axial node length of 3-5 cm is used for the modeling of tight bundles.

The consideration of non-uniform radial grid loss coefficients was assessed in Brynjell-Rahkola et al. (2009), and it was found that the corresponding effect on the void and flow distribution was negligible compared to cases using a constant grid loss coefficient for all channels. This conclusion

[1] *Reference*: Cheng and Todreas (1986) for rod bundle friction factors.

[2] The grid loss coefficient for JAEA-A, B and D rod bundles was not specified in corresponding references. However, based on analysis in section 4.4, the value of 0.5 is reasonable.

is partially applied in our tests depending on the sub-channel configuration of each bundle. For JAEA-A and B bundles, channel No. 3 and 4 are not modeled with spacer grids.

Table XII. VIPRE-01 tight bundles peak-to-average quality ratio (R_f_x) values summary.

Test section	**EPRI** (multiplier)			**HOMO** (multiplier)		
	mean	max	min	mean	max	min
JAEA-A	1.22	1.34	1.14	1.11	1.18	1.08
JAEA-B	1.19	1.30	1.13	1.06	1.13	1.04
JAEA-C	1.49	1.73	1.34	1.42	1.61	1.22
JAEA-D	1.53	1.98	1.37	1.45	1.84	1.28
Toshiba-1	2.95	3.20	2.36	2.71	3.07	2.02
Toshiba-2	2.90	3.81	1.82	2.79	3.62	1.83
Toshiba-3	2.02	2.11	1.77	1.94	2.02	1.75
Toshiba-4	6.47	9.43	4.13	4.80	5.73	3.12

Values for the radial peak-to-average quality ratio (R_f_x) are summarized in Table XII and visualized in Figure 41. As shown, the previous assumption of a constant R_f factor for all the simulated tight bundle data in M2-CISE4 is not appropriate. The EPRI two-phase friction multiplier correlation yields higher R_f_x than the homogeneous model, since the former leads to larger multiplier and higher pressure drops. For some relatively high bundle-averaged critical quality cases, power/heat flux readjustment is necessary to avert peak channel quality overflow in simulation predictions ($x_{peak\ channel} = 1.0$). Sensitivity study reveals that R_f_x is quite insensitive to rod power and mass flux, and thus this approximation is justified. However, the prediction of greater than 1.0 local quality implies that the constitutive models used within VIPRE-01 are not sufficient to accurately model the critical power experiments.

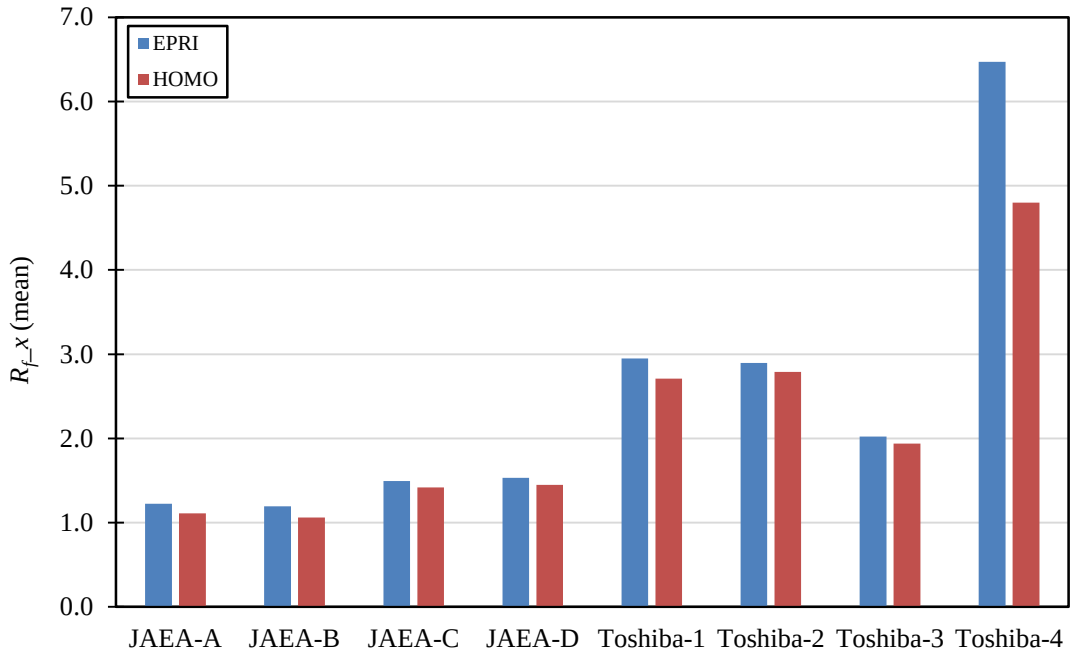

Figure 41. VIPRE-01 tight bundles peak-to-average quality ratio (R_f_x) mean values.

As for the exact flow/quality distribution within each bundle, the JAEA-A & B peak channel is No. 3 (or No. 4), i.e. the corner channel in which the quality is the highest while the mass flux is the lowest, regardless of the radial peaking profile. This is inconsistent with JAEA-A experimental results (Kureta et al., 2002) in which dryout began on the peripheral rod with a flat radial power distribution but switched to the center rod when R_f becomes larger. However, same conclusion was drawn by Nakatsuka et al. (2003) in which the boiling crisis always occurred at the corner channel using improved COBRA-TF sub-channel analysis code by JAERI (Okubo et al., 1993). According to Nakatsuka et al. (2003), the amount of liquid film on the center rod might not be properly evaluated in COBRA-TF, and improvement of the constitutive equations for the tight-lattice configuration was welcome. For instance, with a smaller friction multiplier, the calculated flow distribution would become more uniform, and dryout is more likely to take place in the center channel.

The R_f_x value for each data will be incorporated in the ultimate version of CISE4 based tight bundle critical power correlation, namely M3-CISE4 (Chapter 5), as well as in the mechanistic three-field model (Chapter 6). Sample VIPRE-01 input files for all the eight tight bundle tests are attached in Appendix C.

5. M3-CISE4 Correlation Development and Assessment

5.1. Methodology

The previously developed M2-CISE4 critical quality correlation displayed improvements in tube and annulus data prediction compared to M1-CISE4, but still yields fairly large scatter in tight bundle dryout prediction, as bundle-averaged thermal hydraulic parameters is not capable of effectively capturing the effect of inter-channel turbulent mixing and spacer grids.

As a result, sub-channel analysis using VIPRE-01 has been performed in Chapter 4, and M2-CISE4 will be updated accordingly by replacing the constant radial peaking factor (R_f = 1.1) with data-specific radial peak-to-average quality ratio (R_{f_x}) extracted from VIPRE-01.

The methodology for the development of M3-CISE4 is as follows:

- ✓ Replace the R_f factor in Equation (2) with R_{f_x} (using EPRI or HOMO two-phase friction multiplier model);
- ✓ Calibrate the correlation by modifying exponents on (D_e/D_h) and R_{f_x} terms to fit tight bundle data (average PECP = 1.0) and annulus data as closely as possible (the formulation for tubes is not dependent on these two terms).

5.2. M3-CISE4 Correlation

The up-to-date M3-CISE4 correlation is presented in Equation (9) using EPRI friction multiplier model (in VIPRE-01) and Equation (10) using HOMO friction multiplier model. Its range of validity is the same as that of M2-CISE4, as shown in Table V.

$$\text{EPRI:} \quad x_{cr} = \left(\frac{D_e}{D_h}\right)^{2/3} \times \frac{a \times L_b}{b + L_b} \times R_{f\_}x^{-0.3} \tag{9}$$

$$\text{HOMO:} \quad x_{cr} = \left(\frac{D_e}{D_h}\right)^{2/3} \times \frac{a \times L_b}{b + L_b} \times R_{f\_}x^{-0.38} \tag{10}$$

where

$$a = [1 + 1.481 \times 10^{-4} \left(1 - \frac{P}{P_c}\right)^{-3} G]^{-1} \quad \text{if } G \leq G^*,$$

and

$$a = \left(1 - \frac{P}{P_c}\right) / \left(\frac{G}{1000}\right)^{1/3} \quad \text{if } G > G^*,$$

with

$$G^* = 3375\left(1 - \frac{P}{P_c}\right)^3;$$

$$b = 0.279\left(\frac{P_c}{P} - 1\right)^{0.4} G D_e{}^{1.4}.$$

x_{cr} = critical quality; D_e = hydraulic diameter (m); D_h = heated diameter (m); L_b = boiling length (m); P = exit pressure (MPa); P_c = critical pressure (MPa); G = mass flux (kg/m^2-s); R_f_x = radial peak-to-average quality ratio (from VIPRE-01).

5.3. Results and Discussion

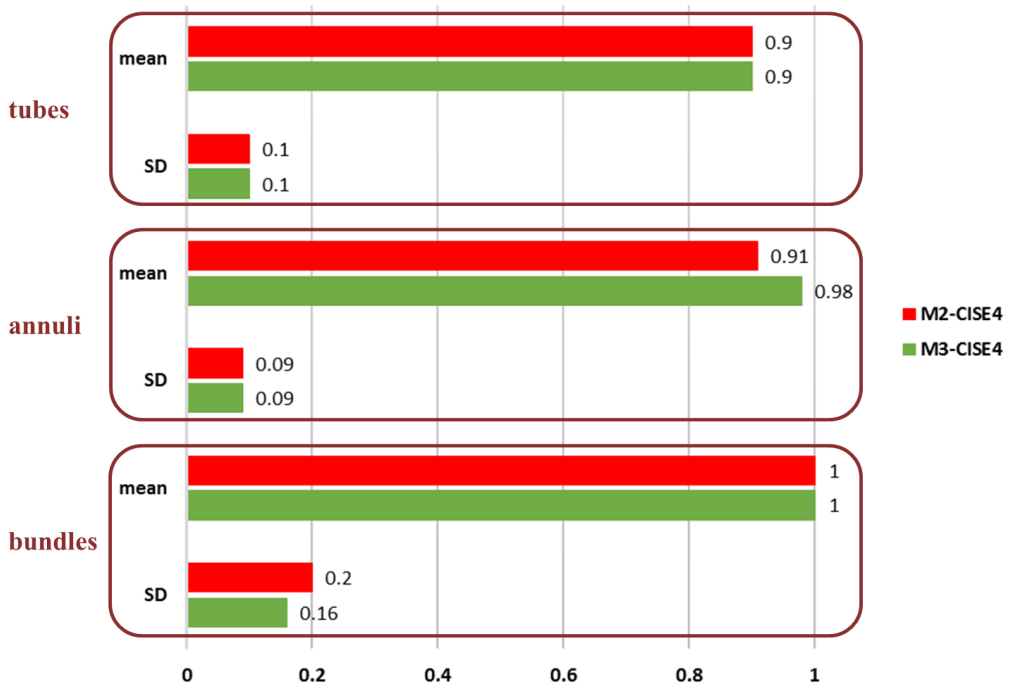

Figure 42. Predicted/experimental critical power (PECP) mean and SD values for tubes, annuli, and tight bundles with M2-CISE4 and M3-CISE4 correlations.

As illustrated in Figure 42, in average M3-CISE4 outperforms its previous version (M2-CISE4) by 7% with respect to annuli data without penalizing the standard deviation. The mean PECP value

for annuli is very close to 1.0 (still slightly conservative), whilst tube dryout prediction performance is unchanged. Moreover, the scatter in tight bundle results is reduced by 4% with M3-CISE4 compared to M2-CISE4, as recapitulated in Table XIII.

Table XIII. PECP mean and SD values for tight bundle test sections with original CISE4, M2-CISE4, and M3-CISE4 correlations.

Correlation		Original CISE4[1]		M2-CISE4		M3-CISE4 (EPRI multiplier)	
Test section		mean	SD	mean	SD	mean	SD
Bundles	JAEA-A	0.72	0.09	0.72	0.09	0.76	0.10
	JAEA-B	1.07	0.12	1.03	0.11	1.10	0.12
	JAEA-C	1.11	0.09	1.02	0.08	1.02	0.06
	JAEA-D	1.19	0.09	1.09	0.08	1.09	0.07
	Toshiba-1	1.28	0.13	1.22	0.10	1.04	0.07
	Toshiba-2	1.27	0.20	1.16	0.16	1.02	0.07
	Toshiba-3	0.97	0.01	0.91	0.02	0.86	0.03
	Toshiba-4	1.49	0.14	1.42	0.12	1.02	0.07
	all bundles	1.06	0.23	1.00	0.20	1.00	0.16

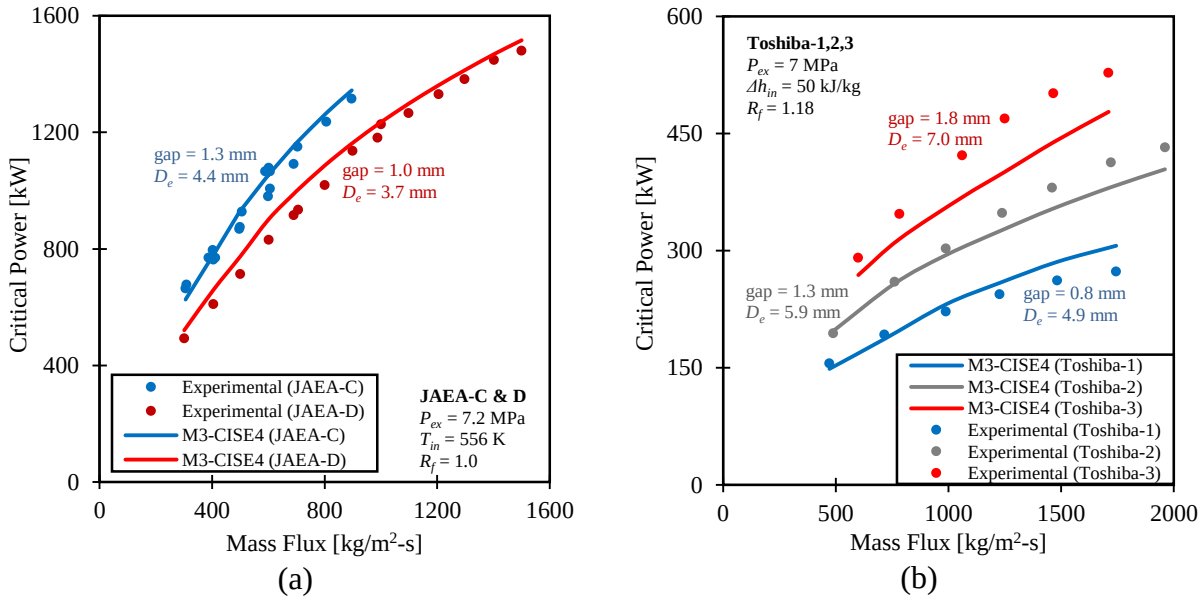

Figure 43. Mass flux and tightness effect on tight bundle critical power (M3-CISE4). (a) JAEA-C & D; (b) Toshiba-1,2,3.

[1] Refer to Todreas and Kazimi (2012) for the formulation of original CISE4.

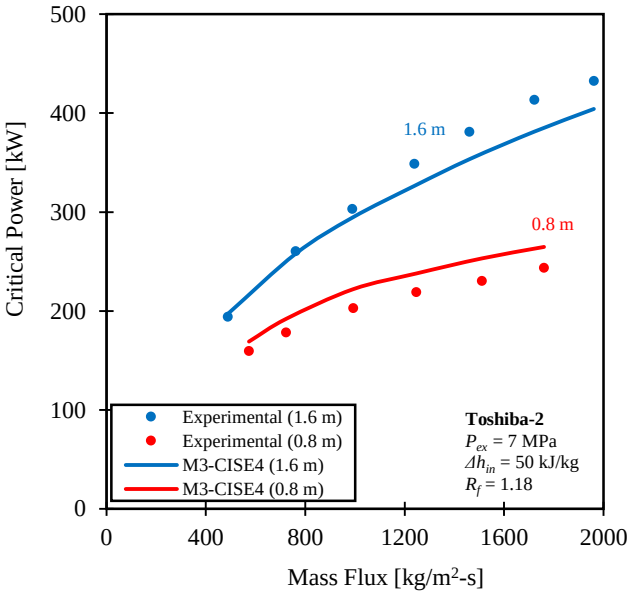

Figure 44. Heated length and APD effect on tight bundle critical power (M3-CISE4).

The M3-CISE4 correlation predicts better quality critical power (reduced scatter), notably for Toshiba-1, 2, and 4 data sets. The effects of bundle tightness, heated length, and axial peaking condition are better captured, as presented in Figure 43 and Figure 44. For Toshiba-2 dryout test in particular, Figure 44 shows much better prediction performance with M3-CISE4 than with M2-CISE4 in Figure 23, since values for the R_f_x factor are very different between the 1.6 m bundle cases (average R_f_x = 2.25 with EPRI multiplier) and the 0.8 m bundle cases (average R_f_x = 3.65 with EPRI multiplier).

Nonetheless, the difference between JAEA-A and B dryout predictions (under-estimation of over 30% for JAEA-A and over-estimation for JAEA-B) remains significant. From JAEA-A to B, the heated length, APD, radial power peaking, and bundle tightness have changed. Unlike the Toshiba-2 test section in which the two bundle configurations (with different lengths and APDs) result in significantly different radial quality peaking factors (R_f_x) as mentioned in the previous paragraph, the sub-channel correction factors between JAEA-A and B are very close (Table XII). Appendix D provides another (approximate) dryout prediction methodology which uses a void fraction criterion in VIPRE-01, and shows similar trend displayed by the two case (JAEA-A & B vs. Toshiba-2). As discussed in section 3.3.4, the difference between uniform (JAEA-A) and double-

humped (JAEA-B) APD profiles can reach up to 15% and is probably unable to be fully captured in sub-channel calculations. VIPRE-01 does not account for enhanced (forced) mixing effect provided by spacers which could further impact the critical power. Besides, discussion in section 4.5 reveals that results given by Nakatsuka et al. (2003) showed similar disagreement between the predictions of the two JAEA test sets. In JAEA-A experiment (Kureta et al., 2002), no thermocouple measuring rod temperatures was positioned on the wall connected to side or corner flow channels, which would lead to inappropriate (overrated) experimental dryout power if the radial quality distribution provided by VIPRE-01 is correct (dryout first occurs in corner channels). Additionally, JAEA-B test (Liu et al., 2004) applied more advanced boiling transition detecting methods (four criteria) than the simple wall temperature rise criterion in JAEA-A (Kureta and Akimoto, 2003). Thermocouple positions in JAEA-B test are unknown, thus no direct conclusion can be drawn on the reliability of the measurements.

5.4. Conclusion

The up-to-date dryout critical power correlation, referred to as M3-CISE4, provides overall high accuracy and high-level of precision when predicting the tubes, annuli, and tight bundles critical power data. Besides one-dimensional bundle-averaged parameters (pressure, mass flux, hydraulic & heated diameter, boiling length), it also contains a sub-channel level parameter – the peak-to-average quality ratio (R_f_x) at the axial location of dryout – in order to model inter-channel mixing and spacer grids, both playing an important role in the evaluation of critical power. The scatter in the PECP values for tight bundles is reduced. Effects of bundle tightness, heated length, radial peaking, and APD are better represented in M3-CISE4 than in its previous versions.

However, the impact of non-uniform APD profile cannot be fully captured by the sub-channel analysis. This could partly explain the difference between JAEA-A and B prediction results. Limitations of modeling in VIPRE-01 (forced mixing, two-phase friction multiplier, etc.) also contribute to the uncertainty of the predicted dryout power. The correctness of measurements may also be challenged due to the positions of thermocouples and different boiling transition detecting criteria between the two test sets.

Another methodology, independent of the empirical CISE4 formulation and namely the three-field model, will be investigated in the next chapter. The RBWR design MCPR will be evaluated in Chapter 7 using both empirical and mechanistic dryout prediction models.

6. Three-Field Model: A Mechanistic Approach

6.1. Introduction

As discussed throughout the thesis, accurate prediction of the dryout critical power is one of the most important missions in BWR type reactor design and safety analysis. This has traditionally been handled by empirical correlations fitted to measurements in electrically heated mock-up rod bundles. Such correlations as CISE4 are widely implemented and largely used in current thermal-hydraulic system codes. However, the simplicity of physical modeling makes them unreliable in certain situations, especially when parameters and working conditions are beyond their validation ranges and when complicated three-dimensional power distributions are present.

During the last three decades, important strides have been made on the mechanistic dryout modeling under typical BWR operating conditions with the ultimate objective to replace empirical correlations. Mechanistic approach in annular flow is referred to as the three-field model (or film flow model). It consists of resolving relevant mass balance equations for each field (liquid film field, entrained droplets field, and vapor field/gas core) within the annular flow regime, up to the film dryout. The three-field model is considered as one of the most promising mathematical tools to accurately predict critical power for tubes, annuli, and BWR fuel bundles, including axially heterogeneous designs.

The model concept is presented in Figure 45 (for a round tube). In annular flow regime, liquid flow flows partly in liquid film adjacent to the wall and partly as droplets in the gas core (vapor). There exists three mass transfer mechanisms: entrainment and deposition of droplets as well as evaporation of liquid film. A set of conservation equations (three) can be expressed to solve for the flow conditions of each field and will be presented in section 6.2. Constitutive relations are needed to close the balance equations system, and will be detailed in section 6.3. In this study, steady-state and constant fluid physical properties are assumed. In section 6.4, results of critical power prediction using the three-field model for tubes, annuli, and tight bundles will be recapitulated and discussed. In tight bundle cases, bundle-averaged parameters are applied.

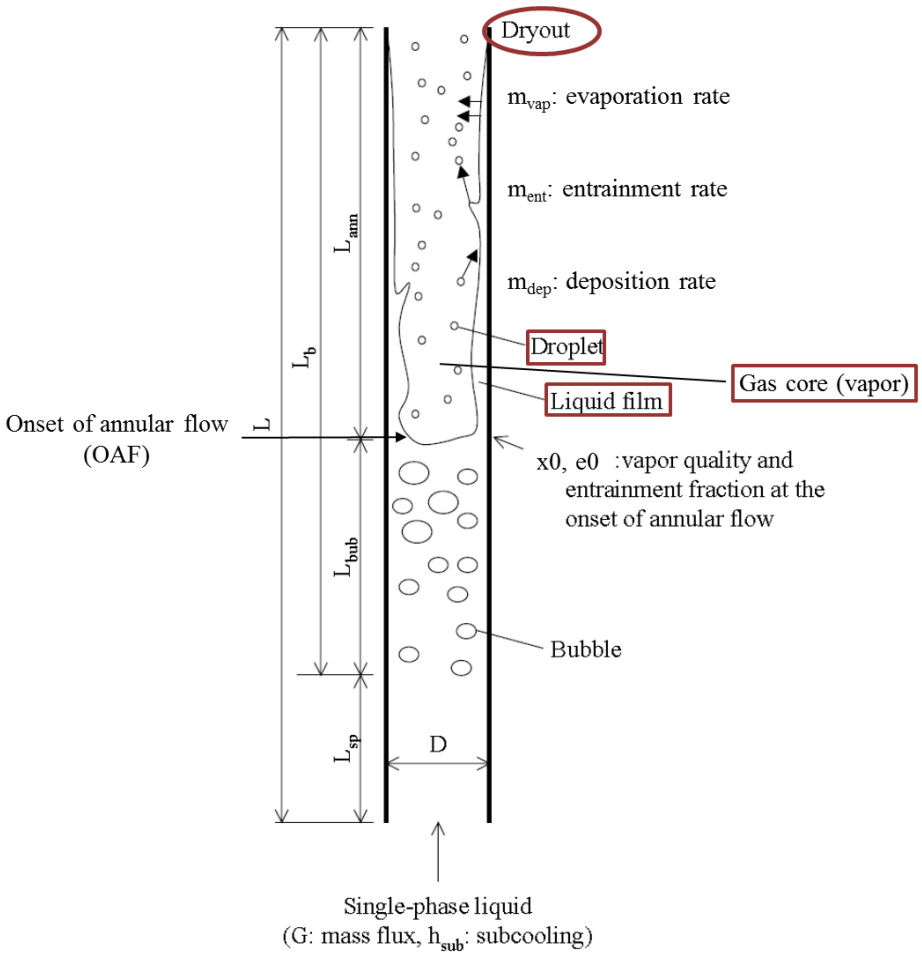

Figure 45. Schematic view[1] of the three-field model (reproduced from Okawa et al., 2003).

6.2. Governing Equations

In a flow channel (tube, annulus, and bundle), conservation of mass can be written for the three fields. The evaporation of droplets into steam is negligible.

Axial variation of film flowrate:

$$\frac{dW_f}{dz} = P_w(m_{dep} - m_{ent} - m_{vap}) \tag{11}$$

[1] The slug/churn flow regime preceding annular flow in the channel is missing here. In fact, interestingly in tight channels the bubbly flow regime may not be present at all and the first regime appearing in the channel is some form of slug flow.

Axial variation of droplet flowrate:

$$\frac{dW_d}{dz} = P_w(m_{ent} - m_{dep}) \tag{12}$$

Axial variation of gas (vapor) flowrate:

$$\frac{dW_g}{dz} = P_w m_{vap} \tag{13}$$

where W_f, W_d, and W_g refer to the mass flowrate of liquid film field, droplet field, and gas core respectively (kg/s); m_{dep}, m_{ent}, and m_{vap} denote the deposition rate, the entrainment rate, and the evaporation rate in the unit of mass flux (kg/m^2-s); P_w is the wetted perimeter (m); z is the upward axial coordinate (m).

The discretized form of the equation set can be written as:

$$\frac{W_f^{i+1} - W_f^i}{\Delta z} = P_w(m_{dep}^i - m_{ent}^i - m_{vap}^i) \tag{14}$$

$$\frac{W_d^{i+1} - W_d^i}{\Delta z} = P_w(m_{ent}^i - m_{dep}^i) \tag{15}$$

$$\frac{W_g^{i+1} - W_g^i}{\Delta z} = P_w m_{vap}^i \tag{16}$$

where Δz is the mesh size (m), and the superscript i denotes the discrete axial node (i = 0 at the onset of annular flow).

6.3. Constitutive Relations

Constitutive relations come from physical or empirical models that are developed and tuned based on separate effects simple geometry (usually round tube) experiments or CFD simulations. They are modifiable and dependent on the application of interest. The closures described in Adamsson and Le Corre (2011) and integrated in the MEFISTO (Mechanistic Film Sub-channel Tool) code

developed by Westinghouse yielded satisfactory prediction of critical power in BWR fuel assemblies. The same formulations, written in Matlab, will be applied in this study, and the model performance will be assessed against the experiments (tubes, annuli, and tight bundles).

6.3.1. Evaporation Rate

The evaporation rate of the liquid film m_{vap} can be calculated by:

$$m_{vap}^{i} = \frac{q^{i}}{h_{fg}} \tag{17}$$

where q is the local heat flux (kW/m^2), and h_{fg} is the latent heat of evaporation (kJ/kg). Liquid and vapor phases are considered to be saturated in diabatic annular flow.

6.3.2. Deposition Rate

The following diffusion equation is used to model the process which controls droplet deposition rate on the liquid film by assuming a net transfer of droplets from high concentration area (gas core) to low concentration area (liquid film):

$$m_{dep}^{i} = k_{dep}^{i} C^{i} \tag{18}$$

where the droplet concentration in gas core C (kg/m^3) is defined as the ratio of mass of all drops to the total volume in which they are contained (i.e. drops + steam), as shown by Equation (19). Assume that the relative velocity (slip) between drops and steam can be neglected. The deposition mass transfer coefficient k_{dep} (m/s) is dependent on C, and various correlations have been established. The model included in Okawa et al. (2003) and Adamsson and Le Corre (2011) is used here due to good agreement with measurements.

$$C^{i} = \frac{W_d^{i}}{\frac{W_d^{i}}{\rho_f} + \frac{W_g^{i}}{\rho_g}} \tag{19}$$

$$k_{dep}^{i} = 0.0632 \left(\frac{C^{i}}{\rho_g}\right)^{-0.5} \Big/ \sqrt{\frac{\rho_g D_e}{\sigma}} \tag{20}$$

ρ is the density (kg/m^3), subscripts f and g refer to saturated liquid and vapor phase, D_e is the hydraulic diameter, σ is the surface tension (N/m).

6.3.3. Entrainment Rate

Various mechanisms come into play concerning the drop formation by entrainment of the liquid film into the gas core, among which breakup of film roll waves due to interfacial shear force is commonly considered as the over-arching driver under BWR conditions. The rate of entrainment is modeled by Adamsson and Le Corre (2011) as:

$$m_{ent}^{i} = k_{ent}^{i}\rho_f(\pi_{ent}^{i})^{n^i} \tag{21}$$

where the non-dimensional entrainment number π_{ent} is expressed as:

$$\pi_{ent}^{i} = \frac{f_i^i \rho_g (J_g^i)^2}{\sigma/\delta^i} \tag{22}$$

The velocity ratio (v_f/v_g) is neglected, and the gas velocity is assumed to be the same as the gas superficial velocity ($v_g = J_g$). f_i is the interfacial friction factor, and when the droplet area in the gas core is neglected, its expression can be found in Equation (23). The liquid film thickness δ in Equation (25) is estimated from the force balance between the interfacial shear force and wall friction force acting on a thin film.

$$f_i^i = 0.005 \times (1 + \frac{75}{A} P_w \delta^i) \tag{23}$$

$$J_g^i = \frac{W_g^i}{A\rho_g} \tag{24}$$

$$\delta^i = (\sqrt{\frac{f_w^i}{f_i^i}\frac{\rho_f}{\rho_g}} + 1)\frac{\rho_g}{\rho_f}\frac{W_f^i}{W_g^i}\frac{A}{P_w} \tag{25}$$

where A denotes the channel area (m^2), f_w is the wall friction factor. In Equation (26), Re_f refers to the film Reynolds number, defined in Equation (27). μ is the dynamic viscosity (kg/m-s).

$$f_w^i = \max(\frac{16}{Re_f^i}, 0.005) \tag{26}$$

$$Re_f^i = \frac{4W_f^i}{\mu_f P_w} \tag{27}$$

Depending on the value of π_{ent}, the empirical constants k_{ent} (m/s) and n in Equation (21) can be obtained as follows:

$$\text{If } \pi_{ent}^i \leq 0.0675, \text{ then } k_{ent}^i = 3.1 \times 10^{-2}, n^i = 2.3; \tag{28}$$

$$\text{If } 0.0675 < \pi_{ent}^i \leq 0.295, \text{ then } k_{ent}^i = 1.6 \times 10^{-3}, n^i = 1.2;$$

$$\text{If } \pi_{ent}^i > 0.295, \text{ then } k_{ent}^i = 6.8 \times 10^{-4}, n^i = 0.5$$

6.3.4. Boundary Conditions

The field mass balance equations (14)-(16) are valid for annular flow only, thus should be integrated from the onset of annular flow (OAF) up to the location of dryout.

Onset of annular flow (OAF)

The transition from slug flow to annular flow is far from clear for researchers. The measurement method can also affect the boundary. One of the most reliable correlations derived from the experimental data is given in Equation (29) and used to determine the point of slug-annular transition.

$$J_g^{*0} = 0.4 + 0.6 J_f^{*0} \tag{29}$$

where the dimensionless superficial velocities J_k^* (subscript k denotes g or f) are defined by:

$$J_k^{*0} = J_k \sqrt{\frac{\rho_k}{gD_e(\rho_f - \rho_g)}} \tag{30}$$

g is the gravitational acceleration (m/s^2). The transition steam quality can be derived from equations (29) and (30):

$$x^0 = \frac{G_g^0}{G} = \frac{0.6+0.4\times\frac{\sqrt{gD_e(\rho_f-\rho_g)\rho_f}}{G}}{0.6+\sqrt{\rho_f/\rho_g}} \quad (31)$$

There exists other methods to determine the OAF. However, a sensitivity study in Adamsson and Le Corre (2011) showed that the exact location of the OAF is of weak importance for the predicted critical power due to relatively long heated lengths.

Moreover, at the elevation where OAF occurs, it is commonly assumed that the deposition and entrainment are in equilibrium, i.e.:

$$m_{dep}^0 = m_{ent}^0 \quad (32)$$

Onset of dryout

The criterion used in Adamsson and Le Corre (2011) and this work for the onset of dryout is to assume complete disappearance of liquid film, i.e. film flowrate/thickness = 0. Other correlations for critical liquid film thickness at dryout can be found in the literature, and it is reported that heat transfer can be deteriorated even when the cross-sectional area-averaged film flowrate is still positive. However, different approaches did not show significant impact on the critical power results. The understanding of the exact physical phenomena leading to film breakup and dry patch formation would be important for a more advanced prediction approach.

6.4. Results and Discussion

Based on the governing equations (section 6.2) and associated closures (section 6.3), critical power can be predicted by adjusting the local heat flux term in Equation (17). Dryout results are compared against experimental data for different geometries, including tubes (Table II), annuli (Table III), as well as tight bundles (Table IV).

6.4.1. Tubes and Annuli

Figure 46 shows the average PECP and associated SD for tubes and annuli with both the latest M3-CISE4 correlation developed in Chapter 5 and the three-field model. It is noticeable that the mechanistic three-field model outperforms the empirical M3-CISE4 notably for the prediction of tube dryout, and the scatter is reduced. While M3-CISE4 gives rise to relatively conservative results, the three-field model predictions agree perfectly (slightly optimistic) with the measurements. It is important to note that unlike the modified CISE4 correlations, the three-field model did not go through any additional tuning when compared against tube and annuli data that were not included in its original validation database.

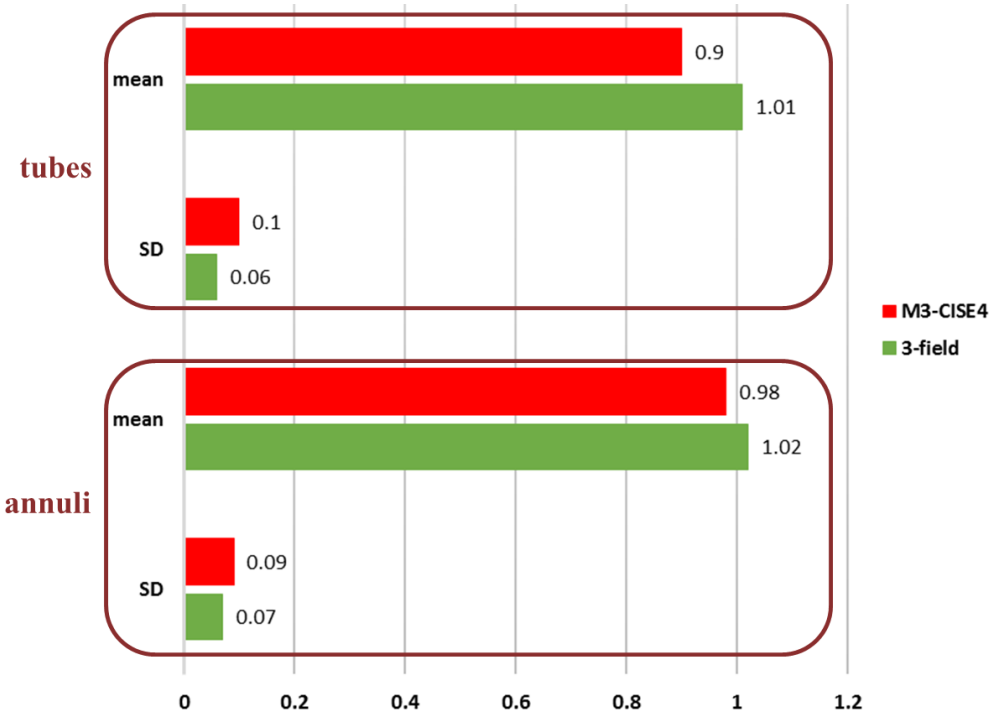

Figure 46. Predicted/experimental critical power (PECP) mean and SD values for tubes and annuli with M3-CISE4 correlation and three-field model.

6.4.2. Tight Bundles

Measurements from the eight tight bundle test sets are correlated by the bundle-averaged one-dimensional three-field model. In the first place, prediction results with no calibration (i.e. without tuning with the R_f_x factor) are presented in Figure 47. Overall, the model over-predicts tight

bundle critical power (mean PECP = 1.33), in particular for Toshiba tests. The scatter in the results is very large (SD = 0.30).

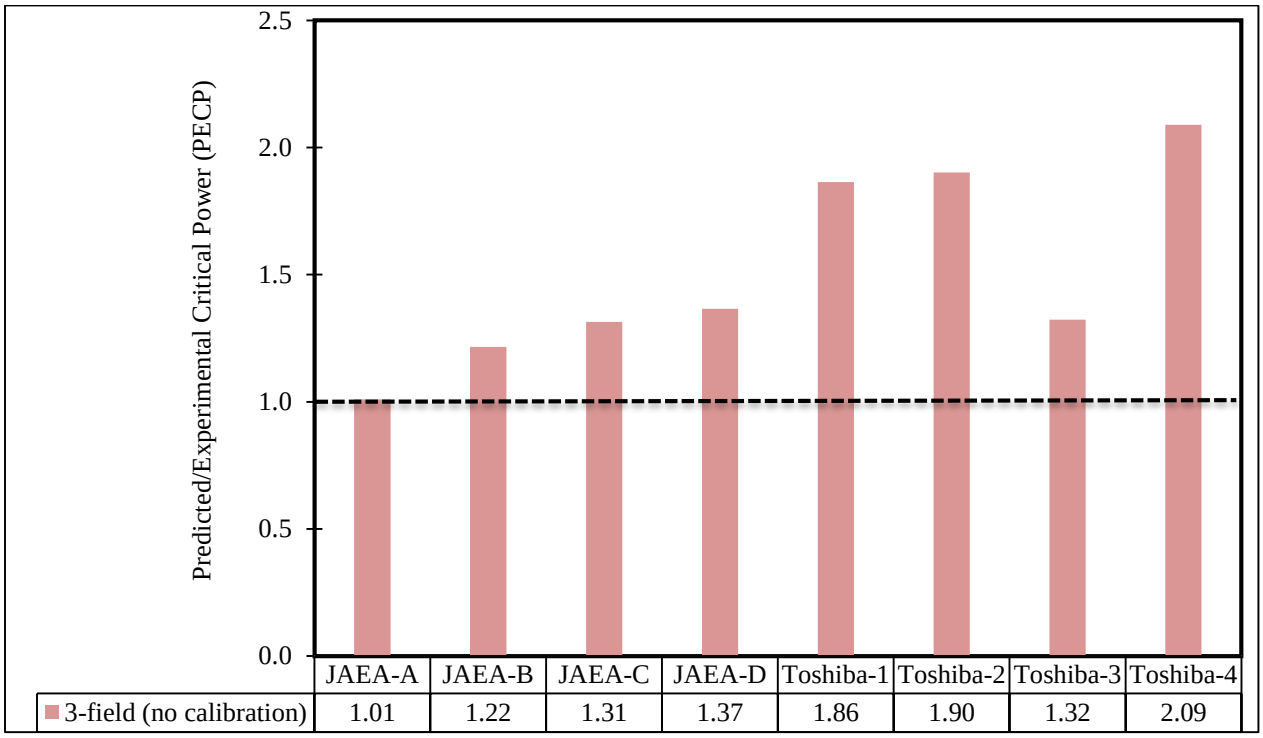

Figure 47. Predicted/experimental critical power (PECP) mean values for tight bundle tests with three-field model (no calibration).

Using the exponent on the radial peak-to-average channel quality ratio (R_f_x) term as a tuning factor to achieve the overall PECP of 1.0, a standard deviation of 0.16 was obtained using the three-field model. Figure 48 plots its performance with regard to each test section and in comparison with M3-CISE4. Results are obtained with the EPRI two-phase friction multiplier model, whilst the homogeneous model yields similar performance and the same level of accuracy (with a slightly different exponent on the R_f_x factor).

The three-field model provides excellent agreement (very slight over-estimation) with JAEA-C and D critical power data. The PECP difference between JAEA-A and B is significantly reduced (from 34% with M3-CISE4 to 20% with three-field model). This may be due to the fact that the mechanistic approach better captures the effect of non-uniform APD, as suggested in Anglart (2010). Concerning Toshiba-1, 2, and 3 data, the divergence between different test sections

becomes much smaller, and the three-field model predictions are relatively conservative. As for Toshiba-4, predicted dryout powers are much lower than measurements. This should be ascribed to the very high and doubtful values for the R_f_x factor (Figure 41) due to its atypical geometry. In the three-field model, the R_f_x factor has a more important weight (exponent = 0.8) than in the M3-CISE4 formulation (exponent = 0.3), since the latter includes a D_e/D_h term aiming to (partially) capture the radial quality distribution and bundle tightness effect in the absence of the sub-channel analysis.

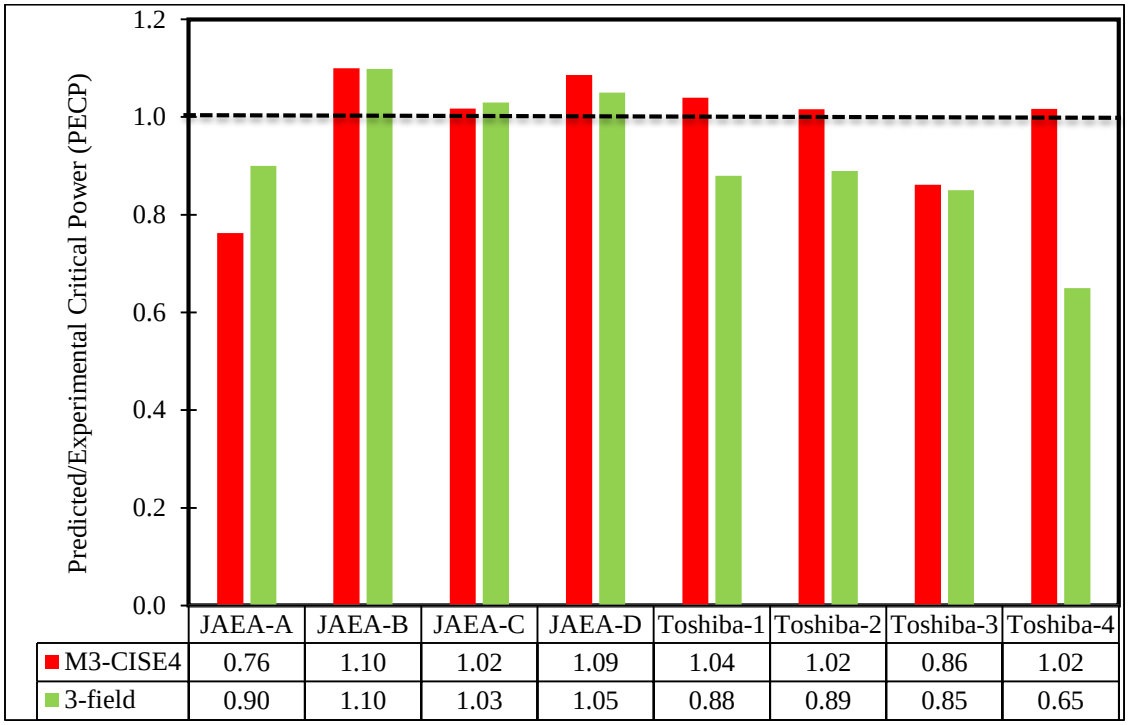

	JAEA-A	JAEA-B	JAEA-C	JAEA-D	Toshiba-1	Toshiba-2	Toshiba-3	Toshiba-4
M3-CISE4	0.76	1.10	1.02	1.09	1.04	1.02	0.86	1.02
3-field	0.90	1.10	1.03	1.05	0.88	0.89	0.85	0.65

Figure 48. Predicted/experimental critical power (PECP) mean values for tight bundle tests with M3-CISE4 correlation and three-field model.

6.5. Conclusion

With the use of the three-field model made up of equations and closures described in this chapter, accurate prediction of dryout can be achieved for tubes and annuli. Similar conclusion can be drawn for tight bundles, even though the standard deviation is not further reduced compared to the empirical M3-CISE4 correlation and results for Toshiba-4 are inadequate.

One of the main influencing factors not being accounted for in this analysis is the spacer grid effect, usually seen as a local enhancing effect on the droplet deposition rate due to turbulence enhancement downstream the grids. A multiplier representative of such effect was added on the standard (without enhancement) deposition rate model in Adamsson and Le Corre (2011), though a calibration process is required to tune the spacer effect based on experimental data, as the effect is highly complex and dependent on the details of specific spacer designs. Since the RBWR features relatively low mass fluxes, the spacer factor is expected to be not significant.

Different constitutive relations could be investigated, in particular for the rates of deposition and entrainment. It is worthwhile to note that the liquid film boiling induced droplet entrainment, if not comparable to the wave breakup mechanism, is the second entrainment driving force and may become more important with higher heat fluxes and shorter channels than in conventional BWR bundles, which is the case of an RBWR.

The onset of annular flow location is shown to be of little importance if the channel length is long enough. In a tighter and shorter bundle than typical BWRs, sensitivity study reveals that a different slug-annular transition criterion does not dramatically alter the predicted critical power: if Equation (29) is replaced with $J_g^{*0} = 1$ as recommended by Hewitt and Govan (1990), the predicted dryout power is lower by less than 5%.

The dryout may occur before the liquid film completely vanishes, since the film is wavy and dry spots may appear triggering dryout, and also the local heat flux may destabilize the film and break it up. However, various models and correlations did not lead to different critical power results, and the criterion of zero film flowrate is applied, hence eliminating otherwise uncertainties of an empirical model.

The major issue with picking a different set of constitutive relations is that all these closures may provide perfect results for some conditions while being significantly biased for others. The models applied in this thesis (section 6.3, which are the same as in MEFISTO code) yield accurate tube and annulus dryout predictions as well as very satisfactory results for most of the tight bundle

cases. The inadequate Toshiba-4 predicted critical power should be (mainly) due to the lack of reliability in VIPRE-01 when it deals with such an irregular configuration.

Last but not least, the sub-channel level three-field model, as described in Adamsson and Le Corre (2011), will account for film cross-flow effects and eliminate the need for a R_f_x factor, and might provide even better tight bundle dryout prediction than the one-dimensional model investigated in the thesis.

7. MCPR Evaluation of RBWR Designs

The ultimate objective of the tight bundle critical power prediction investigation is to evaluate the Minimum Critical Power Ratio (MCPR) of the RBWR based on appropriate models (CISE4 based correlations, three-field model, and CHF look-up table). In order to maintain the integrity of fuel cladding, the MCPR should be ensured to remain above the steady-state design limit value of 1.3 which covers 0.1 for uncertainty in data and 0.2 for margin against transients.

The two selected RBWR designs, AC and TB2, have their thermal-hydraulic design parameters presented in Table I. In the first place, three CISE4 based correlations (original CISE4, M1-CISE4, and M2-CISE4) and the CHF look-up table are applied on the peak assembly (note the core radial power peaking factor of 1.3 for AC and 1.2 for TB2), and results are shown in Table XIV. The methodology applied in the look-up table approach is described in Kolev (2007) except that: (1) the dryout crisis is not assumed to occur at the exit of the hot bundle, but at the end of the upper fissile zone; (2) the same bundle geometry factor (D_e/D_h) as in the M2-CISE4 formulation is taken into account.

Table XIV. Critical quality and MCPR evaluation of RBWR-AC and RBWR-TB2 with four different models.

Design	RBWR-AC				RBWR-TB2			
Flow rate	Nominal		120%[1]		Nominal		120%	
Correlation	x_{cr}	MCPR	x_{cr}	MCPR	x_{cr}	MCPR	x_{cr}	MCPR
Original CISE4	0.59	1.13	0.55	1.26	0.65	1.30	0.60	1.46
M1-CISE4	0.55	1.06	0.50	1.15	0.58	1.16	0.53	1.28
M2-CISE4	0.53	1.01	0.48	1.11	0.57	1.15	0.53	1.28
Look-up table	0.71	1.35	0.63	1.43	0.59	1.19	0.55	1.34

As presented in Table XIV, the predicted critical quality and MCPR values by M1-CISE4 and M2-CISE4 correlations are very close, especially for RBWR-TB2. The original CISE4 yields relatively optimistic prediction. The look-up table method predicts much higher results for RBWR-AC

[1] In an RBWR, the coolant flow rate in the hot assembly is designed to be 1.2 times the average flow rate.

compared to CISE4, but similar values for TB2 as the local heat flux values are used. The RBWR-TB2 upper fissile zone maximum axial peaking at the beginning of cycle (BOC) is over twice as much as that of AC, as shown in Figure 4. The applicability of CHF look-up table for rod bundle geometry and more specifically for tight lattice bundles remains to be verified. A tentative conclusion is that typical BWR MCPR limit of 1.3 is not achieved by either design with the first two modified versions of CISE4 correlation.

The up-to-date and improved M3-CISE4 correlation as well as the three-field model will be used to evaluate the MCPR of RBWR-TB2, final candidate of the Hitachi project. Sub-channel modeling is performed in VIPRE-01, and its scheme (1/6 bundle, 134 channels) is presented in Figure 49. Rod-to-rod gap is 2.17 mm, and rod-to-box gap is 1.69 mm. Both flat and center-peak (R_f = 1.1) radial peaking conditions are investigated. Spacer grids are modeled.

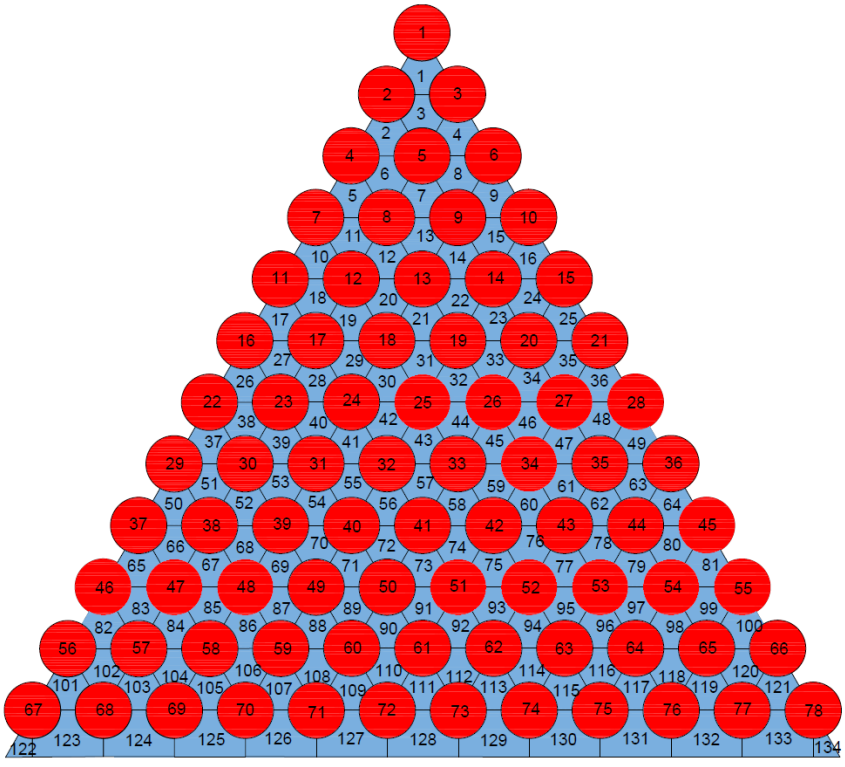

Figure 49. RBWR-TB2 bundle sub-channel scheme.

The EPRI and HOMO friction multiplier models result in very close critical quality and MCPR values, hence only EPRI results are presented. The R_f_x factor is equal to 1.09 for a flat bundle

and 1.25 for a center-peak radial peaking bundle (which is the limiting value as the peak quality channel is at the center), regardless of the flow condition (insensitive for a change of 20% in mass flux).

Table XV. Critical quality and MCPR evaluation of RBWR-TB2 with M3-CISE4 correlation and three-field model.

Design	**RBWR-TB2**							
Flow rate	**Nominal**				**120%**			
Radial peaking	**Flat**		**Center-peak**		**Flat**		**Center-peak**	
Correlation	**x_{cr}**	**MCPR**	**x_{cr}**	**MCPR**	**x_{cr}**	**MCPR**	**x_{cr}**	**MCPR**
M3-CISE4	0.62	1.24	0.59	1.19	0.57	1.39	0.55	1.33
Three-field model	0.81	1.60	0.72	1.44	0.79	1.85	0.70	1.63

As shown in Table XV, the M3-CISE4 correlation yields higher MCPR values than its previous versions (Table XIV), and the design limit is achieved at 120% coolant flow rate (which is the case in the RBWR hot assembly). The three-field model gives rise to remarkably higher critical quality and MCPR results, and shows comfortable margins to the 1.3 limit. As suggested in Liu et al. (2007) and from tube PECP results[1], the critical power prediction with CISE4 based correlations tends to be conservative when the tight bundle is extended from experimental test size to the real 397-rod geometry (RBWR-TB2).

Table XVI. Sensitivity of MCPR for RBWR-TB2 with M3-CISE4 correlation and three-field model to design parameters.

Design	**RBWR-TB2**				
Parameter	**Power (core)**	**Mass Flux (hot assembly)**	***R_f_x* (center peak)**	**MCPR (M3-CISE4)**	**MCPR (3-field)**
Initial Parameters	3926 MW	688 kg/m^2-s	1.25	1.33	1.63
Power Change	110%	-	-	91%	91%
Flow Change	-	95%	-	97%	96%
R_f_x Change	-	-	112%	97%	92%
All Changes	110%	95%	112%	86%	80%
Final Parameters	4319 MW	653 kg/m^2-s	1.40	1.14	1.30

[1] Tube geometry is closest to the RBWR bundle in terms of tightness (1.0 for tubes and 0.93 for RBWR).

Table XVI presents the sensitivity of the RBWR-TB2 MCPR value to design parameters (power, flow, and radial quality peaking factor) using M3-CISE4 and three-field model in order to account for assumed engineering uncertainties. A 10% higher power, 5% lower flow rate, combined with 12% higher radial peak-to-average quality ratio would lead to 14% MCPR downgrade with M3-CISE4 and 20% with three-field model.

The VIPRE-01 input file for the RBWR-TB2 bundle (center-peak, EPRI multiplier) is attached in Appendix E.

8. Summary, Conclusions, and Future Work

8.1. Summary and Conclusions

The thesis investigates unique features of the dryout critical power in an axially heterogeneous tight lattice bundle and provides best-estimate prediction approaches (M3-CISE4 correlation and three-field model) which can be applied on the RBWR design.

Based on the assessment of the previously derived M1-CISE4 correlation against over 1350 critical power data with tube, annulus, and tight bundle geometries that are representative of the RBWR flow characteristics, an updated correlation, M2-CISE4, is developed to improve the prediction with regard to tube and annulus geometry. These data are integrated in our database for a better understanding of different parameter effects and calibration of updated models. Tubes are the closest to the RBWR geometry in terms of tightness (1.0 for tubes and 0.93 for RBWR); annuli have the same hydraulic-over-heated-diameter term as appeared in rod bundles (though its value is quite different from that in bundles), and some of the selected test sections include non-uniform APD profiles.

The key parameters that influence critical power are identified through the assessment of M2-CISE4, and such effects as inter-channel mixing and spacer grids can be captured only via sub-channel analysis with the code VIPRE-01. The applicability of VIPRE-01 for tight bundle configuration has been verified under single-phase and two-phase flow conditions, and intra-assembly radial quality distribution profiles have been retrieved for the eight tight bundle test sections. For the selected test cases, in single-phase VIPRE-01 results agree perfectly with CFD solutions, whereas in two-phase VIPRE-01 results match well with measurements and NASCA code values on center (peak) channels but show disagreements on peripheral channels. Further benchmark requires more sub-channel level data.

The critical power correlation is further updated and improved, and the up-to-date M3-CISE4 includes data-specific radial peak-to-average quality ratio (R_{f_x}) term extracted from sub-channel analysis for the tight bundle tests by JAEA and Toshiba. As a result, M3-CISE4 is able to outperform its previous versions by improving annuli dryout prediction and reducing the spread in

tight bundle results. The effects of bundle tightness, heated length, and axial peaking condition are better captured. However, the impact of non-uniform axial power distribution may not be fully represented by the M3-CISE4 formulation, even though the magnitude of the impact should be less than 15% (section 3.3.4).

The mechanistic dryout modeling approach in annular flow regime, namely three-field model, has also been investigated for all the three geometries (tube, annulus, tight bundle). This model yields excellent agreement with measured results for tubes and annuli, while tight bundle dryout prediction scatter is at the same level as M3-CISE4. The effect of non-uniform axial peaking is better captured, since local heat flux is part of the calculations. Among the eight tight bundle test sections, JAEA-C and D sets are the closest in configuration (bundle geometry and tightness, APD profile, radial peaking) to the RBWR design, and their predicted critical power results match very well with experimental data by both M3-CISE4 and three-field model.

Finally, the MCPR of the RBWR has been evaluated based on models investigated in the thesis. While the typical BWR steady-state design limit of 1.3 is not achieved with the first two modified versions of CISE4 correlation (M1 and M2-CISE4), M3-CISE4 yields slightly higher than 1.3 value for MCPR. The three-field model predicts more comfortable margins for the RBWR-TB2.

8.2. Recommendations for Future Work

Despite improvements in the critical power prediction shown in this work, there is still room to further improve the performance of critical power prediction models, both the empirical M3-CISE4 and mechanistic three-field.

More experimental data of tight bundles are necessary to help calibrate correlations. On the other hand, new independent critical power database is required for the validation of M3-CISE4 as well as bundle-averaged three-field model and to judge whether or not these models are decently predictive. The availability of original data instead of those extracted from published papers is vital to the dryout prediction accuracy. Critical power experiments should ideally use similar bundle geometry as in an RBWR (hydraulic diameter, bundle tightness, channel box shape, heated

length, spacer grids configuration, etc.) and apply similar operation conditions (pressure, mass velocity, inlet condition, APD, etc.) with sensitivity survey. Measurements of sub-channel void fraction will allow a more reliable validation of VIPRE-01 for tight bundle applications. If possible, thermocouples should be positioned on not only center rods but also peripheral rods facing side and corner sub-channels such that the radial location of dryout will not be contested.

In the critical quality - boiling length formulation (e.g. CISE4), a sensitivity study on the impact of boiling length starting point is recommended. It is commonly considered that the boiling length starts at the elevation of onset of nucleate boiling (or onset of saturated boiling). However, Yang et al. (2006) suggested that a boiling length starting from other elevations such as the onset of annular flow point might result in smaller dryout prediction errors.

Constitutive models (in particular void/quality relation, two-phase friction multiplier model, and turbulent mixing settings) in VIPRE-01, as well as closure terms in the three-field model (in particular spacer enhanced deposition and film boiling induced entrainment rates) require future investigations to be more representative of tight bundle features.

A more advanced approach coupling local channel flow conditions and the three-field model (sub-channel level three-field model) offers potentials for a more accurate prediction of dryout critical power in axially heterogeneous tight bundle designs.

Appendix A: VIPRE-01 Single-Phase Benchmark Input Files

Test case #1:

```
1,0,0,1,0                                                    *vipre.1
JAEA 14-rod bundle (Kureta 2008)                             *vipre.2
*
*
geom,10,10,10,0,0,0                                          *geom.1
0.3,0.0,0.5                                                  *geom.2
1,11.8499e-6,10.7521e-3,10.7521e-3,1,3,0.0013,7.5187e-3,     *geom.4
2,23.6999e-6,21.5042e-3,21.5042e-3,2,3,0.0013,8.6580e-3,7,0.0013,9.9673e-3,
3,23.6999e-6,21.5042e-3,21.5042e-3,1,4,0.0013,8.6366e-3,
4,23.6999e-6,21.5042e-3,21.5042e-3,2,5,0.0013,7.5203e-3,8,0.0013,10.027e-3,
5,11.8499e-6,10.7521e-3,10.7521e-3,1,10,0.00065,9.9913e-3,
6,5.4999e-6,8.1133e-3,3.5840e-3,1,7,0.0010,9.9053e-3,
7,43.9984e-6,36.4942e-3,21.5042e-3,1,8,0.0010,14.958e-3,
8,43.9984e-6,36.4942e-3,21.5042e-3,1,9,0.0010,11.154e-3,
9,10.9997e-6,16.2267e-3,7.1681e-3,1,10,0.0010,8.9040e-3,
10,21.9992e-6,18.2471e-3,10.7521e-3
*
*
prop,0,1,2,1                                                 *prop.1
*
*
rods,1,5,0,1,0,0,0,0,0,0,0,0                                 *rods.1
0.24,0.03,0,0                                                *rods.2
4                                                            *rods.3
0.0,0.0,0.0001,1.0,0.2399,1.0,0.24,0.0                       *rods.4
*
*rods geometry input                                         *rods.9
1,1,1.,1,1,0.1667,2,0.1667,3,0.1667,
2,1,1.,1,2,0.1667,7,0.25,6,0.0833,
3,1,1.,1,1,0.0833,3,0.1667,5,0.0833,4,0.1667,
4,1,1.,1,2,0.1667,3,0.1667,7,0.25,4,0.1667,8,0.25,
5,1,1.,1,4,0.1667,5,0.1667,8,0.25,10,0.25,9,0.1667,
0
*
1,dumy,13.69e-3,0.0,0                                        *rods.68
*
*
oper,1,2,0,1,0,1,0,0,0,0                                     *oper.1
-1.0,0.0,0.0,0.0,                                            *oper.2
0                                                            *oper.3
7200000,558.15,1000.0,0.0,0.0                                *oper.5
```

```
0                                                    *oper.12
*
*
corr,0,2,0                                           *corr.1
chll,chll,homo,none                                  *corr.2
ditb,chen,chen,epri,cond,g5.7,0                      *corr.6
1,0,0.0                                              *corr.16
*
*
drag,1,0,0                                           *drag1
0.316,-0.25,0.,94.0485,-1.,0.                        *drag2
0.5,0                                                *drag5
*
*
cont                                                 *cont.1
0.0,0,200,750,2,2,0,0                                *cont.2
0.1,0.00001,0.001,0.05,0.01,0.9,1.5,1.0              *cont.3
0,0,0,0,0,0,1,1,0,0,0,1,0,2,0                        *cont.6
100.,0,0,0,0,0                                       *cont.7
*
*
endd
0
```

Test case #2: (adiabatic, mixing coefficient β = 0.01)

```
1,0,0,1,0                                                    *vipre.1
Toshiba-1 7-rod bundle (Yamamoto 2006) 500mm                 *vipre.2
*
*
geom,4,4,10,0,0,0                                            *geom.1
0.5,0.0,0.5                                                  *geom.2
1,12.4618e-6,16.9646e-3,16.9646e-3,1,2,0.0008,8.7898e-3,     *geom.4
2,42.4032e-6,28.5646e-3,16.9646e-3,2,3,2.2041e-3,7.7782e-3,4,2.2041e-3,7.7905e-3,
3,9.0578e-6,7.2177e-3,2.8274e-3,0,
4,9.0578e-6,7.2177e-3,2.8274e-3,0
*
*
prop,0,1,2,1                                                 *prop.1
*
*
rods,1,3,0,1,0,0,0,0,0,0,0,0                                 *rods.1
0.5,0.0,0,0                                                  *rods.2
4                                                            *rods.3
0.0,0.0,0.00001,1.0,0.49999,1.0,0.5,0.0                      *rods.4
*
*rods geometry input                                         *rods.9
1,1,1.18,1,1,0.1667,
2,1,0.97,1,1,0.1667,2,0.25,4,0.0833,
3,1,0.97,1,1,0.1667,2,0.25,3,0.0833,
0
*
1,dumy,10.8e-3,0.0,0                                         *rods.68
*
*
oper,1,2,0,1,0,1,0,0,0,0                                     *oper.1
-1.0,0.0,0.0,0.0,                                            *oper.2
0                                                            *oper.3
7200000,558.15,1000.0,0.0,0.0                                *oper.5
0                                                            *oper.12
*
*
corr,0,2,0                                                   *corr.1
chll,chll,homo,none                                          *corr.2
ditb,chen,chen,epri,cond,g5.7,0                              *corr.6
1,0,0.0                                                      *corr.16
*
*
mixx,0,0,0                                                   *mixx.1
0.8,0.01,0.0                                                 *mixx.2
```

```
*
*
drag,1,0,0                                  *drag1
0.316,-0.25,0.,94.0485,-1.,0.               *drag2
0.5                                         *drag5
*
*
cont                                        *cont.1
0.0,0,200,750,2,2,0,0                       *cont.2
0.1,0.00001,0.001,0.05,0.01,0.9,1.5,1.0     *cont.3
0,0,0,0,0,0,1,1,0,0,0,1,0,2,0               *cont.6
100.,0,0,0,0,0                              *cont.7
*
*
endd
0
```

Appendix B: VIPRE-01 Two-Phase Benchmark Input Files

Test case #1:

```
1,0,0,1,0                                                    *vipre.1
JAEA 14-rod bundle (Kureta 2008)                             *vipre.2
*
*
geom,10,10,20,0,0,0                                          *geom.1
0.3,0.0,0.5                                                  *geom.2
1,11.8499e-6,10.7521e-3,10.7521e-3,1,3,0.0013,7.5187e-3,     *geom.4
2,23.6999e-6,21.5042e-3,21.5042e-3,2,3,0.0013,8.6580e-3,7,0.0013,9.9673e-3,
3,23.6999e-6,21.5042e-3,21.5042e-3,1,4,0.0013,8.6366e-3,
4,23.6999e-6,21.5042e-3,21.5042e-3,2,5,0.0013,7.5203e-3,8,0.0013,10.027e-3,
5,11.8499e-6,10.7521e-3,10.7521e-3,1,10,0.00065,9.9913e-3,
6,5.4999e-6,8.1133e-3,3.5840e-3,1,7,0.0010,9.9053e-3,
7,43.9984e-6,36.4942e-3,21.5042e-3,1,8,0.0010,14.958e-3,
8,43.9984e-6,36.4942e-3,21.5042e-3,1,9,0.0010,11.154e-3,
9,10.9997e-6,16.2267e-3,7.1681e-3,1,10,0.0010,8.9040e-3,
10,21.9992e-6,18.2471e-3,10.7521e-3
*
*
prop,0,1,2,1                                                 *prop.1
*
*
rods,1,5,0,1,0,0,0,0,0,0,0,0                                 *rods.1
0.24,0.03,0,0                                                *rods.2
2                                                            *rods.3
0.0,1.0,0.24,1.0                                             *rods.4
*rods geometry input                                         *rods.9
1,1,1.,1,1,0.1667,2,0.1667,3,0.1667,
2,1,1.,1,2,0.1667,7,0.25,6,0.0833,
3,1,1.,1,1,0.0833,3,0.1667,5,0.0833,4,0.1667,
4,1,1.,1,2,0.1667,3,0.1667,7,0.25,4,0.1667,8,0.25,
5,1,1.,1,4,0.1667,5,0.1667,8,0.25,10,0.25,9,0.1667,
0
1,dumy,13.69e-3,0.0,0                                        *rods.68
*
*
oper,1,2,0,1,0,1,0,0,0,0                                     *oper.1
-1.0,0.0,0.0,0.0,                                            *oper.2
0                                                            *oper.3
100000,363.15,382.0,1.7857,0.0                               *oper.5
0                                                            *oper.12
*
```

```
*
corr,0,2,0                                  *corr.1
chll,chll,homo,none                         *corr.2
ditb,chen,chen,epri,cond,g5.7,0             *corr.6
1,0,0.0                                     *corr.16
*
*
mixx,3,0,0                                  *mixx.1
0.8,0.035,-0.1                              *mixx.2
*
*
drag,1,0,0                                  *drag1
0.15139,-0.18,0.,94.0485,-1.,0.             *drag2
0.5                                         *drag5
*
*
grid,0,1                                    *grid.1
0.5                                         *grid.2
-1,2                                        *grid.4
0.0,1,0.28,1                                *grid.6
0
*
*
cont                                        *cont.1
0.0,0,100,750,2,2,0,0                       *cont.2
0.1,0.00001,0.001,0.05,0.01,0.9,1.5,1.0     *cont.3
0,0,0,0,0,0,1,1,0,0,0,1,0,2,0               *cont.6
100.,0,0,0,0,0                              *cont.7
*
*
endd
0
```

Test case #2: (side peak)

```
1,0,0,1,0                                                    *vipre.1
JAEA-C 37-rod bundle (Liu 2007)                              *vipre.2
*
*
geom,14,14,50,0,0,0                                          *geom.1
1.26,0.0,0.5                                                 *geom.2
1,22.1806e-6,20.4204e-3,20.4204e-3,1,3,1.3e-3,8.0499e-3,     *geom.4
2,22.1806e-6,20.4204e-3,20.4204e-3,2,3,1.3e-3,8.1668e-3,6,1.3e-3,8.2581e-3,
3,22.1806e-6,20.4204e-3,20.4204e-3,1,4,1.3e-3,8.3782e-3,
4,22.1806e-6,20.4204e-3,20.4204e-3,1,8,1.3e-3,8.2801e-3,
5,22.1806e-6,20.4204e-3,20.4204e-3,2,6,1.3e-3,8.1951e-3,10,1.3e-3,9.5826e-3,
6,22.1806e-6,20.4204e-3,20.4204e-3,1,7,1.3e-3,8.3525e-3,
7,22.1806e-6,20.4204e-3,20.4204e-3,2,8,1.3e-3,8.2011e-3,11,1.3e-3,9.5812e-3,
8,22.1806e-6,20.4204e-3,20.4204e-3,1,9,1.3e-3,8.3481e-3,
9,22.1806e-6,20.4204e-3,20.4204e-3,1,12,1.3e-3,9.5899e-3,
10,41.5989e-6,34.7204e-3,20.4204e-3,2,11,1.05e-3,14.2983e-3,13,1.05e-3,9.4566e-3,
11,41.5989e-6,34.7204e-3,20.4204e-3,1,12,1.05e-3,14.2897e-3,
12,41.5989e-6,34.7204e-3,20.4204e-3,1,14,1.05e-3,9.5151e-3,
13,5.3942e-6,7.7624e-3,3.4034e-3,
14,5.3942e-6,7.7624e-3,3.4034e-3
*
*
prop,0,1,2,1                                                 *prop.1
*
*
rods,1,10,0,1,0,0,0,0,0,0,0                                  *rods.1
1.26,0.0,0,0                                                 *rods.2
24                                                           *rods.3
0.0,0.315,0.108,0.315,0.10800001,0.492,0.165,0.492,          *rods.4
0.16500001,0.617,0.253,0.617,0.25300001,2.235,0.472,2.235,
0.47200001,0.547,0.778,0.547,0.77800001,2.179,0.861,2.179,
0.86100001,2.102,0.908,2.102,0.90800001,1.975,0.959,1.975,
0.95900001,1.848,0.991,1.848,0.99100001,0.353,1.076,0.353,
1.07600001,0.201,1.133,0.201,1.13300001,0.174,1.260,0.174
*
*rods geometry input                                          *rods.9
1,1,0.8726,1,1,0.1667,
2,1,0.8726,1,1,0.1667,2,0.1667,3,0.1667,
3,1,0.8726,1,1,0.1667,3,0.1667,4,0.1667,
4,1,0.8726,1,2,0.1667,5,0.1667,6,0.1667,
5,1,0.8726,1,2,0.1667,3,0.1667,4,0.1667,6,0.1667,7,0.1667,8,0.1667,
6,1,0.8726,1,4,0.1667,8,0.1667,9,0.1667,
7,1,1.1344,1,5,0.1667,10,0.25,13,0.0833,
8,1,1.1344,1,5,0.1667,6,0.1667,7,0.1667,10,0.25,11,0.25,
```

```
9,1,1.1344,1,7,0.1667,8,0.1667,9,0.1667,11,0.25,12,0.25,
10,1,1.1344,1,9,0.1667,12,0.25,14,0.0833,
0
*
1,dumy,13.0e-3,0.0,0                                    *rods.68
*
*
oper,1,2,0,2,0,1,0,0,0,0                                *oper.1
-1.0,0.0,0.0,0.0,                                       *oper.2
0                                                       *oper.3
7200000,556.00,400.00,0.47090,0.0                       *oper.5
0                                                       *oper.12
*
*
corr,0,2,0                                              *corr.1
chll,chll,homo,none                                     *corr.2
ditb,chen,chen,epri,cond,g5.7,0                         *corr.6
1,0,0.0                                                 *corr.16
*
*
mixx,3,0,0                                              *mixx.1
0.8,0.035,-0.1                                          *mixx.2
*
*
drag,1,0,0                                              *drag1
0.15139,-0.18,0,94.0485,-1,0,                           *drag2
0.5                                                     *drag5
*
*
grid,0,1                                                *grid.1
0.5                                                     *grid.2
-1,4                                                    *grid.4
0.21,1,0.51,1,0.73,1,1.03,1                             *grid.6
0
*
*
cont                                                    *cont.1
0.0,0,200,750,2,2,0,0                                   *cont.2
0.1,0.00001,0.001,0.05,0.01,0.9,1.5,1.0                 *cont.3
0,0,0,0,0,0,1,1,0,0,0,1,0,2,0                           *cont.6
100.,0,0,0,0,0                                          *cont.7
*
*
endd
0
```

Appendix C: VIPRE-01 Tight Bundle Tests Sample Input Files

JAEA-A:

R_f = 1.307
P = 7.2 MPa
G = 300 kg/m^2-s
T_{in} = 554.8 K
Average heat flux = 171.09 kW/m^2
Two-phase friction multiplier model: EPRI

```
1,0,0,1,0                                                    *vipre.1
JAEA-A 7-rod bundle (Kureta 2003)                            *vipre.2
*
*
geom,4,4,36,0,0,0                                            *geom.1
1.8,0.0,0.5                                                  *geom.2
1,17.1842e-6,19.3208e-3,19.3208e-3,1,2,1.0e-3,6.9854e-3,     *geom.4
2,11.4561e-6,20.5593e-3,12.8805e-3,2,3,0.5e-3,7.4210e-3,4,0.5e-3,7.4225e-3,
3,5.7281e-6,14.1190e-3,6.4403e-3,
4,5.7281e-6,14.1190e-3,6.4403e-3
*
*
prop,0,1,2,1                                                 *prop.1
*
*
rods,1,3,0,1,0,0,0,0,0,0,0,0                                 *rods.1
1.8,0.0,0,0                                                  *rods.2
2                                                            *rods.3
0.0,1.0,1.8,1.0                                              *rods.4
*
*rods geometry input                                          *rods.9
1,1,1.307,1,1,0.1667,
2,1,0.949,1,1,0.1667,2,0.1667,3,0.1667,
3,1,0.949,1,1,0.1667,2,0.1667,4,0.1667,
0
*
1,dumy,12.3e-3,0.0,0                                         *rods.68
*
*
oper,1,2,0,2,0,1,0,0,0,0                                     *oper.1
-1.0,0.0,0.0,0.0,                                            *oper.2
0                                                            *oper.3
7200000,554.8,300.00,0.17109,0.0                             *oper.5
```

```
0                                                    *oper.12
*
*
corr,0,2,0                                           *corr.1
chll,chll,epri,none                                  *corr.2
ditb,chen,chen,epri,cond,g5.7,0                      *corr.6
1,0,0.0                                              *corr.16
*
*
mixx,3,0,0                                           *mixx.1
0.8,0.035,-0.1                                       *mixx.2
*
*
drag,1,0,0                                           *drag1
0.15139,-0.18,0,94.0485,-1,0,                        *drag2
0.5                                                  *drag5
*
*
grid,0,1                                             *grid.1
0.5                                                  *grid.2
2,6                                                  *grid.4
1,2                                                  *grid.5
0.05,1,0.35,1,0.65,1,0.95,1,1.25,1,1.55,1            *grid.6
0
*
*
cont                                                 *cont.1
0.0,0,200,750,2,2,0,0                                *cont.2
0.1,0.00001,0.001,0.05,0.01,0.9,1.5,1.0              *cont.3
0,0,0,0,0,0,1,1,0,0,0,1,0,2,0                        *cont.6
100.,0,0,0,0,0                                       *cont.7
*
*
endd
0
```

JAEA-B:

R_f = 1.277
P = 7.2 MPa
G = 600 kg/m^2-s
T_{in} = 555.9 K
Average heat flux = 417.38 kW/m^2
Two-phase friction multiplier model: HOMO

```
1,0,0,1,0                                                    *vipre.1
JAEA-B 7-rod bundle (Liu 2004)                               *vipre.2
*
*
geom,4,4,40,0,0,0                                            *geom.1
1.26,0.0,0.5                                                 *geom.2
1,22.1806e-6,20.4204e-3,20.4204e-3,1,2,1.3e-3,7.5467e-3,     *geom.4
2,14.7871e-6,21.8697e-3,13.6136e-3,2,3,0.65e-3,7.8460e-3,4,0.65e-3,7.9988e-3,
3,7.3935e-6,15.0629e-3,6.8068e-3,
4,7.3935e-6,15.0629e-3,6.8068e-3
*
*
prop,0,1,2,1                                                 *prop.1
*
*
rods,1,3,0,1,0,0,0,0,0,0,0,0                                 *rods.1
1.26,0.0,0,0                                                 *rods.2
24                                                           *rods.3
0.0,0.321,0.098,0.321,0.09800001,0.462,0.147,0.462,          *rods.4
0.14700001,0.565,0.241,0.565,0.24100001,2.114,0.462,2.114,
0.46200001,0.547,0.759,0.547,0.75900001,2.204,0.846,2.204,
0.84600001,2.158,0.895,2.158,0.89500001,2.002,0.951,2.002,
0.95100001,1.830,0.977,1.830,0.97700001,0.386,1.049,0.386,
1.04900001,0.246,1.147,0.246,1.14700001,0.193,1.260,0.193
*
*rods geometry input                                          *rods.9
1,1,1.277,1,1,0.1667,
2,1,0.954,1,1,0.1667,2,0.1667,3,0.1667,
3,1,0.954,1,1,0.1667,2,0.1667,4,0.1667
0
*
1,dumy,13.0e-3,0.0,0                                         *rods.68
*
*
oper,1,2,0,2,0,1,0,0,0,0                                     *oper.1
-1.0,0.0,0.0,0.0,                                            *oper.2
```

```
0                                                    *oper.3
7200000,555.89,600.00,0.41738,0.0                    *oper.5
0                                                    *oper.12
*
*
corr,0,2,0                                           *corr.1
chll,chll,homo,none                                  *corr.2
ditb,chen,chen,epri,cond,g5.7,0                      *corr.6
1,0,0.0                                              *corr.16
*
*
mixx,3,0,0                                           *mixx.1
0.8,0.035,-0.1                                       *mixx.2
*
*
drag,1,0,0                                           *drag1
0.15139,-0.18,0,94.0485,-1,0,                        *drag2
0.5                                                  *drag5
*
*
grid,0,1                                             *grid.1
0.5                                                  *grid.2
2,4                                                  *grid.4
1,2                                                  *grid.5
0.22,1,0.52,1,0.73,1,1.0,1                           *grid.6
0
*
*
cont                                                 *cont.1
0.0,0,200,750,2,2,0,0                                *cont.2
0.1,0.00001,0.001,0.05,0.01,0.9,1.5,1.0              *cont.3
0,0,0,0,0,0,1,1,0,0,0,1,0,2,0                        *cont.6
100.,0,0,0,0,0                                       *cont.7
*
*
endd
0
```

JAEA-C:

R_f = 1.006
P = 7.2 MPa
G = 600 kg/m^2-s
T_{in} = 556 K
Average heat flux = 553.15 kW/m^2
Two-phase friction multiplier model: EPRI

```
1,0,0,1,0                                                    *vipre.1
JAEA-C 37-rod bundle (Liu 2007)                              *vipre.2
*
*
geom,14,14,42,0,0,0                                          *geom.1
1.26,0.0,0.5                                                 *geom.2
1,22.1806e-6,20.4204e-3,20.4204e-3,1,3,1.3e-3,8.0499e-3,     *geom.4
2,22.1806e-6,20.4204e-3,20.4204e-3,2,3,1.3e-3,8.1668e-3,6,1.3e-3,8.2581e-3,
3,22.1806e-6,20.4204e-3,20.4204e-3,1,4,1.3e-3,8.3782e-3,
4,22.1806e-6,20.4204e-3,20.4204e-3,1,8,1.3e-3,8.2801e-3,
5,22.1806e-6,20.4204e-3,20.4204e-3,2,6,1.3e-3,8.1951e-3,10,1.3e-3,9.5826e-3,
6,22.1806e-6,20.4204e-3,20.4204e-3,1,7,1.3e-3,8.3525e-3,
7,22.1806e-6,20.4204e-3,20.4204e-3,2,8,1.3e-3,8.2011e-3,11,1.3e-3,9.5812e-3,
8,22.1806e-6,20.4204e-3,20.4204e-3,1,9,1.3e-3,8.3481e-3,
9,22.1806e-6,20.4204e-3,20.4204e-3,1,12,1.3e-3,9.5899e-3,
10,41.5989e-6,34.7204e-3,20.4204e-3,2,11,1.05e-3,14.2983e-3,13,1.05e-3,9.4566e-3,
11,41.5989e-6,34.7204e-3,20.4204e-3,1,12,1.05e-3,14.2897e-3,
12,41.5989e-6,34.7204e-3,20.4204e-3,1,14,1.05e-3,9.5151e-3,
13,5.3942e-6,7.7624e-3,3.4034e-3,
14,5.3942e-6,7.7624e-3,3.4034e-3
*
*
prop,0,1,2,1                                                 *prop.1
*
*
rods,1,10,0,1,0,0,0,0,0,0,0,0                                *rods.1
1.26,0.0,0,0                                                 *rods.2
24                                                           *rods.3
0.0,0.315,0.108,0.315,0.10800001,0.492,0.165,0.492,          *rods.4
0.16500001,0.617,0.253,0.617,0.25300001,2.235,0.472,2.235,
0.47200001,0.547,0.778,0.547,0.77800001,2.179,0.861,2.179,
0.86100001,2.102,0.908,2.102,0.90800001,1.975,0.959,1.975,
0.95900001,1.848,0.991,1.848,0.99100001,0.353,1.076,0.353,
1.07600001,0.201,1.133,0.201,1.13300001,0.174,1.260,0.174
*
*rods geometry input                                          *rods.9
```

```
1,1,1.006,1,1,0.1667,
2,1,1.006,1,1,0.1667,2,0.1667,3,0.1667,
3,1,1.006,1,1,0.1667,3,0.1667,4,0.1667,
4,1,1.006,1,2,0.1667,5,0.1667,6,0.1667,
5,1,1.006,1,2,0.1667,3,0.1667,4,0.1667,6,0.1667,7,0.1667,8,0.1667,
6,1,1.006,1,4,0.1667,8,0.1667,9,0.1667,
7,1,0.993,1,5,0.1667,10,0.25,13,0.0833,
8,1,0.993,1,5,0.1667,6,0.1667,7,0.1667,10,0.25,11,0.25,
9,1,0.993,1,7,0.1667,8,0.1667,9,0.1667,11,0.25,12,0.25,
10,1,0.993,1,9,0.1667,12,0.25,14,0.0833,
0
*
1,dumy,13.0e-3,0.0,0                                    *rods.68
*
*
oper,1,2,0,2,0,1,0,0,0,0                                *oper.1
-1.0,0.0,0.0,0.0,                                       *oper.2
0                                                       *oper.3
7200000,556.00,600.00,0.55315,0.0                       *oper.5
0                                                       *oper.12
*
*
corr,0,2,0                                              *corr.1
chll,chll,epri,none                                     *corr.2
ditb,chen,chen,epri,cond,g5.7,0                         *corr.6
1,0,0.0                                                 *corr.16
*
*
mixx,3,0,0                                              *mixx.1
0.8,0.035,-0.1                                          *mixx.2
*
*
drag,1,0,0                                              *drag1
0.15139,-0.18,0,94.0485,-1,0,                           *drag2
0.5                                                     *drag5
*
*
grid,0,1                                                *grid.1
0.5                                                     *grid.2
-1,4                                                    *grid.4
0.21,1,0.51,1,0.73,1,1.03,1                             *grid.6
0
*
*
cont                                                    *cont.1
0.0,0,200,750,2,2,0,0                                   *cont.2
```

```
0.1,0.00001,0.001,0.05,0.01,0.9,1.5,1.0                    *cont.3
0,0,0,0,0,0,1,1,0,0,0,1,0,2,0                              *cont.6
100.,0,0,0,0,0                                             *cont.7
*
*
endd
0
```

JAEA-D:

R_f = 1.097
P = 7.2 MPa
G = 800 kg/m^2-s
T_{in} = 556 K
Average heat flux = 468.74 kW/m^2
Two-phase friction multiplier model: HOMO

```
1,0,0,1,0                                                    *vipre.1
JAEA-D 37-rod bundle (Liu 2007)                              *vipre.2
*
*
geom,14,14,42,0,0,0                                          *geom.1
1.26,0.0,0.5                                                 *geom.2
1,18.5043e-6,20.4204e-3,20.4204e-3,1,3,1.0e-3,8.0459e-3,     *geom.4
2,18.5043e-6,20.4204e-3,20.4204e-3,2,3,1.0e-3,8.0460e-3,6,1.0e-3,8.0704e-3,
3,18.5043e-6,20.4204e-3,20.4204e-3,1,4,1.0e-3,8.1310e-3,
4,18.5043e-6,20.4204e-3,20.4204e-3,1,8,1.0e-3,8.0704e-3,
5,18.5043e-6,20.4204e-3,20.4204e-3,2,6,1.0e-3,8.0392e-3,10,1.0e-3,9.2815e-3,
6,18.5043e-6,20.4204e-3,20.4204e-3,1,7,1.0e-3,8.1232e-3,
7,18.5043e-6,20.4204e-3,20.4204e-3,2,8,1.0e-3,8.0392e-3,11,1.0e-3,9.2815e-3,
8,18.5043e-6,20.4204e-3,20.4204e-3,1,9,1.0e-3,8.1111e-3,
9,18.5043e-6,20.4204e-3,20.4204e-3,1,12,1.0e-3,9.2831e-3,
10,35.1339e-6,34.4204e-3,20.4204e-3,2,11,0.75e-3,14.0000e-3,13,0.75e-3,9.2668e-3,
11,35.1339e-6,34.4204e-3,20.4204e-3,1,12,0.75e-3,14.0241e-3,
12,35.1339e-6,34.4204e-3,20.4204e-3,1,14,0.75e-3,9.2732e-3,
13,4.1125e-6,7.5892e-3,3.4034e-3,
14,4.1125e-6,7.5892e-3,3.4034e-3
*
*
prop,0,1,2,1                                                 *prop.1
*
*
rods,1,10,0,1,0,0,0,0,0,0,0,0                                *rods.1
1.26,0.0,0,0                                                 *rods.2
24                                                           *rods.3
0.0,0.315,0.108,0.315,0.10800001,0.492,0.165,0.492,          *rods.4
0.16500001,0.617,0.253,0.617,0.25300001,2.235,0.472,2.235,
0.47200001,0.547,0.778,0.547,0.77800001,2.179,0.861,2.179,
0.86100001,2.102,0.908,2.102,0.90800001,1.975,0.959,1.975,
0.95900001,1.848,0.991,1.848,0.99100001,0.353,1.076,0.353,
1.07600001,0.201,1.133,0.201,1.13300001,0.174,1.260,0.174
*
*rods geometry input                                          *rods.9
```

```
1,1,1.097,1,1,0.1667,
2,1,1.097,1,1,0.1667,2,0.1667,3,0.1667,
3,1,1.097,1,1,0.1667,3,0.1667,4,0.1667,
4,1,1.097,1,2,0.1667,5,0.1667,6,0.1667,
5,1,1.097,1,2,0.1667,3,0.1667,4,0.1667,6,0.1667,7,0.1667,8,0.1667,
6,1,1.097,1,4,0.1667,8,0.1667,9,0.1667,
7,1,0.898,1,5,0.1667,10,0.25,13,0.0833,
8,1,0.898,1,5,0.1667,6,0.1667,7,0.1667,10,0.25,11,0.25,
9,1,0.898,1,7,0.1667,8,0.1667,9,0.1667,11,0.25,12,0.25,
10,1,0.898,1,9,0.1667,12,0.25,14,0.0833,
0
*
1,dumy,13.0e-3,0.0,0                                    *rods.68
*
*
oper,1,2,0,2,0,1,0,0,0,0                                *oper.1
-1.0,0.0,0.0,0.0,                                       *oper.2
0                                                       *oper.3
7200000,556.00,800.00,0.46874,0.0                       *oper.5
0                                                       *oper.12
*
*
corr,0,2,0                                              *corr.1
chll,chll,homo,none                                     *corr.2
ditb,chen,chen,epri,cond,g5.7,0                         *corr.6
1,0,0.0                                                 *corr.16
*
*
mixx,3,0,0                                              *mixx.1
0.8,0.035,-0.1                                          *mixx.2
*
*
drag,1,0,0                                              *drag1
0.15139,-0.18,0,94.0485,-1,0,                           *drag2
0.5                                                     *drag5
*
*
grid,0,1                                                *grid.1
0.5                                                     *grid.2
-1,4                                                    *grid.4
0.21,1,0.51,1,0.73,1,1.03,1                             *grid.6
0
*
*
cont                                                    *cont.1
0.0,0,200,750,2,2,0,0                                   *cont.2
```

```
0.1,0.00001,0.001,0.05,0.01,0.9,1.5,1.0                    *cont.3
0,0,0,0,0,0,1,1,0,0,0,1,0,2,0                              *cont.6
100.,0,0,0,0,0                                             *cont.7
*
*
endd
0
```

Toshiba-1:

R_f = 1.18
Two-phase friction multiplier model: EPRI

```
1,0,0,1,0                                                    *vipre.1
Toshiba-1 7-rod bundle (Yamamoto 2006)                       *vipre.2
*
*
geom,4,4,40,0,0,0                                            *geom.1
2.0,0.0,0.5                                                  *geom.2
1,12.4618e-6,16.9646e-3,16.9646e-3,1,2,0.0008,8.7898e-3,     *geom.4
2,42.4032e-6,28.5646e-3,16.9646e-3,2,3,2.2041e-3,7.7782e-3,4,2.2041e-3,7.7905e-3,
3,9.0578e-6,7.2177e-3,2.8274e-3,0,
4,9.0578e-6,7.2177e-3,2.8274e-3,0
*
*
prop,0,1,2,1                                                 *prop.1
*
*
rods,1,3,0,1,0,0,0,0,0,0,0,0                                 *rods.1
1.6,0.4,0,0                                                  *rods.2
10                                                           *rods.3
0.0,0.707,0.188,0.707,0.188001,1.0,0.493,1.0,                *rods.4
0.493001,1.204,1.091,1.204,1.091001,1.0,1.394,1.0,
1.394001,0.707,1.6,0.707
*
*rods geometry input                                          *rods.9
1,1,1.18,1,1,0.1667,
2,1,0.97,1,1,0.1667,2,0.25,4,0.0833,
3,1,0.97,1,1,0.1667,2,0.25,3,0.0833,
0
*
1,dumy,10.8e-3,0.0,0                                         *rods.68
*
*
oper,0,2,0,2,0,6,0,0,0,0                                     *oper.1
-1.0,0.0,0.0,0.0,                                            *oper.2
0                                                            *oper.3
7000000,1217440,472.22,0.33108,0.0                           *oper.5
7000000,1217440,716.67,0.39804,0.0
7000000,1217440,988.89,0.54560,0.0
7000000,1217440,1227.78,0.64377,0.0
7000000,1217440,1483.33,0.69031,0.0
7000000,1217440,1744.44,0.70133,0.0
```

```
0                                                    *oper.12
*
*
corr,0,2,0                                           *corr.1
chll,chll,epri,none                                  *corr.2
ditb,chen,chen,epri,cond,g5.7,0                      *corr.6
1,0,0.0                                              *corr.16
*
*
mixx,3,0,0                                           *mixx.1
0.8,0.035,-0.1                                       *mixx.2
*
*
drag,1,0,0                                           *drag1
0.15139,-0.18,0,94.0485,-1,0,                        *drag2
0.5                                                  *drag5
*
*
grid,0,1                                             *grid.1
0.55                                                 *grid.2
-1,5                                                 *grid.4
0.0,1,0.45,1,0.9,1,1.35,1,1.8,1                      *grid.6
0
*
*
cont                                                 *cont.1
0.0,0,200,750,2,2,0,0                                *cont.2
0.1,0.00001,0.001,0.05,0.01,0.9,1.5,1.0              *cont.3
0,0,0,0,0,0,1,1,0,0,0,1,0,2,0                        *cont.6
100.,0,0,0,0,0                                       *cont.7
*
*
endd
0
```

Toshiba-2:

R_f = 1.18
Heated length = 1.6 m
Two-phase friction multiplier model: HOMO

```
1,0,0,1,0                                                    *vipre.1
Toshiba-2 7-rod bundle (Yamamoto 2006) 1.6m                  *vipre.2
*
*
geom,4,4,40,0,0,0                                            *geom.1
2.0,0.0,0.5                                                  *geom.2
1,17.5930e-6,16.9646e-3,16.9646e-3,1,2,0.0013,8.9825e-3,     *geom.4
2,50.6458e-6,29.0646e-3,16.9646e-3,2,3,2.5711e-3,8.1299e-3,4,2.5711e-3,8.1861e-3,
3,10.7079e-6,7.4295e-3,2.8274e-3,0,
4,10.7079e-6,7.4295e-3,2.8274e-3,0
*
*
prop,0,1,2,1                                                 *prop.1
*
*
rods,1,3,0,1,0,0,0,0,0,0,0,0                                 *rods.1
1.6,0.4,0,0                                                  *rods.2
10                                                           *rods.3
0.0,0.707,0.188,0.707,0.188001,1.0,0.493,1.0,                *rods.4
0.493001,1.204,1.091,1.204,1.091001,1.0,1.394,1.0,
1.394001,0.707,1.6,0.707
*
*rods geometry input                                          *rods.9
1,1,1.18,1,1,0.1667,
2,1,0.97,1,1,0.1667,2,0.25,4,0.0833,
3,1,0.97,1,1,0.1667,2,0.25,3,0.0833,
0
*
1,dumy,10.8e-3,0.0,0                                         *rods.68
*
*
oper,0,2,0,2,0,7,0,0,0,0                                     *oper.1
-1.0,0.0,0.0,0.0,                                            *oper.2
0                                                            *oper.3
7000000,1217440,488.89,0.51191,0.0                           *oper.5
7000000,1217440,761.11,0.68643,0.0
7000000,1217440,988.89,0.79890,0.0
7000000,1217440,1238.89,0.91912,0.0
7000000,1217440,1461.11,1.00444,0.0
```

```
7000000,1217440,1722.22,1.08975,0.0
7000000,1217440,1961.11,1.14017,0.0
0                                                    *oper.12
*
*
corr,0,2,0                                           *corr.1
chll,chll,homo,none                                  *corr.2
ditb,chen,chen,epri,cond,g5.7,0                      *corr.6
1,0,0.0                                              *corr.16
*
*
mixx,3,0,0                                           *mixx.1
0.8,0.035,-0.1                                       *mixx.2
*
*
drag,1,0,0                                           *drag1
0.15139,-0.18,0,94.0485,-1,0,                        *drag2
0.5                                                  *drag5
*
*
grid,0,1                                             *grid.1
0.65                                                 *grid.2
-1,5                                                 *grid.4
0.0,1,0.45,1,0.9,1,1.35,1,1.8,1                      *grid.6
0
*
*
cont                                                 *cont.1
0.0,0,200,750,2,2,0,0                                *cont.2
0.1,0.00001,0.001,0.05,0.01,0.9,1.5,1.0              *cont.3
0,0,0,0,0,0,1,1,0,0,0,1,0,2,0                        *cont.6
100.,0,0,0,0,0                                       *cont.7
*
*
endd
0
```

Toshiba-3:

R_f = 1.18
Two-phase friction multiplier model: EPRI

```
1,0,0,1,0                                                    *vipre.1
Toshiba-3 7-rod bundle (Yamamoto 2006)                       *vipre.2
*
*
geom,4,4,40,0,0,0                                            *geom.1
2.0,0.0,0.5                                                  *geom.2
1,22.9407e-6,16.9646e-3,16.9646e-3,1,2,0.0018,9.2844e-3,     *geom.4
2,59.8854e-6,29.5646e-3,16.9646e-3,2,3,2.9881e-3,8.4376e-3,4,2.9881e-3,8.4210e-3,
3,12.6771e-6,7.6703e-3,2.8274e-3,0,
4,12.6771e-6,7.6703e-3,2.8274e-3,0
*
*
prop,0,1,2,1                                                 *prop.1
*
*
rods,1,3,0,1,0,0,0,0,0,0,0,0                                 *rods.1
1.6,0.4,0,0                                                  *rods.2
12                                                           *rods.3
0.0,0.0,0.000001,0.707,0.188,0.707,0.188001,1.0,             *rods.4
0.493,1.0,0.493001,1.204,1.091,1.204,1.091001,1.0,
1.394,1.0,1.394001,0.707,1.599999,0.707,1.6,0.0
*
*rods geometry input                                          *rods.9
1,1,1.18,1,1,0.1667,
2,1,0.97,1,1,0.1667,2,0.25,4,0.0833,
3,1,0.97,1,1,0.1667,2,0.25,3,0.0833,
0
*
1,dumy,10.8e-3,0.0,0                                         *rods.68
*
*
oper,0,2,0,2,0,6,0,0,0,0                                     *oper.1
-1.0,0.0,0.0,0.0,                                            *oper.2
0                                                            *oper.3
7000000,1217440,600.00,0.76787,0.0                           *oper.5
7000000,1217440,783.33,0.91524,0.0
7000000,1217440,1061.11,1.11302,0.0
7000000,1217440,1250.00,1.23713,0.0
7000000,1217440,1466.67,1.32244,0.0
7000000,1217440,1711.11,1.39225,0.0
```

```
0                                                    *oper.12
*
*
corr,0,2,0                                           *corr.1
chll,chll,epri,none                                  *corr.2
ditb,chen,chen,epri,cond,g5.7,0                      *corr.6
1,0,0.0                                              *corr.16
*
*
mixx,3,0,0                                           *mixx.1
0.8,0.035,-0.1                                       *mixx.2
*
*
drag,1,0,0                                           *drag1
0.15139,-0.18,0,94.0485,-1,0,                        *drag2
0.5                                                  *drag5
*
*
grid,0,1                                             *grid.1
0.75                                                 *grid.2
-1,5                                                 *grid.4
0.0,1,0.45,1,0.9,1,1.35,1,1.8,1                      *grid.6
0
*
*
cont                                                 *cont.1
0.0,0,200,750,2,2,0,0                                *cont.2
0.1,0.00001,0.001,0.05,0.01,0.9,1.5,1.0              *cont.3
0,0,0,0,0,0,1,1,0,0,0,1,0,2,0                        *cont.6
100.,0,0,0,0,0                                       *cont.7
*
*
endd
0
```

Toshiba-4:

R_f = 1.15 (side peak)
Two-phase friction multiplier model: HOMO

```
1,0,0,1,0                                                    *vipre.1
Toshiba-4 14-rod bundle (Yamamoto 2006) side-peak            *vipre.2
*
*
geom,36,36,40,0,0,0                                          *geom.1
2.0,0.0,0.5                                                  *geom.2
1,50.0918e-6,25.6139e-3,8.4823e-3,2,2,3.7816e-3,10.8394e-3,6,2.5500e-3,10.4617e-3,  *geom.4
2,65.2934e-6,29.0646e-3,16.9646e-3,2,3,3.7816e-3,12.1014e-3,8,1.3e-3,9.7151e-3,
3,65.2934e-6,29.0646e-3,16.9646e-3,2,4,3.7816e-3,12.1006e-3,10,1.3e-3,9.7045e-3,
4,65.2934e-6,29.0646e-3,16.9646e-3,2,5,3.7816e-3,10.7915e-3,12,1.3e-3,9.6883e-3,
5,50.0918e-6,25.6139e-3,8.4823e-3,1,14,2.5500e-3,10.4623e-3,
6,28.7064e-6,24.3612e-3,5.6549e-3,2,7,1.3e-3,6.7366e-3,15,1.9e-3,11.5983e-3,
7,17.5930e-6,16.9646e-3,11.3097e-3,2,8,1.3e-3,7.0319e-3,16,1.3e-3,7.0306e-3,
8,17.5930e-6,16.9646e-3,16.9646e-3,1,9,1.3e-3,6.9412e-3,
9,17.5930e-6,16.9646e-3,16.9646e-3,2,10,1.3e-3,7.0272e-3,18,1.3e-3,7.0198e-3,
10,17.5930e-6,16.9646e-3,16.9646e-3,1,11,1.3e-3,6.9688e-3,
11,17.5930e-6,16.9646e-3,16.9646e-3,2,12,1.3e-3,7.0123e-3,20,1.3e-3,6.9922e-3,
12,17.5930e-6,16.9646e-3,16.9646e-3,1,13,1.3e-3,6.9773e-3,
13,17.5930e-6,16.9646e-3,11.3097e-3,2,14,1.3e-3,6.7459e-3,22,1.3e-3,7.0009e-3,
14,28.7064e-6,24.3612e-3,5.6549e-3,1,23,1.9e-3,11.5797e-3,
15,28.7064e-6,24.3612e-3,5.6549e-3,2,16,1.3e-3,6.7747e-3,24,2.5500e-3,9.4578e-3,
16,17.5930e-6,16.9646e-3,11.3097e-3,1,17,1.3e-3,6.9335e-3,
17,17.5930e-6,16.9646e-3,16.9646e-3,2,18,1.3e-3,7.0356e-3,26,1.3e-3,7.0033e-3,
18,17.5930e-6,16.9646e-3,16.9646e-3,1,19,1.3e-3,6.9391e-3,
19,17.5930e-6,16.9646e-3,16.9646e-3,2,20,1.3e-3,7.0695e-3,28,1.3e-3,7.0171e-3,
20,17.5930e-6,16.9646e-3,16.9646e-3,1,21,1.3e-3,6.9631e-3,
21,17.5930e-6,16.9646e-3,16.9646e-3,2,22,1.3e-3,7.0146e-3,30,1.3e-3,6.9862e-3,
22,17.5930e-6,16.9646e-3,11.3097e-3,1,23,1.3e-3,6.7765e-3,
23,28.7064e-6,24.3612e-3,5.6549e-3,1,32,2.5500e-3,9.3871e-3,
24,28.7064e-6,24.3612e-3,5.6549e-3,2,25,1.3e-3,6.7302e-3,33,1.9e-3,12.5578e-3,
25,17.5930e-6,16.9646e-3,11.3097e-3,2,26,1.3e-3,7.0005e-3,33,1.3e-3,9.4491e-3,
26,17.5930e-6,16.9646e-3,16.9646e-3,1,27,1.3e-3,6.9620e-3,
27,17.5930e-6,16.9646e-3,16.9646e-3,2,28,1.3e-3,7.0096e-3,34,1.3e-3,9.7269e-3,
28,17.5930e-6,16.9646e-3,16.9646e-3,1,29,1.3e-3,6.9370e-3,
29,17.5930e-6,16.9646e-3,16.9646e-3,2,30,1.3e-3,7.1120e-3,35,1.3e-3,9.7142e-3,
30,17.5930e-6,16.9646e-3,16.9646e-3,1,31,1.3e-3,6.9581e-3,
31,17.5930e-6,16.9646e-3,11.3097e-3,2,32,1.3e-3,6.8363e-3,36,1.3e-3,9.5120e-3,
32,28.7064e-6,24.3612e-3,5.6549e-3,1,36,1.9e-3,12.7148e-3,
33,82.7385e-6,45.5462e-3,8.4823e-3,1,34,3.7816e-3,13.5631e-3,
34,65.2934e-6,29.0646e-3,16.9646e-3,1,35,3.7816e-3,12.1078e-3,
```

```
35,65.2934e-6,29.0646e-3,16.9646e-3,1,36,3.7816e-3,13.6612e-3,
36,82.7385e-6,45.5462e-3,8.4823e-3,0
*
*
prop,0,1,2,1                                                    *prop.1
*
*
rods,1,14,0,1,0,0,0,0,0,0,0,0                                   *rods.1
1.6,0.4,0,0                                                     *rods.2
10                                                              *rods.3
0.0,0.707,0.188,0.707,0.188001,1.0,0.493,1.0,                   *rods.4
0.493001,1.204,1.091,1.204,1.091001,1.0,1.394,1.0,
1.394001,0.707,1.6,0.707
*
*rods geometry input                                             *rods.9
1,1,0.96,1,1,0.25,2,0.25,6,0.1667,7,0.1667,8,0.1667,
2,1,0.96,1,2,0.25,3,0.25,8,0.1667,9,0.1667,10,0.1667
3,1,0.96,1,3,0.25,4,0.25,10,0.1667,11,0.1667,12,0.1667,
4,1,0.96,1,4,0.25,5,0.25,12,0.1667,13,0.1667,14,0.1667,
5,1,1.15,1,7,0.1667,8,0.1667,9,0.1667,16,0.1667,17,0.1667,18,0.1667,
6,1,0.96,1,9,0.1667,10,0.1667,11,0.1667,18,0.1667,19,0.1667,20,0.1667,
7,1,0.96,1,11,0.1667,12,0.1667,13,0.1667,20,0.1667,21,0.1667,22,0.1667,
8,1,1.15,1,15,0.1667,16,0.1667,17,0.1667,24,0.1667,25,0.1667,26,0.1667,
9,1,1.15,1,17,0.1667,18,0.1667,19,0.1667,26,0.1667,27,0.1667,28,0.1667,
10,1,0.96,1,19,0.1667,20,0.1667,21,0.1667,28,0.1667,29,0.1667,30,0.1667,
11,1,0.96,1,21,0.1667,22,0.1667,23,0.1667,30,0.1667,31,0.1667,32,0.1667,
12,1,0.96,1,25,0.1667,26,0.1667,27,0.1667,33,0.25,34,0.25,
13,1,0.96,1,27,0.1667,28,0.1667,29,0.1667,34,0.25,35,0.25,
14,1,0.96,1,29,0.1667,30,0.1667,31,0.1667,35,0.25,36,0.25,
0
*
1,dumy,10.8e-3,0.0,0                                            *rods.68
*
*
oper,0,2,0,2,0,6,0,0,0,0                                        *oper.1
-1.0,0.0,0.0,0.0,                                               *oper.2
0                                                               *oper.3
7000000,1217437,501.43,0.34967,0.0                              *oper.5
7000000,1217437,754.48,0.43884,0.0
7000000,1217437,1001.96,0.50294,0.0
7000000,1217437,1258.55,0.54356,0.0
7000000,1217437,1505.99,0.52802,0.0
7000000,1217437,1764.45,0.60020,0.0
0                                                               *oper.12
*
*
```

```
corr,0,2,0                                  *corr.1
chll,chll,homo,none                         *corr.2
ditb,chen,chen,epri,cond,g5.7,0             *corr.6
1,0,0.0                                     *corr.16
*
*
mixx,3,0,0                                  *mixx.1
0.8,0.035,-0.1                              *mixx.2
*
*
drag,1,0,0                                  *drag1
0.15139,-0.18,0,94.0485,-1,0,               *drag2
0.5                                         *drag5
*
*
grid,0,1                                    *grid.1
0.25                                        *grid.2
-1,5                                        *grid.4
0.0,1,0.45,1,0.9,1,1.35,1,1.8,1             *grid.6
0
*
*
cont                                        *cont.1
0.0,0,200,750,2,2,0,0                       *cont.2
0.1,0.00001,0.005,0.05,0.01,0.9,1.5,1.0     *cont.3
0,0,0,0,0,0,1,1,0,0,0,1,0,2,0               *cont.6
100.,0,0,0,0,0                              *cont.7
*
*
endd
0
```

Appendix D: Tight Bundle Critical Quality Comparison

JAEA-A & B Comparison vs. Toshiba-2 Comparison

This appendix provides another (approximate) dryout prediction methodology using a void fraction criterion in VIPRE-01, and illustrates predicted vs. experimental critical quality for JAEA-A & B and Toshiba-2 test cases.

In VIPRE-01, two different void fraction values are calculated on each axial node of each sub-channel (Stewart et al., 2011a): one (so-called equilibrium void fraction) with the pre-selected empirical correlation as a function of flow, slip ratio and equilibrium quality; the other (so-called dynamic void fraction) based on the vapor mass conservation equation. The dynamic void fraction is physically more meaningful because it is solved via the transport equation for vapor provided by the drift flux model.

The following two figures plot respectively JAEA-A & B and Toshiba-2 tight bundle experimental vs. predicted critical quality under similar conditions. The predicted critical quality is performed in VIPRE-01 by setting a dynamic void fraction criterion of 95% (Weisman, 1992) at the peak sub-channel outlet. This methodology is not supposed to provide accurate dryout prediction but is able to illustrate some physical trends within the two cases. As shown, the relative distances between experimental and VIPRE-01 critical quality values for JAEA-A & B case (Figure 50) and those for Toshiba-2 case (Figure 51) are alike. However, as discussed in section 5.3, the sub-channel correction factor (R_f_x) barely differs between JAEA-A and B tests, unlike Toshiba-2 test in which R_f_x values are significantly different between the two bundle configurations.

Future work on direct coupling of the sub-channel level flow information with the three-field model could potentially explain the trends shown in the experiments.

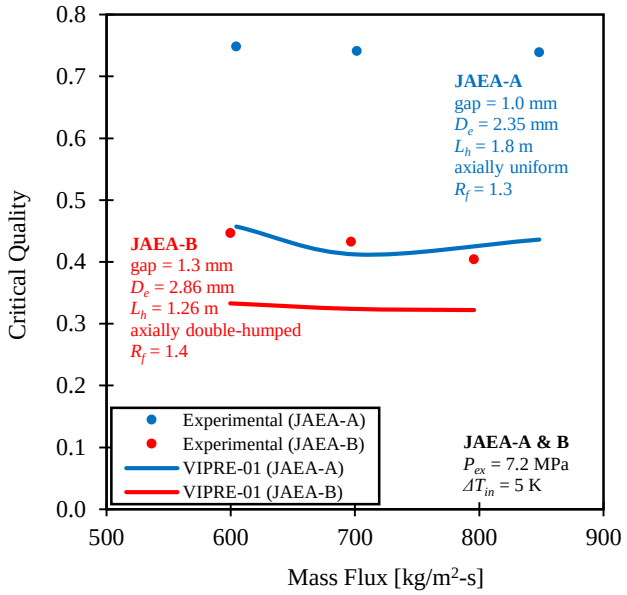

Figure 50. JAEA-A & B experimental vs. VIPRE-01 critical quality.

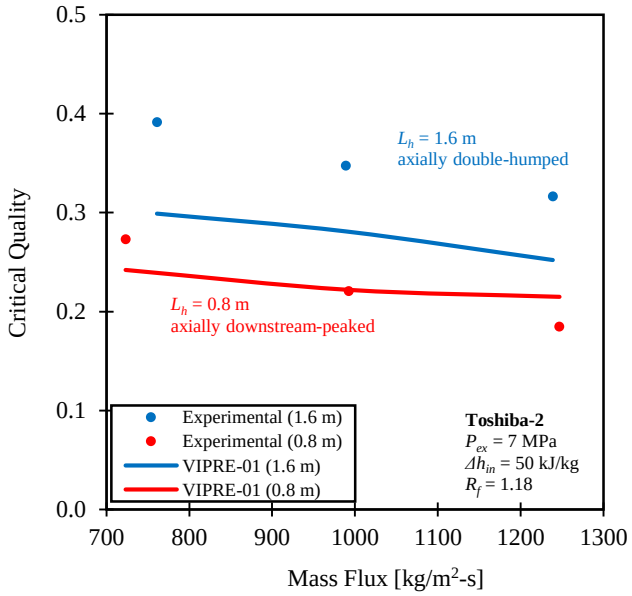

Figure 51. Toshiba-2 experimental vs. VIPRE-01 critical quality.

Appendix E: VIPRE-01 RBWR-TB2 Bundle Input File

RBWR-TB2: (center-peak R_f = 1.1, EPRI friction multiplier model)

```
1,0,0,1,0                                                    *vipre.1
RBWR-TB2                                                     *vipre.2
*
*
geom,134,134,30,0,0,0                                        *geom.1
1.015,0.0,0.5                                                *geom.2
1,17.6597e-6,11.3097e-3,11.3097e-3,1,3,2.17e-3,5.4366e-3,    *geom.4
2,17.6597e-6,11.3097e-3,11.3097e-3,2,3,2.17e-3,5.4366e-3,6,2.17e-3,5.4366e-3,
3,17.6597e-6,11.3097e-3,11.3097e-3,1,4,2.17e-3,5.4366e-3,
4,17.6597e-6,11.3097e-3,11.3097e-3,1,8,2.17e-3,5.4366e-3,
5,17.6597e-6,11.3097e-3,11.3097e-3,2,6,2.17e-3,5.4366e-3,11,2.17e-3,5.4366e-3,
6,17.6597e-6,11.3097e-3,11.3097e-3,1,7,2.17e-3,5.4366e-3,
7,17.6597e-6,11.3097e-3,11.3097e-3,2,8,2.17e-3,5.4366e-3,13,2.17e-3,5.4366e-3,
8,17.6597e-6,11.3097e-3,11.3097e-3,1,9,2.17e-3,5.4366e-3,
9,17.6597e-6,11.3097e-3,11.3097e-3,1,15,2.17e-3,5.4366e-3,
10,17.6597e-6,11.3097e-3,11.3097e-3,2,11,2.17e-3,5.4366e-3,18,2.17e-3,5.4366e-3,
11,17.6597e-6,11.3097e-3,11.3097e-3,1,12,2.17e-3,5.4366e-3,
12,17.6597e-6,11.3097e-3,11.3097e-3,2,13,2.17e-3,5.4366e-3,20,2.17e-3,5.4366e-3,
13,17.6597e-6,11.3097e-3,11.3097e-3,1,14,2.17e-3,5.4366e-3,
14,17.6597e-6,11.3097e-3,11.3097e-3,2,15,2.17e-3,5.4366e-3,22,2.17e-3,5.4366e-3,
15,17.6597e-6,11.3097e-3,11.3097e-3,1,16,2.17e-3,5.4366e-3,
16,17.6597e-6,11.3097e-3,11.3097e-3,1,24,2.17e-3,5.4366e-3,
17,17.6597e-6,11.3097e-3,11.3097e-3,2,18,2.17e-3,5.4366e-3,27,2.17e-3,5.4366e-3,
18,17.6597e-6,11.3097e-3,11.3097e-3,1,19,2.17e-3,5.4366e-3,
19,17.6597e-6,11.3097e-3,11.3097e-3,2,20,2.17e-3,5.4366e-3,29,2.17e-3,5.4366e-3,
20,17.6597e-6,11.3097e-3,11.3097e-3,1,21,2.17e-3,5.4366e-3,
21,17.6597e-6,11.3097e-3,11.3097e-3,2,22,2.17e-3,5.4366e-3,31,2.17e-3,5.4366e-3,
22,17.6597e-6,11.3097e-3,11.3097e-3,1,23,2.17e-3,5.4366e-3,
23,17.6597e-6,11.3097e-3,11.3097e-3,2,24,2.17e-3,5.4366e-3,33,2.17e-3,5.4366e-3,
24,17.6597e-6,11.3097e-3,11.3097e-3,1,25,2.17e-3,5.4366e-3,
25,17.6597e-6,11.3097e-3,11.3097e-3,1,35,2.17e-3,5.4366e-3,
26,17.6597e-6,11.3097e-3,11.3097e-3,2,27,2.17e-3,5.4366e-3,38,2.17e-3,5.4366e-3,
27,17.6597e-6,11.3097e-3,11.3097e-3,1,28,2.17e-3,5.4366e-3,
28,17.6597e-6,11.3097e-3,11.3097e-3,2,29,2.17e-3,5.4366e-3,40,2.17e-3,5.4366e-3,
29,17.6597e-6,11.3097e-3,11.3097e-3,1,30,2.17e-3,5.4366e-3,
30,17.6597e-6,11.3097e-3,11.3097e-3,2,31,2.17e-3,5.4366e-3,42,2.17e-3,5.4366e-3,
31,17.6597e-6,11.3097e-3,11.3097e-3,1,32,2.17e-3,5.4366e-3,
32,17.6597e-6,11.3097e-3,11.3097e-3,2,33,2.17e-3,5.4366e-3,44,2.17e-3,5.4366e-3,
33,17.6597e-6,11.3097e-3,11.3097e-3,1,34,2.17e-3,5.4366e-3,
34,17.6597e-6,11.3097e-3,11.3097e-3,2,35,2.17e-3,5.4366e-3,46,2.17e-3,5.4366e-3,
35,17.6597e-6,11.3097e-3,11.3097e-3,1,36,2.17e-3,5.4366e-3,
```

36,17.6597e-6,11.3097e-3,11.3097e-3,1,48,2.17e-3,5.4366e-3,
37,17.6597e-6,11.3097e-3,11.3097e-3,2,38,2.17e-3,5.4366e-3,51,2.17e-3,5.4366e-3,
38,17.6597e-6,11.3097e-3,11.3097e-3,1,39,2.17e-3,5.4366e-3,
39,17.6597e-6,11.3097e-3,11.3097e-3,2,40,2.17e-3,5.4366e-3,53,2.17e-3,5.4366e-3,
40,17.6597e-6,11.3097e-3,11.3097e-3,1,41,2.17e-3,5.4366e-3,
41,17.6597e-6,11.3097e-3,11.3097e-3,2,42,2.17e-3,5.4366e-3,55,2.17e-3,5.4366e-3,
42,17.6597e-6,11.3097e-3,11.3097e-3,1,43,2.17e-3,5.4366e-3,
43,17.6597e-6,11.3097e-3,11.3097e-3,2,44,2.17e-3,5.4366e-3,57,2.17e-3,5.4366e-3,
44,17.6597e-6,11.3097e-3,11.3097e-3,1,45,2.17e-3,5.4366e-3,
45,17.6597e-6,11.3097e-3,11.3097e-3,2,46,2.17e-3,5.4366e-3,59,2.17e-3,5.4366e-3,
46,17.6597e-6,11.3097e-3,11.3097e-3,1,47,2.17e-3,5.4366e-3,
47,17.6597e-6,11.3097e-3,11.3097e-3,2,48,2.17e-3,5.4366e-3,61,2.17e-3,5.4366e-3,
48,17.6597e-6,11.3097e-3,11.3097e-3,1,49,2.17e-3,5.4366e-3,
49,17.6597e-6,11.3097e-3,11.3097e-3,1,63,2.17e-3,5.4366e-3,
50,17.6597e-6,11.3097e-3,11.3097e-3,2,51,2.17e-3,5.4366e-3,66,2.17e-3,5.4366e-3,
51,17.6597e-6,11.3097e-3,11.3097e-3,1,52,2.17e-3,5.4366e-3,
52,17.6597e-6,11.3097e-3,11.3097e-3,2,53,2.17e-3,5.4366e-3,68,2.17e-3,5.4366e-3,
53,17.6597e-6,11.3097e-3,11.3097e-3,1,54,2.17e-3,5.4366e-3,
54,17.6597e-6,11.3097e-3,11.3097e-3,2,55,2.17e-3,5.4366e-3,70,2.17e-3,5.4366e-3,
55,17.6597e-6,11.3097e-3,11.3097e-3,1,56,2.17e-3,5.4366e-3,
56,17.6597e-6,11.3097e-3,11.3097e-3,2,57,2.17e-3,5.4366e-3,72,2.17e-3,5.4366e-3,
57,17.6597e-6,11.3097e-3,11.3097e-3,1,58,2.17e-3,5.4366e-3,
58,17.6597e-6,11.3097e-3,11.3097e-3,2,59,2.17e-3,5.4366e-3,74,2.17e-3,5.4366e-3,
59,17.6597e-6,11.3097e-3,11.3097e-3,1,60,2.17e-3,5.4366e-3,
60,17.6597e-6,11.3097e-3,11.3097e-3,2,61,2.17e-3,5.4366e-3,76,2.17e-3,5.4366e-3,
61,17.6597e-6,11.3097e-3,11.3097e-3,1,62,2.17e-3,5.4366e-3,
62,17.6597e-6,11.3097e-3,11.3097e-3,2,63,2.17e-3,5.4366e-3,78,2.17e-3,5.4366e-3,
63,17.6597e-6,11.3097e-3,11.3097e-3,1,64,2.17e-3,5.4366e-3,
64,17.6597e-6,11.3097e-3,11.3097e-3,1,80,2.17e-3,5.4366e-3,
65,17.6597e-6,11.3097e-3,11.3097e-3,2,66,2.17e-3,5.4366e-3,83,2.17e-3,5.4366e-3,
66,17.6597e-6,11.3097e-3,11.3097e-3,1,67,2.17e-3,5.4366e-3,
67,17.6597e-6,11.3097e-3,11.3097e-3,2,68,2.17e-3,5.4366e-3,85,2.17e-3,5.4366e-3,
68,17.6597e-6,11.3097e-3,11.3097e-3,1,69,2.17e-3,5.4366e-3,
69,17.6597e-6,11.3097e-3,11.3097e-3,2,70,2.17e-3,5.4366e-3,87,2.17e-3,5.4366e-3,
70,17.6597e-6,11.3097e-3,11.3097e-3,1,71,2.17e-3,5.4366e-3,
71,17.6597e-6,11.3097e-3,11.3097e-3,2,72,2.17e-3,5.4366e-3,89,2.17e-3,5.4366e-3,
72,17.6597e-6,11.3097e-3,11.3097e-3,1,73,2.17e-3,5.4366e-3,
73,17.6597e-6,11.3097e-3,11.3097e-3,2,74,2.17e-3,5.4366e-3,91,2.17e-3,5.4366e-3,
74,17.6597e-6,11.3097e-3,11.3097e-3,1,75,2.17e-3,5.4366e-3,
75,17.6597e-6,11.3097e-3,11.3097e-3,2,76,2.17e-3,5.4366e-3,93,2.17e-3,5.4366e-3,
76,17.6597e-6,11.3097e-3,11.3097e-3,1,77,2.17e-3,5.4366e-3,
77,17.6597e-6,11.3097e-3,11.3097e-3,2,78,2.17e-3,5.4366e-3,95,2.17e-3,5.4366e-3,
78,17.6597e-6,11.3097e-3,11.3097e-3,1,79,2.17e-3,5.4366e-3,
79,17.6597e-6,11.3097e-3,11.3097e-3,2,80,2.17e-3,5.4366e-3,97,2.17e-3,5.4366e-3,
80,17.6597e-6,11.3097e-3,11.3097e-3,1,81,2.17e-3,5.4366e-3,
81,17.6597e-6,11.3097e-3,11.3097e-3,1,99,2.17e-3,5.4366e-3,

82,17.6597e-6,11.3097e-3,11.3097e-3,2,83,2.17e-3,5.4366e-3,102,2.17e-3,5.4366e-3,
83,17.6597e-6,11.3097e-3,11.3097e-3,1,84,2.17e-3,5.4366e-3,
84,17.6597e-6,11.3097e-3,11.3097e-3,2,85,2.17e-3,5.4366e-3,104,2.17e-3,5.4366e-3,
85,17.6597e-6,11.3097e-3,11.3097e-3,1,86,2.17e-3,5.4366e-3,
86,17.6597e-6,11.3097e-3,11.3097e-3,2,87,2.17e-3,5.4366e-3,106,2.17e-3,5.4366e-3,
87,17.6597e-6,11.3097e-3,11.3097e-3,1,88,2.17e-3,5.4366e-3,
88,17.6597e-6,11.3097e-3,11.3097e-3,2,89,2.17e-3,5.4366e-3,108,2.17e-3,5.4366e-3,
89,17.6597e-6,11.3097e-3,11.3097e-3,1,90,2.17e-3,5.4366e-3,
90,17.6597e-6,11.3097e-3,11.3097e-3,2,91,2.17e-3,5.4366e-3,110,2.17e-3,5.4366e-3,
91,17.6597e-6,11.3097e-3,11.3097e-3,1,92,2.17e-3,5.4366e-3,
92,17.6597e-6,11.3097e-3,11.3097e-3,2,93,2.17e-3,5.4366e-3,112,2.17e-3,5.4366e-3,
93,17.6597e-6,11.3097e-3,11.3097e-3,1,94,2.17e-3,5.4366e-3,
94,17.6597e-6,11.3097e-3,11.3097e-3,2,95,2.17e-3,5.4366e-3,114,2.17e-3,5.4366e-3,
95,17.6597e-6,11.3097e-3,11.3097e-3,1,96,2.17e-3,5.4366e-3,
96,17.6597e-6,11.3097e-3,11.3097e-3,2,97,2.17e-3,5.4366e-3,116,2.17e-3,5.4366e-3,
97,17.6597e-6,11.3097e-3,11.3097e-3,1,98,2.17e-3,5.4366e-3,
98,17.6597e-6,11.3097e-3,11.3097e-3,2,99,2.17e-3,5.4366e-3,118,2.17e-3,5.4366e-3,
99,17.6597e-6,11.3097e-3,11.3097e-3,1,100,2.17e-3,5.4366e-3,
100,17.6597e-6,11.3097e-3,11.3097e-3,1,120,2.17e-3,5.4366e-3,
101,17.6597e-6,11.3097e-3,11.3097e-3,2,102,2.17e-3,5.4366e-3,123,2.17e-3,6.1340e-3,
102,17.6597e-6,11.3097e-3,11.3097e-3,1,103,2.17e-3,5.4366e-3,
103,17.6597e-6,11.3097e-3,11.3097e-3,2,104,2.17e-3,5.4366e-3,124,2.17e-3,6.1340e-3,
104,17.6597e-6,11.3097e-3,11.3097e-3,1,105,2.17e-3,5.4366e-3,
105,17.6597e-6,11.3097e-3,11.3097e-3,2,106,2.17e-3,5.4366e-3,125,2.17e-3,6.1340e-3,
106,17.6597e-6,11.3097e-3,11.3097e-3,1,107,2.17e-3,5.4366e-3,
107,17.6597e-6,11.3097e-3,11.3097e-3,2,108,2.17e-3,5.4366e-3,126,2.17e-3,6.1340e-3,
108,17.6597e-6,11.3097e-3,11.3097e-3,1,109,2.17e-3,5.4366e-3,
109,17.6597e-6,11.3097e-3,11.3097e-3,2,110,2.17e-3,5.4366e-3,127,2.17e-3,6.1340e-3,
110,17.6597e-6,11.3097e-3,11.3097e-3,1,111,2.17e-3,5.4366e-3,
111,17.6597e-6,11.3097e-3,11.3097e-3,2,112,2.17e-3,5.4366e-3,128,2.17e-3,6.1340e-3,
112,17.6597e-6,11.3097e-3,11.3097e-3,1,113,2.17e-3,5.4366e-3,
113,17.6597e-6,11.3097e-3,11.3097e-3,2,114,2.17e-3,5.4366e-3,129,2.17e-3,6.1340e-3,
114,17.6597e-6,11.3097e-3,11.3097e-3,1,115,2.17e-3,5.4366e-3,
115,17.6597e-6,11.3097e-3,11.3097e-3,2,116,2.17e-3,5.4366e-3,130,2.17e-3,6.1340e-3,
116,17.6597e-6,11.3097e-3,11.3097e-3,1,117,2.17e-3,5.4366e-3,
117,17.6597e-6,11.3097e-3,11.3097e-3,2,118,2.17e-3,5.4366e-3,131,2.17e-3,6.1340e-3,
118,17.6597e-6,11.3097e-3,11.3097e-3,1,119,2.17e-3,5.4366e-3,
119,17.6597e-6,11.3097e-3,11.3097e-3,2,120,2.17e-3,5.4366e-3,132,2.17e-3,6.1340e-3,
120,17.6597e-6,11.3097e-3,11.3097e-3,1,121,2.17e-3,5.4366e-3,
121,17.6597e-6,11.3097e-3,11.3097e-3,1,133,2.17e-3,6.1340e-3,
122,4.6969e-6,4.9413e-3,1.8850e-3,1,123,1.6938e-3,6.0577e-3,
123,29.2450e-6,20.6797e-3,11.3097e-3,1,124,1.6938e-3,9.3824e-3,
124,29.2450e-6,20.6797e-3,11.3097e-3,1,125,1.6938e-3,9.3824e-3,
125,29.2450e-6,20.6797e-3,11.3097e-3,1,126,1.6938e-3,9.3824e-3,
126,29.2450e-6,20.6797e-3,11.3097e-3,1,127,1.6938e-3,9.3824e-3,
127,29.2450e-6,20.6797e-3,11.3097e-3,1,128,1.6938e-3,9.3824e-3,

```
128,29.2450e-6,20.6797e-3,11.3097e-3,1,129,1.6938e-3,9.3824e-3,
129,29.2450e-6,20.6797e-3,11.3097e-3,1,130,1.6938e-3,9.3824e-3,
130,29.2450e-6,20.6797e-3,11.3097e-3,1,131,1.6938e-3,9.3824e-3,
131,29.2450e-6,20.6797e-3,11.3097e-3,1,132,1.6938e-3,9.3824e-3,
132,29.2450e-6,20.6797e-3,11.3097e-3,1,133,1.6938e-3,9.3824e-3,
133,29.2450e-6,20.6797e-3,11.3097e-3,1,134,1.6938e-3,6.0577e-3,
134,4.6969e-6,4.9413e-3,1.8850e-3
*
*
prop,0,1,2,1                                                    *prop.1
*
*
rods,1,78,0,1,0,0,0,0,0,0,0,0                                   *rods.1
1.015,0.0,0,0                                                   *rods.2
40                                                              *rods.3
0.0,0.79,0.028,0.79,0.02800001,0.95,0.057,0.95,                 *rods.4
0.05700001,1.11,0.084,1.11,0.08400001,1.20,0.112,1.20,
0.11200001,1.26,0.168,1.26,0.16800001,1.22,0.193,1.22,
0.19300001,1.37,0.223,1.37,0.22300001,0.27,0.501,0.27,
0.50100001,0.32,0.569,0.32,0.56900001,0.37,0.638,0.37,
0.63800001,0.51,0.777,0.51,0.77700001,2.83,0.804,2.83,
0.80400001,2.59,0.857,2.59,0.85700001,2.57,0.884,2.57,
0.88400001,2.49,0.909,2.49,0.90900001,2.37,0.938,2.37,
0.93800001,2.25,0.965,2.25,0.96500001,3.01,0.992,3.01,
0.99200001,0.79,1.003,0.79,1.00300001,1.04,1.015,1.04,
*
*rods geometry input                                             *rods.9
1,1,1.1,1,1,0.1667,
2,1,1.09,1,1,0.1667,2,0.1667,3,0.1667,
3,1,1.09,1,1,0.1667,3,0.1667,4,0.1667,
4,1,1.08,1,2,0.1667,5,0.1667,6,0.1667,
5,1,1.08,1,2,0.1667,3,0.1667,4,0.1667,6,0.1667,7,0.1667,8,0.1667,
6,1,1.08,1,4,0.1667,8,0.1667,9,0.1667,
7,1,1.07,1,5,0.1667,10,0.1667,11,0.1667,
8,1,1.07,1,5,0.1667,6,0.1667,7,0.1667,11,0.1667,12,0.1667,13,0.1667,
9,1,1.07,1,7,0.1667,8,0.1667,9,0.1667,13,0.1667,14,0.1667,15,0.1667,
10,1,1.07,1,9,0.1667,15,0.1667,16,0.1667,
11,1,1.06,1,10,0.1667,17,0.1667,18,0.1667,
12,1,1.06,1,10,0.1667,11,0.1667,12,0.1667,18,0.1667,19,0.1667,20,0.1667,
13,1,1.06,1,12,0.1667,13,0.1667,14,0.1667,20,0.1667,21,0.1667,22,0.1667,
14,1,1.06,1,14,0.1667,15,0.1667,16,0.1667,22,0.1667,23,0.1667,24,0.1667,
15,1,1.06,1,16,0.1667,24,0.1667,25,0.1667,
16,1,1.05,1,17,0.1667,26,0.1667,27,0.1667,
17,1,1.05,1,17,0.1667,18,0.1667,19,0.1667,27,0.1667,28,0.1667,29,0.1667,
18,1,1.05,1,19,0.1667,20,0.1667,21,0.1667,29,0.1667,30,0.1667,31,0.1667,
19,1,1.05,1,21,0.1667,22,0.1667,23,0.1667,31,0.1667,32,0.1667,33,0.1667,
```

20,1,1.05,1,23,0.1667,24,0.1667,25,0.1667,33,0.1667,34,0.1667,35,0.1667,
21,1,1.05,1,25,0.1667,35,0.1667,36,0.1667,
22,1,1.04,1,26,0.1667,37,0.1667,38,0.1667,
23,1,1.04,1,26,0.1667,27,0.1667,28,0.1667,38,0.1667,39,0.1667,40,0.1667,
24,1,1.04,1,28,0.1667,29,0.1667,30,0.1667,40,0.1667,41,0.1667,42,0.1667,
25,1,1.04,1,30,0.1667,31,0.1667,32,0.1667,42,0.1667,43,0.1667,44,0.1667,
26,1,1.04,1,32,0.1667,33,0.1667,34,0.1667,44,0.1667,45,0.1667,46,0.1667,
27,1,1.04,1,34,0.1667,35,0.1667,36,0.1667,46,0.1667,47,0.1667,48,0.1667,
28,1,1.04,1,36,0.1667,48,0.1667,49,0.1667,
29,1,1.03,1,37,0.1667,50,0.1667,51,0.1667,
30,1,1.03,1,37,0.1667,38,0.1667,39,0.1667,51,0.1667,52,0.1667,53,0.1667,
31,1,1.03,1,39,0.1667,40,0.1667,41,0.1667,53,0.1667,54,0.1667,55,0.1667,
32,1,1.03,1,41,0.1667,42,0.1667,43,0.1667,55,0.1667,56,0.1667,57,0.1667,
33,1,1.03,1,43,0.1667,44,0.1667,45,0.1667,57,0.1667,58,0.1667,59,0.1667,
34,1,1.03,1,45,0.1667,46,0.1667,47,0.1667,59,0.1667,60,0.1667,61,0.1667,
35,1,1.03,1,47,0.1667,48,0.1667,49,0.1667,61,0.1667,62,0.1667,63,0.1667,
36,1,1.03,1,49,0.1667,63,0.1667,64,0.1667,
37,1,1.02,1,50,0.1667,65,0.1667,66,0.1667,
38,1,1.02,1,50,0.1667,51,0.1667,52,0.1667,66,0.1667,67,0.1667,68,0.1667,
39,1,1.02,1,52,0.1667,53,0.1667,54,0.1667,68,0.1667,69,0.1667,70,0.1667,
40,1,1.02,1,54,0.1667,55,0.1667,56,0.1667,70,0.1667,71,0.1667,72,0.1667,
41,1,1.02,1,56,0.1667,57,0.1667,58,0.1667,72,0.1667,73,0.1667,74,0.1667,
42,1,1.02,1,58,0.1667,59,0.1667,60,0.1667,74,0.1667,75,0.1667,76,0.1667,
43,1,1.02,1,60,0.1667,61,0.1667,62,0.1667,76,0.1667,77,0.1667,78,0.1667,
44,1,1.02,1,62,0.1667,63,0.1667,64,0.1667,78,0.1667,79,0.1667,80,0.1667,
45,1,1.02,1,64,0.1667,80,0.1667,81,0.1667,
46,1,1.0,1,65,0.1667,82,0.1667,83,0.1667,
47,1,1.0,1,65,0.1667,66,0.1667,67,0.1667,83,0.1667,84,0.1667,85,0.1667,
48,1,1.0,1,67,0.1667,68,0.1667,69,0.1667,85,0.1667,86,0.1667,87,0.1667,
49,1,1.0,1,69,0.1667,70,0.1667,71,0.1667,87,0.1667,88,0.1667,89,0.1667,
50,1,1.0,1,71,0.1667,72,0.1667,73,0.1667,89,0.1667,90,0.1667,91,0.1667,
51,1,1.0,1,73,0.1667,74,0.1667,75,0.1667,91,0.1667,92,0.1667,93,0.1667,
52,1,1.0,1,75,0.1667,76,0.1667,77,0.1667,93,0.1667,94,0.1667,95,0.1667,
53,1,1.0,1,77,0.1667,78,0.1667,79,0.1667,95,0.1667,96,0.1667,97,0.1667,
54,1,1.0,1,79,0.1667,80,0.1667,81,0.1667,97,0.1667,98,0.1667,99,0.1667,
55,1,1.0,1,81,0.1667,99,0.1667,100,0.1667,
56,1,0.95,1,82,0.1667,101,0.1667,102,0.1667,
57,1,0.95,1,82,0.1667,83,0.1667,84,0.1667,102,0.1667,103,0.1667,104,0.1667,
58,1,0.95,1,84,0.1667,85,0.1667,86,0.1667,104,0.1667,105,0.1667,106,0.1667,
59,1,0.95,1,86,0.1667,87,0.1667,88,0.1667,106,0.1667,107,0.1667,108,0.1667,
60,1,0.95,1,88,0.1667,89,0.1667,90,0.1667,108,0.1667,109,0.1667,110,0.1667,
61,1,0.95,1,90,0.1667,91,0.1667,92,0.1667,110,0.1667,111,0.1667,112,0.1667,
62,1,0.95,1,92,0.1667,93,0.1667,94,0.1667,112,0.1667,113,0.1667,114,0.1667,
63,1,0.95,1,94,0.1667,95,0.1667,96,0.1667,114,0.1667,115,0.1667,116,0.1667,
64,1,0.95,1,96,0.1667,97,0.1667,98,0.1667,116,0.1667,117,0.1667,118,0.1667,
65,1,0.95,1,98,0.1667,99,0.1667,100,0.1667,118,0.1667,119,0.1667,120,0.1667,

```
66,1,0.95,1,100,0.1667,120,0.1667,121,0.1667,
67,1,0.9,1,101,0.1667,122,0.0833,123,0.25,
68,1,0.9,1,101,0.1667,102,0.1667,103,0.1667,123,0.25,124,0.25,
69,1,0.9,1,103,0.1667,104,0.1667,105,0.1667,124,0.25,125,0.25,
70,1,0.9,1,105,0.1667,106,0.1667,107,0.1667,125,0.25,126,0.25,
71,1,0.9,1,107,0.1667,108,0.1667,109,0.1667,126,0.25,127,0.25,
72,1,0.9,1,109,0.1667,110,0.1667,111,0.1667,127,0.25,128,0.25,
73,1,0.9,1,111,0.1667,112,0.1667,113,0.1667,128,0.25,129,0.25,
74,1,0.9,1,113,0.1667,114,0.1667,115,0.1667,129,0.25,130,0.25,
75,1,0.9,1,115,0.1667,116,0.1667,117,0.1667,130,0.25,131,0.25,
76,1,0.9,1,117,0.1667,118,0.1667,119,0.1667,131,0.25,132,0.25,
77,1,0.9,1,119,0.1667,120,0.1667,121,0.1667,132,0.25,133,0.25,
78,1,0.9,1,121,0.1667,133,0.25,134,0.0833,
0
*
1,dumy,7.2e-3,0.0,0                                    *rods.68
*
*
oper,0,2,0,2,0,2,0,0,0,0                               *oper.1
-1.0,0.0,0.0,0.0,                                      *oper.2
0                                                      *oper.3
7200000,1250000,573.20,0.71789,0.0                     *oper.5
7200000,1250000,687.84,0.71789,0.0
0                                                      *oper.12
*
*
corr,0,2,0                                             *corr.1
chll,chll,epri,none                                    *corr.2
ditb,chen,chen,epri,cond,g5.7,0                        *corr.6
1,0,0.0                                                *corr.16
*
*
mixx,3,0,0                                             *mixx.1
0.8,0.035,-0.1                                         *mixx.2
*
*
drag,1,0,0                                             *drag1
0.15139,-0.18,0,94.0485,-1,0,                          *drag2
0.5                                                    *drag5
*
*
grid,0,3                                               *grid.1
71.4,1.62,1.22                                         *grid.2
-1,7                                                   *grid.4
0.0,1,0.187,2,0.374,2,0.561,2,0.748,2,0.935,2,1.015,3  *grid.6
0
```

```
*
*
cont                                                    *cont.1
0.0,0,200,750,2,2,0,0                                   *cont.2
0.1,0.0001,0.001,0.05,0.01,0.9,1.5,0.9                  *cont.3
0,0,0,0,0,0,1,1,0,0,0,1,0,2,0                           *cont.6
100.,0,0,0,0,0                                          *cont.7
*
*
endd
0
```

References

Adamsson, C., Anglart, H., 2010. Influence of Axial Power Distribution on Dryout: Film-flow Models and Experiments. *Nuclear Engineering and Design*, 240, 1495-1505.

Adamsson, C., Le Corre, J.M., 2011. Modeling and Validation of a Mechanistic Tool (MEFISTO) for the Prediction of Critical Power in BWR Fuel Assemblies. *Nuclear Engineering and Design*, 241, 2843-2858.

Anglart, H., 2010. Study of the Influence of Axial Power Distribution on Dryout. *Proc. of the 18th International Conference on Nuclear Engineering (ICONE-18)*, Xi'an, China, Paper 29050.

Beus, S.G., Humphreys, D.A., 1979. Critical Heat Flux Tests with High Pressure Water in an Internally Heated Annulus with Alternating Axial Heat Flux Distribution (AWBA Development Program). DOE Research and Development Report, WAPD-TM-1451.

Beus, S.G., Seebold, O.P., 1981. Critical Heat Flux Experiments in an Internally Heated Annulus with a Non-Uniform, Alternate High and Low Axial Heat Flux Distribution (AWBA Development Program). DOE Research and Development Report, WAPD-TM-1475.

Brynjell-Rahkola, K., Le Corre, J.M., Adamsson, C., 2009. Validation of VIPRE-W Sub-channel Void Predictions using NUPEC/BFBT Measurements. *Proc. of the 13th International Topical Meeting on Nuclear Reactor Thermal-hydraulics (NURETH-13)*, Kanazawa City, Japan, N13P1080.

Caraghiaur, D., Anglart, H., Frid, W., 2009. Experimental Investigation of Turbulent Flow through Spacer Grids in Fuel Rod Bundles. *Nuclear Engineering and Design*, 239, 2013-2021.

Cheng, S.K., Todreas, N.E., 1986. Hydrodynamic Models and Correlations for Bare and Wire-Wrapped Hexagonal Rod Bundles - Bundle Friction Factors, Subchannel Friction Factors and Mixing Parameters. *Nuclear Engineering and Design*, 92, 227-251.

Conboy, T.M., 2010. Assessment of Helical-Cruciform Fuel Rods for High Power Density LWRs. MIT, Ph.D. Thesis.

Downar, T., Kazimi, M.S., 2015. Analysis of RBWR-AC and TB2 Design with SERPENT/PARCS/PATHS Code System. Hitachi Final Report.

Gaspari, G. P., Hassid, A., Lucchini, F., 1975. A Rod-Centered Subchannel Analysis with Turbulent (Enthalpy) Mixing For Critical Heat Flux Prediction in Rod Clusters Cooled By Boiling Water. *Proc. of International Heat Transfer Conference*, Tokyo, Japan, CONF-740925.

Groeneveld, D.C., Shan, J.Q., Vasic, A.Z., Leung, L.K.H., Durmayaz, A., Yang, J., Cheng, S.C., Tanase, A., 2007. The 2006 CHF Look-up Table. *Nuclear Engineering and Design*, 237, 1909-1922.

Hewitt, G.F., Govan, A.H., 1990. Phenomenological Modeling of Non-equilibrium Flows with Phase Change. *International Journal of Heat and Mass Transfer*, 33, 229-242.

Holloway, M., McClusky, H.L., Beasley, D.E., 2003. The Effect of Support Grid Features on Local, Single-phase Heat Transfer Measurements in Rod Bundles. *Proc. of ASME Summer Heat Transfer Conference (HT2003)*, Las Vegas, USA, HT2003-47433.

INL (Idaho National Laboratory), 2001. RELAP5/MOD3.3 Beta Code Manual. NUREG/CR-5535/Rev 1, Information Systems Laboratories, Inc.

Janssen, E., Kervinen, J.A., 1963. Burnout Conditions for Single Rod in Annular Geometry, Water at 600 to 1400 Psia. Atomic Power Equipment Department, General Electric Company, GEAP-3899.

Kolev, N.I., 2007. Check of the 2005-Look Up Table for Prediction of CHF in Bundles. *Nuclear Engineering and Design*, 237, 978-981.

Kureta, M., Akimoto, H., Yamamoto, K., Okada, H., 2002. Critical Heat Flux Experiment for Reduced-Moderation Water Reactor (RMWR). *Proc. of International Congress on Advances in Nuclear Power Plants (ICAPP)*, Hollywood, Florida, USA, Paper No. 1129.

Kureta, M., Akimoto, H., 2003. Critical Power Correlation for Axially Uniformly Heated Tight-Lattice Bundles. *Nuclear Technology*, 143, 89-100.

Kureta, M., 2007. Experimental Study of Three-Dimensional Void Fraction Distribution in Heated Tight-Lattice Rod Bundles Using Three-Dimensional Neutron Tomography. *Journal of Power and Energy Systems*, 1(3), 225-238.

Kureta, M., Tamai, H., Yoshida, H., Ohnuki, A., Akimoto, H., 2008. Development of Design Technology on Thermal-hydraulic Performance in Tight-lattice Rod Bundles: V - Estimation of Void Fraction. *Journal of Power and Energy Systems*, 2(1), 271-282.

Liu, W., Kureta, M., Akimoto, H., 2004. Critical Power in 7-Rod Tight Lattice Bundle. *JSME International Journal*, 47(2), 299-305.

Liu, W., Kureta, M., Yoshida, H., Ohnuki, A., Akimoto, H., 2007. An Improved Critical Power Correlation for Tight-Lattice Rod Bundles. *Journal of Nuclear Science and Technology*, 44(4), 558-571.

Mortimore, E.P., Beus, S.G., 1979. Critical Heat Flux Experiments with a Local Hot Patch in an Internally Heated Annulus (LWBR Development Program). DOE Research and Development Report, WAPD-TM-1419.

Nakatsuka, T., Tamai, H., Kureta, M., Okubo, T., Akimoto, H., Iwamura, T., 2003. Subchannel Analysis of CHF Experiments for Tight-Lattice Core. GENES4/ANP2003, Kyoto, Japan, Paper 1148.

Neykov, B., Aydogan, F., Hochreiter, L., Ivanov, K., Utsuno, H., Kasahara, F., Sartori, E., Martin, M., 2006. NUPEC BWR Full-size Fine-mesh Bundle Test (BFBT) Benchmark, Volume I: Specifications. OECD 2006, NEA No. 6212, NEA/NSC/DOC(2005)5, ISBN 92-64-01088-2.

Okawa, T., Kotani, A., Kataoka, I., Naito, M., 2003. Prediction of Critical Heat Flux in Annular Flow Using a Film Flow Model. *Journal of Nuclear Science and Technology*, 40(6), 388-396.

Okubo, T., Ezzidi, A., Murao, Y., 1993. Assessment of Models in COBRA-TF Code for Liquid Entrainments in Film-Mist Flow. JAERI-M 93-069.

Passerini, S., Kazimi, M.S., 2012. Sustainability Features of Nuclear Fuel Cycle Options. Sustainability, 4, 2377-2398.

Rehme, K., Trippe, G., 1980. Pressure Drop and Velocity Distribution in Rod Bundles with Spacer Grids. *Nuclear Engineering and Design*, 62, 349-359.

Rowe, D.S., Macduff, R.B., Collingham, R.E., 1990. Thermal-hydraulic Subchannel Model Based on Void Drift. *Proc. of the 9th International Heat Transfer Conference*, Jerusalem, Israel, Paper No. 9-TPF-02.

Shirvan, K., 2013. RBWR Project Summary (based on slides from MIT, U-M and UCB).

Shirvan, K., Andrews, N., Kazimi, M.S., 2013. Best Estimate Void Fraction and Critical Power Correlations for Tight Lattice BWR Bundles. *Proc. of International Congress on Advances in Nuclear Power Plants (ICAPP)*, Jeju Island, Korea, Paper No. FA159.

Shirvan, K., Kazimi, M.S., 2015. Reduced Moderated Boiling Water Reactor Thermal Hydraulics and Safety Assessment. Hitachi Technical Report.

Stewart, C.W., Cuta, J.M., Montgomery, S.D., Kelly, J.M., Basehore, K.L., George, T.L., Rowe, D.S., Gose, G.C., Westacott, J.L., 2011a. VIPRE-01: A Thermal-Hydraulic Code for Reactor Cores. Volume 1: Mathematical Modeling. Computer Code Manual. NP-2511-CCM-A, Volume 1, Revision 4.3, Research Project 1584-1.

Stewart, C.W., Cuta, J.M., Montgomery, S.D., Kelly, J.M., Basehore, K.L., George, T.L., Rowe, D.S., Gose, G.C., Westacott, J.L., 2011b. VIPRE-01: A Thermal-Hydraulic Code for Reactor Cores. Volume 2: Users Manual. Computer Code Manual. NP-2511-CCM-A, Volume 2, Revision 4.4, Research Project 1584-1.

Sung, Y.X., Schueren, P., Meliksetian, A., 1999. VIPRE-01 Modeling and Qualification for Pressurized Water Reactor Non-LOCA Thermal-Hydraulic Safety Analysis. Westinghouse Electric Company LLC, WCAP-15306-NP-A.

Takeda, R., Aoyama, M., Moriwaki, M., Uchikawa, S., Yokomizo, O., Ochiai, K., 1995. General Features of Resource-renewable BWR (RBWR) and Scenario of Long-term Energy Supply. *Proc. of International Conference on Evaluation of Emerging Nuclear Fuel Cycle Systems*, Versailles, France, P.938.

Tamai, H., Yoshida, H., Akimoto, H., 2003. Numerical Simulation on Film Flow Distribution and Boiling Transition in Tight-Lattice Rod Bundles with Spacer. GENES4/ANP2003, Kyoto, Japan, Paper 1021.

Tamai, H., Kureta, M., Yoshida, H., Akimoto, H., 2004. Pressure Drop Characteristics in Tight-Lattice Bundles for Reduced-Moderation Water Reactors. *JSME International Journal*, 47(2), 293-298.

Thompson, B., Macbeth, R.V., 1964. Boiling Water Heat Transfer Burnout in Uniformly Heated Round Tubes: a Compilation of World Data with Accurate Correlations. United Kingdom Atomic Energy Authority, AEEW-R356.

Todreas, N.E., Kazimi, M.S., 2012. Nuclear Systems, Volume 1: Thermal Hydraulic Fundamentals. Second Edition, CRC Press, Taylor & Francis Group.

Todreas, N.E., Rohsenow, W.M., 1965. The Effect of Non-uniform Axial Heat Flux Distribution on the Critical Heat Flux. MIT, Report No. 9843-37.

Uchikawa, S., Okubo, T., Nakano, Y., 2009. Breeder-type Operation Based on the LWR-MOX Fuel Technologies in Light Water Reactors with Hard Neutron Spectrum (FLWR). *Proc. of International Congress on Advances in Nuclear Power Plants (ICAPP)*, Tokyo, Japan, Paper 9022.

Weisman, J., 1992. The Current Status of Theoretically Based Approaches to the Prediction of the Critical Heat Flux in Flow Boiling. *Nuclear Technology*, 99, 1-21.

Yamamoto, T., Akiba, M., Morooka, S., Shirakawa, K., Abe, N., 2006. Thermal Hydraulic Performance of Tight Lattice Bundle. *JSME International Journal*, 49(2), 334-342.

Yang, J., Groeneveld, D.C., Leung, L.K.H., Cheng, S.C., El Nakla M.A., 2006. An Experimental and Analytical Study of the Effect of Axial Power Profile on CHF. *Nuclear Engineering and Design*, 236, 1384-1395.